INFORMATION TO USERS

This manuscript has been reproduced from the microfilm master. UMI films the text directly from the original or copy submitted. Thus, some thesis and dissertation copies are in typewriter face, while others may be from any type of computer printer.

The quality of this reproduction is dependent upon the quality of the copy submitted. Broken or indistinct print, colored or poor quality illustrations and photographs, print bleedthrough, substandard margins, and improper alignment can adversely affect reproduction.

In the unlikely event that the author did not send UMI a complete manuscript and there are missing pages, these will be noted. Also, if unauthorized copyright material had to be removed, a note will indicate the deletion.

Oversize materials (e.g., maps, drawings, charts) are reproduced by sectioning the original, beginning at the upper left-hand corner and continuing from left to right in equal sections with small overlaps.

Photographs included in the original manuscript have been reproduced xerographically in this copy. Higher quality 6" x 9" black and white photographic prints are available for any photographs or illustrations appearing in this copy for an additional charge. Contact UMI directly to order.

ProQuest Information and Learning
300 North Zeeb Road, Ann Arbor, MI 48106-1346 USA
800-521-0600

DYNAMIC RESPONSE OF FLUID-LOADED COMPOSITE PLATES TO STATIONARY AND MOVING LOADS

BY

HUSAIN AL-GAHTANI

A Thesis Presented to the

DEANSHIP OF GRADUATE STUDIES

KING FAHD UNIVERSITY OF PETROLEUM & MINERALS

DHAHRAN, SAUDI ARABIA

In Partial Fulfillment of the
Requirements for the Degree of

MASTER OF SCIENCE

In

MECHANICAL ENGINEERING

Rabi I 1422

MAY 2001

UMI Number: 1406104

Bell & Howell Information and Learning Company
300 North Zeeb Road
P.O. Box 1346
Ann Arbor, MI 48106-1346

KING FAHD UNIVERSITY OF PETROLEUM AND MINERALS

DHAHRAN 31261, SAUDI ARABIA

DEANSHIP OF GRADUATE STUDIES

This thesis, written by **HUSAIN MUHAMMAD AL-GAHTANI** under the direction of his Thesis Advisor and approved by his Thesis Committee, has been presented to and accepted by the Dean of Graduate Studies, in partial fulfillment of the requirements for the degree of **MASTER OF SCIENCE IN MECHANICAL ENGINEERING.**

THESIS COMMITTEE

June 19, 2001
Dr. SAIF AL-KAABI (Chairman)

19 June 2001
Dr. MOHAMMAD KHAN (Member)

June 19, 2001
Dr. MOHAMMAD HAMDAN (Member)

June 19, 2001
Dr. BASSEM AL-BEDOOR (Member)

Dr. YAGOUB AL-NASSAR (Member)

Department Chairman

Dean, College of Graduate Studies

3/4/1422
Date

عمادة الدراسات العليا
DEANSHIP OF GRADUATE STUDIES

Dedicated

to

my PARENTS and ALL OF MY FAMILY

for

their moral support

Acknowledgments

Above and first of all, I thank and pray to Allah for His guidance and protection throughout my life, including the years of this study. I am happy to have had a chance to His name, in the sincerest way, through this small accomplishment, and I ask Him, with hope only in Him, to accept my efforts. And secondly may peace be upon His Prophet, MOHAMMED.

Acknowledgment is due to the King Fahd University of Petroleum and Minerals for supporting this research.

I wish to dedicate this thesis with heartful thanks to my parents, brothers, sisters family members, friend, teachers and any person who supported or helped me in one way or another in this life.

I would like to express my sincere thanks to my advisor Dr. Saif Ahmad Al-Kaabi, for sharing with me his profound knowledge and expertise in the field of wave propagation. I also wish to thank his support, patience, comments, constructive criticism and, of course, encouragement.

I would also like to pay thanks to the other members of my advisory committee: Dr. M. A. Khan, Dr. M Hamdan, Dr. B. Al-Bedoor and Dr. Y. Al-Nassar, who have been sincere and co-operative whenever I called. Hope this work will be just the onset of my research endeavor.

CONTENTS

List of Tables

List of Figures

THESIS ABSTRACT

Name: HUSAIN AL-GAHTANI

Title: DYNAMIC RESPONSE OF FLUID-LOADED COMPOSITE PLATES TO STATIONARY AND MOVING LOADS

Degree: MASTER OF SCIENCE

Major Field: MECHANICAL ENGINEERING

Date of Degree: MAY 2001

Laminated composite plates are important elements in different structural applications due to their high strength to weight ratio. They are exposed to several types of loading such as fluid loading. This type of loading can be widely found in nuclear reactors and marine structures. Other type of loading is the one in which the load is moving. The moving load might be a conventional vehicle, a loading airplane, or a train. Studying the combined effects of the two types of loading is of great importance in order to find critical values of load velocity leading to significant vibrations, which subsequently lead to some annoying or maybe failure problems. In the present work, Liquid-loaded laminated composite plates are investigated under stationary and moving loads. Dispersion curves are calculated under different liquid loading conditions. Transient normal displacements are computed for 3, 6, and 12-ply laminated plates at three different locations along three main directions, namely, 0°, 45° and 90° direction. In addition, Group velocities are compared along these directions. For comparison purposes, the response is simulated for an isotropic plate at three different locations. Effect of liquid loading on these responses and group velocities is studied. For a single moving load, critical velocities of the load are computed for isotropic and laminated plates under different conditions. For double moving loads, effects of phase difference between loads and velocity of the loads on the maximum displacement of both isotropic and laminated plates are investigated. A higher order approximate solution in conjunction with Fourier transforms technique is used to model the dynamic behavior of the plate. This solution is based on the plate bending theory, which includes the effects of transverse shear and rotary inertia.

King Fahd University of Petroleum and Minerals, Dhahran.

MAY 2001

ملخص الرسالة

الاسم : حسين محمد القحطاني

العنوان : الاستجابة الديناميكية للألواح متعددة الطبقات المحملة بالسوائل من الجانبين بفعل الحمل الثابت أو المتحرك

الدرجة : ماجستير في العلوم

التخصص : الهندسة الميكانيكية

التاريخ : مايو ٢٠٠١

تعد الألواح الطبقية من الأجزاء المهمة في العديد من التطبيقات الإنشائية، نظرا لارتفاع نسبة المتانة إلى الوزن. وهذا النوع من الألواح يتعرض إلى أنواع عديدة من الأحمال كحمل السوائل الذي نجده بكثرة في المفاعلات النووية و الإنشاءات البحرية. النوع الآخر من الحمل هو الذي تكون فيه القوة متحركة.هذه القوة قد تكون مركبة متحركة، طائرة تهبط، أو قطار متحرك. وتعد دراسة الآثار المشتركة لهذين النوعين من الأحمال ذات أهمية قصوى وذلك لإيجاد قيم حرجة لسرعة القوى المتحركة والتي تؤدي إلى اهتزازات عالية المؤدية بدورها إلى مشاكل مزعجة أو مشاكل فشل. في هذا البحث ، تم دراسة الاستجابة العابرة للألواح الطبقية المحملة بسائلين على كلا الجانبين بفعل الحمل الثابت أو المتحرك. في البداية حسبت منحنيات التشتت للألواح تحت ظروف حمل متغيرة. ومن ثم تم حساب الاستجابة العابرة للألواح ذات ٣، ٦ و ١٢ طبقة في ثلاث مواقع مختلفة على امتداد ثلاث اتجاهات مختلفة وهي ٠ ، ٤٥ ، ٩٠° . كما تم حساب السرعة الجماعية في هذه الاتجاهات الثلاثة. ولغرض المقارنة،، تم حساب الاستجابة للوح موحد الخواص في ثلاث مواقع مختلفة. أما بالنسبة للحمل الأحادي المتحرك فقد حسبت السرعات الحرجة للحمل للألواح متعددة الطبقات و الألواح أحادية الخواص تحت ظروف مختلفة. وللحمل المزدوج المتحرك فقد تم دراسة تأثير اختلاف الطور وسرعة حركة الحمل على الاستجابة العظمى لكلا النوعين من الألواح.وقد تم استخدام حل تقريبي ذي درجة أعلى مقترنا بطريقة فوريه للتحويل. هذا الحل في الأساس يعتمد على نظرية انحناء الألواح والذي يأخذ بعين الاعتبار تأثير القوة القاصة و تأثير العطالة الدورانية.

جامعة الملك فهد للبترول والمعادن
الظهران، المملكة العربية السعودية
مايو ٢٠٠١

CHAPTER 1

INTRODUCTION

Plates are important elements of machines and structures. With the increasing use of such structures, the need for dynamic analysis of their characteristics has become evident. Moreover, laminated composite plates have become increasingly popular for a wide range of applications, especially for high performance structural components. They are used as primary structural components in modern applications due to their high ratio of strength and stiffness to weight. Such applications include aircraft and automotive structures.

Propagation of waves in plates is of great interest in seismology, ultrasonic material characterization, and ultrasonic nondestructive evaluation of defects. Therefore, this type of study has been the subject of numerous investigations in recent years.

Since plates are widely used in numerous applications, they are exposed to several types of loading. One type of loading is fluid loading on either or both sides of plates. This type of loading can be widely found in nuclear reactors and marine structures. Other type of loading is the one in which the load is moving. In this type, the problem of calculating the dynamic response of plates is very important in many engineering applications, which include for instance various transport systems. The moving load might be a conventional vehicle, a landing airplane, or a train. Studying such cases is of great importance in order to find critical values of load velocity leading to significant vibrations, which subsequently lead to some annoying or maybe failure problems.

1.1 LITERATURE SURVEY

The effect of fluid loading on the flexural vibrations of infinite isotropic plates has received wide attention by many researchers. Schroter and Fahy [1] analyzed the acoustic interaction between a layer of compressible fluid and a coupled isotropic, infinite panel, which separates the layer from a half-space of identical fluid. The response of the panel when driven by a point harmonic force was evaluated using Hankel Transformation in conjunction with complex variable integration techniques. Dispersion curves of the half-space/panel/layer coupled system were presented.

Dabirikhan and Turner [2] studied the coupling of the lowest antisymmetric modes *(A_o)* and interface Scholte modes *(AS)* in fluid-loaded isotropic plates. They presented the phase velocity dispersion curves of A_o and AS modes for a fluid loaded aluminum plate for various values of fluid density.

Selezov and Tkachenko [3] investigated the propagation of unsteady flexural waves in an elastic isotropic plate, placed on the surface of a finite depth liquid. The motion of the plate was described by a refined theory that included the inertia of rotation and the shear deformation, while the fluid was regarded as an inviscid fluid. They used the Fourier transformation approach to solve the governing equations of motions of the model.

S. Soedel and W. Soedel [4] developed equations of motion of elastic isotropic plates carrying liquids. The liquid was treated as incompressible with free surface oscillations. A closed form solution leading in the natural frequencies and modes of the plate-liquid combination was employed. The harmonic response of the liquid-plate system to a dynamic pressure distribution and also to point load on the plate was expressed in terms of the plate liquid modes.

Jurnu Wu and Zhu [5] studied theoretically the influence of liquid layer on the propagation of "Lamb" waves in an isotropic plate of finite thickness. The dispersion

equations of Lamb waves in this system were derived. Numerical solutions of the equations showed that the plane velocity of Lamb waves changed with the thickness of the liquid layers.

Sean Wu and Zhu [6] examined the effect of mean flow on dynamic responses on an infinite isotropic plate subjected to a time-dependent force excitation. An analysis of the transient response problem of isotropic plates with arbitrary shape in contact with fluid whose surface was excited by a general dynamic pressure was presented by Kosuke Nagaya [7]. Both Laplace and Fourier transformation were utilized to study the response of different shape plates, namely circular, rectangular, rectangular with round corners and oval plates.

Bao et al. [8] presented dispersion curves of lower modes of isotropic plate loaded with two different fluids. Experimental dispersion curves of a poly-ethylenethorephtalate film loaded with different types of fluids on both sides were presented by Desmet et al. [9]. The effect of fluid properties on the dispersion curves was studied.

Dickey et al. [10] developed dispersion curves of isotropic plates loaded with fluids on either or both sides using the impedance method. It was found that there can be

no local maxima at the critical frequency in the response of a fluid-loaded plate because the fluid presents infinite impedance.

Langley [11] used the harmonic Green function to study the sound fields of an infinite fluid-plate system excited by a point force. The plate was modeled as a linear elastic, isotropic, homogeneous layer of constant thickness bounding two different homogeneous fluid half spaces. Experimental and theoretical analysis of dispersion curves of a fluid layer between two elastic isotropic plates was investigated by Hassan and Nagy [12].

For the moving load problem, Nugroho et al. [13] investigated the displacement of an elastic, isotropic plate resting on fluid when two types of moving loads are applied: point and distributed circular loads. Two types of approaches were used, namely, Fast Fourier Transformation (FFT) and large-time asymptotic analysis.

The dynamic responses of an infinite homogeneous isotropic plate on an elastic foundation subjected to constant amplitude or harmonic moving loads were studied by Kim, S et al. [14] using formulations in the transformed field domains of time, space, and moving space. Effect of load speed on the maximum displacement was presented. For moving harmonic loads, critical velocities were studied for different frequencies. Furthermore, the effect of multiple loads was discussed. Several issues were investigated

such as phase between loads and effect of velocity on the maximum displacement in this type of loading. It was found that when the loads were moving, a change in phase between the loads could significantly reduce the maximum displacement.

Dieterman and Metrikine [15] determined the critical (resonance) velocities of a harmonically varying point load moving uniformly along an elastic isotropic layer as a function of the load frequency. It was proved in their study that the critical velocity of the load was equal to the group velocity of the waves generated by the load. Moreover, the critical depths of the plate were determined as a function of the load velocity. Fourier integral transformation was used in this analysis too.

Barber [16] investigated the normal surface displacement of isotropic elastic half-space, due to a normal point force, which moves with constant speed. The Smirnov-Sobolev technique was used to reduce the problem to a linear superposition of two-dimensional stress and displacement fields.

Finite Element Method (FEM) was utilized to evaluate the dynamic response of pavements subjected to a constant-amplitude-moving load by Zaman et al. [17]. The pavement-foundation system was modeled by a series of thick isotropic plate elements supported by discrete springs and dashpots at the nodal points representing the viscoelastic foundation. The moving loads were represented by masses each supported by

a spring and dashpot suspension system and having a specified horizontal velocity and acceleration. The accuracy of this algorithm was verified by comparing the finite element solution with the available analytical results. A parametric study was conducted to determine the effects of various parameters on the dynamic response of pavements to moving loads.

Bodin et al. [18] formulated a self-consistent boundary-value problem for isotropic plate subjected to moving loads using Hamilton Principle. The equations of energy and momentum were derived. Pesterev and Bergman [19] calculated the response of a general class of nonconservative linear distributed parameter systems excited by a moving concentrated load. A method of solution based on the series expansion of the response in terms of complex eigenfunctions of the continuous system was proposed. A set of ordinary differential equations in the time-dependent coefficients of the expansions was presented.

1.2 OBJECTIVE OF PRESENT WORK

Since all of the previous works were performed primarily for isotropic plates using classical theory, the main objective of our present work is to analyze the laminated composite plates with fluid loading on either or both sides. Several aspects are studied under this type of loading such as transient responses and dispersion curves. Dispersion

means that a pulse consisting of a range of frequencies does not retain its initial shape as it propagates through the dispersive medium. When the phase velocity depend on frequency or (wavelength), then the propagating wave is dispersive. Such dispersion may be caused by:

1. the presence of specimen boundaries (geometric dispersion).
2. the frequency dependence of material constants (material dispersion).
3. the scattering of waves by densely distributed fine inhomogeneities in a material (scattering dispersion).
4. the absorption or dissipation of wave energy into heat or other forms of energy in an irreversible process (disspative dispersion).

The effects of various properties of both plate and liquid are investigated. These properties include density, thickness, depth and plate type.

Moreover, laminated composite plates under moving loads are investigated. Critical velocities of the moving load are studied with and without fluid loading. The effect of fluid depth on those velocities is studied as well. Finally, plates under two moving loads are analyzed. Effects of the moving load speeds and phase differences are presented.

Due to the complexity of the analytical solution for multilayered laminates, and because thin composite plates are investigated here, a higher order approximate solution will be considered. This solution is based on the plate bending theory, which includes the effects of transverse shear and rotary inertia. This solution is an extension of Mindlin's plate theory for homogeneous isotropic plates [20]. Such an extension was originally due to Yang, Norris, and Stavsky [21] who extended Mindlin's theory to laminates consisting of an arbitrary number of anisotropic layers.

The original classical plate theory is based on the Kirchhoff hypothesis, which assumes that a line normal to the midplane before deformation remains straight and normal to the midplane after deformation, and hence neglects transverse shear deformation effects. For homogeneous, isotropic linear elastic thin plates, the effects of the transverse shear deformation are negligible. However, these effects are significant in the case of laminated composite plates due to the relatively low transverse shear modulus. As a result, the higher order laminated plate theory, which incorporates the effects of transverse shear deformation, and rotary inertia should be used in the analysis of composite plates. There are two good textbooks written by Whitney [22] and Cacote [23], which cover in detail the theoretical background of this theory.

1.3 THESIS OUTLINE

Three types of plates, namely 3, 6 and 12 plys plates under fluid loading are studied. Dispersion curves and transverse displacement plots are introduced for these plates. Effects of several parameters are precisely discussed. These parameters include: fluid heights, fluid densities, and types of plates. Furthermore, for moving loads, several issues are studied. Effects of load speed at different frequencies as well as the effect of fluid loading are taken into account when studying the response to moving loads.

The thesis begins with introductory chapter (Chapter 1) in which important previous works in the field of wave propagation in plates are introduced. A brief section of the main object of the present work is then written.

The second chapter is devoted primarily to theoretical formulation of the present problem. It starts with general assumptions on which the solution of the laminated plates is based. Geometry of the laminated composite plate loaded by liquid is then presented. Next, equations of motion for all types of loading are introduced. The methodology, type and difficulty of the problem solution are treated as well in this chapter.

Results, discussions and interpretations are the main subject of Chapter 3. Dispersion curves are computed for various liquid loadings. Transient responses of laminated composite and isotropic plates are then investigated under different loading conditions. Group velocity is also discussed and calculated as well. For single moving load, the critical velocity of the load is investigated under different loading conditions for both isotropic and laminated plates. This chapter is concluded by studying isotropic and laminated plates subjected to double moving loads. Effects of phase difference and speed of the two loads are discussed.

Major conclusions and remarks are presented in the last chapter. Moreover, some suggestions are introduced for future work in this area. The thesis closes with Appendices providing some expressions mentioned in the course of the text.

CHAPTER 2

THEORETICAL FORMULATIONS

2.1 STATIONARY LOADS

2.1.1 PROBLEM STATEMENT

The problem under consideration is described in Figure 2.1. The plate is modeled as laminated orthotropic plate, which is constructed of an arbitrary number of transversely isotropic laminas. Schematic diagram of one lamina is declared in Figure 2.2. A plate with a thickness H is loaded, in general, by two liquids; liquid 1 and liquid 2, having heights of H_1 and H_2, respectively. The plate is subjected to a concentrated vertical force f(t) in the negative z-direction. This force can be stationary or moving.

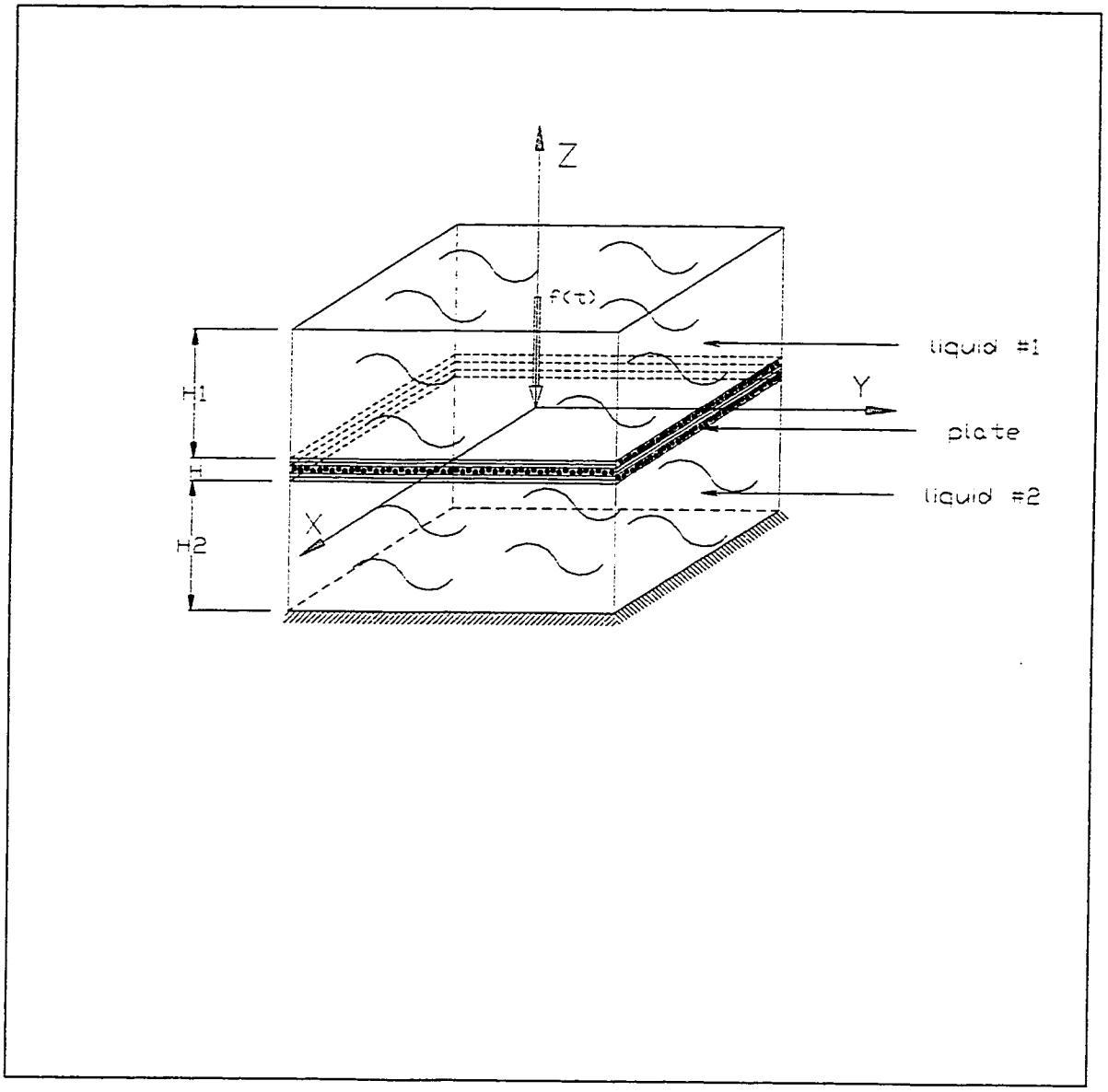

Figure 2.1: Geometric representation of a fluid loaded composite plate

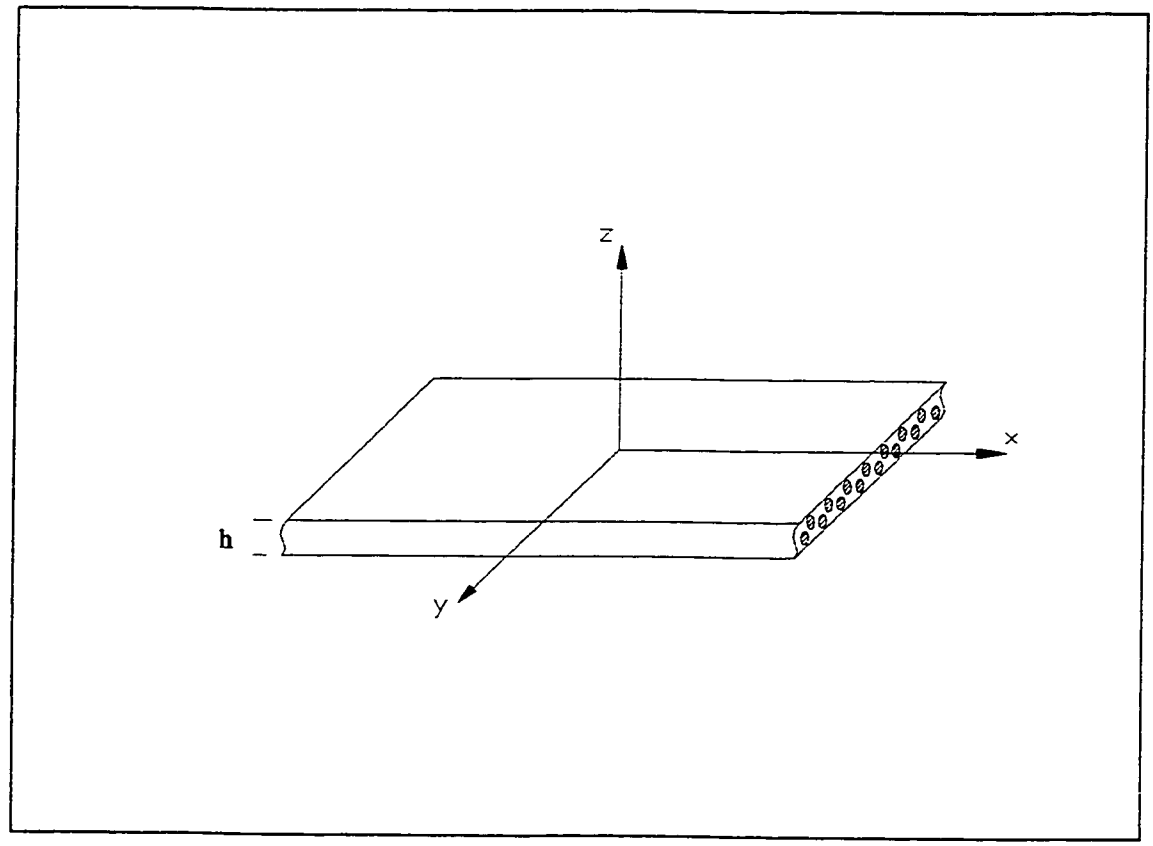

Figure 2.2: Geometry of a single lamina

2.1.2 GENERAL ASSUMPTIONS

The formulation of the governing equations of the preceding problem is mainly based on the following basic assumptions [22]:

1. The plate is constructed of an arbitrary number of layers of transversely isotropic laminas bonded together. However, the orthotropic axes of material symmetry of an individual layer need not coincide with the x-y axes of the plate.
2. The plate is thin, i.e., the thickness H is much smaller than other physical dimensions.
3. The material of each lamina is elastic and homogeneous (the fiber diameters and the lamina thickness are small compared to the dominant wave length).
4. The displacements of the mid-plane are small compared to the plate thickness.
5. In order to include in-plane force effects, nonlinear terms in the equations of motion involving products of stresses and plate slopes are retained. All other nonlinear terms are neglected.

6. Tangential displacements ***u*** (in x-direction) and **v** (in y-direction) are linear functions of the z-coordinate.
7. There are no body forces.
8. The deformations are such that straight lines, initially normal to the plate middle surface, remain straight lines but no longer normal to the middle surface, which means that deformations due to transverse shear are considered. In addition, the effects of rotary inertia are included.
9. The transverse normal strain e_{zz} is negligible.
10. The liquid is assumed inviscid and incompressible and potential flow theory is adapted.

2.1.3 EQUATIONS OF MOTIONS

2.1.3.1 Upper Liquid. Both liquids satisfy the Laplace equation, which is considered the governing equation of motion for them.

The upper liquid is assumed to have a depth H_1, and its top surface is free. The liquid is assumed to be incompressible and must satisfy

$$\nabla^2\Phi_1 = 0, \tag{2.1}$$

where $\Phi_1 = \Phi_1$ (x, y, z, t) is the velocity potential.

The boundary condition at the free surface of the upper liquid ($z = H/2 + H_1$) is that the pressure must be zero. The other boundary condition ($z=H/2$) is that the normal velocity of solid is equal to the normal velocity of the liquid i.e. continuous contact. So one can write,

$$\rho_1 \left.\frac{\partial \Phi_1}{\partial t}\right|_{z=H_1+\frac{H}{2}} = 0$$

$$\left.\frac{\partial \Phi_1}{\partial z}\right|_{z=\frac{H}{2}} = \frac{\partial w_0}{\partial t} \qquad (2.2)$$

where ρ_1 is the density of the upper liquid and w_o is the normal displacement of the plate.

2.1.3.2 Lower Liquid. Similarly, equations for the lower liquid can be written as:

$$\nabla^2 \Phi_2 = 0, \qquad (2.3)$$

where $\Phi_2 = \Phi_2$ (x,y,z,t) is a velocity potential.

The boundary condition is such that the velocity of the lower liquid is equal to zero at z = -(H_2+H/2) and equal to the plate velocity at z = - H/2. So one can write:

$$\left.\frac{\partial \Phi_2}{\partial z}\right|_{z=-(H_2+\frac{H}{2})} = 0$$

$$\left.\frac{\partial \Phi_2}{\partial z}\right|_{z=-\frac{H}{2}} = \frac{\partial w_0}{\partial t} \qquad (2.4)$$

2.1.3.3 Plate. For convenience, we use the common (x, y, z) for the coordinate and (u, v, w) for the corresponding displacement components. The displacement components are assumed to be of the form:

$$u(x,y,z,t) = u_0(x,y,t) + z\psi_x(x,y,t)$$

$$v(x,y,z,t) = v_0(x,y,t) + z\psi_y(x,y,t)$$

$$w(x,y,z,t) = w_0(x,y,t)$$

where u_o and v_o are the mid-plane displacement components in the x- and y-axis, respectively; and ψ_x and ψ_y denote the rotations of a line element, originally perpendicular to the longitudinal plane, about the y- and x-axes respectively. (See Figures 2.3 and 2.4.)

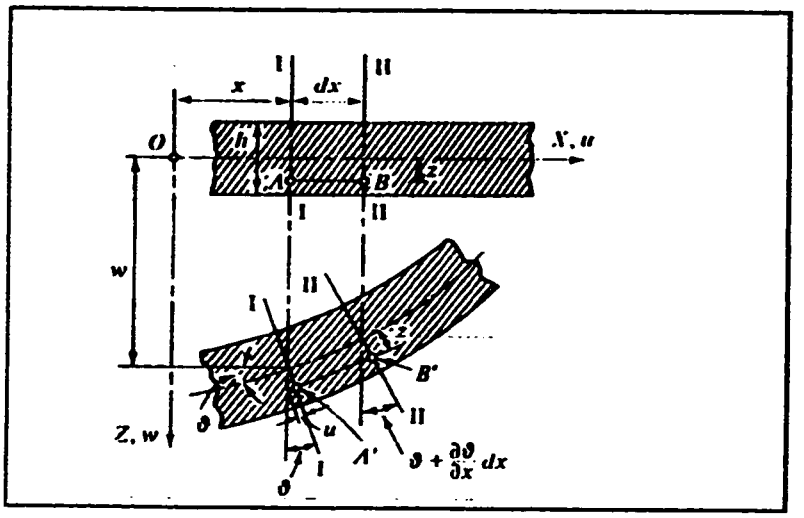

Figure 2.3: Section before and after deflection.

Source: Szilard [24]

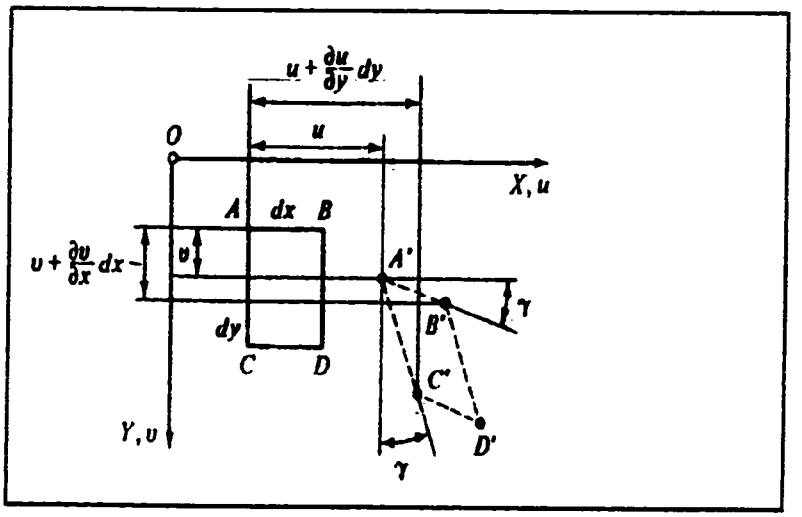

Figure 2.4: Angular distortion.

Source: Szilard [24]

The stress-strain constitutive equations for the k[th] layer is given by:

$$\begin{Bmatrix} \sigma_x^{(k)} \\ \sigma_y^{(k)} \\ \tau_{yz}^{(k)} \\ \tau_{xz}^{(k)} \\ \tau_{xy}^{(k)} \end{Bmatrix} = \begin{bmatrix} Q_{11}^{(k)} & Q_{12}^{(k)} & 0 & 0 & Q_{16}^{(k)} \\ Q_{12}^{(k)} & Q_{22}^{(k)} & 0 & 0 & Q_{26}^{(k)} \\ 0 & 0 & Q_{44}^{(k)} & Q_{45}^{(k)} & 0 \\ 0 & 0 & Q_{45}^{(k)} & Q_{55}^{(k)} & 0 \\ Q_{16}^{(k)} & Q_{26}^{(k)} & 0 & 0 & Q_{66}^{(k)} \end{bmatrix} \begin{Bmatrix} \varepsilon_x^{(k)} \\ \varepsilon_y^{(k)} \\ \gamma_{yz}^{(k)} \\ \gamma_{xz}^{(k)} \\ \gamma_{xy}^{(k)} \end{Bmatrix} \tag{2.6}$$

where the reduced stiffness terms $Q_{ij}^{(k)}$ are given by :

$$Q_{ij}^{(k)} = C_{ij}^{(k)} - \frac{C_{i3}^{(k)} C_{j3}^{(k)}}{C_{33}^{(k)}} \begin{cases} \text{i, j} = 1,2,6 \Rightarrow \text{plane} - \text{stress reduced stiffness} \\ \text{i, j} = 4,5 \Rightarrow \text{transverse shear stiffness} \end{cases} \tag{2.7}$$

with $C_{ij}^{(k)}$ terms denoting anisotropic stiffnesses.

The force and moment resultants per unit length are defined as follows:

$$(N_x, N_y, N_{xy}) = \int_{-H/2}^{H/2} \left(\sigma_x^{(k)}, \sigma_y^{(k)}, \tau_{xy}^{(k)} \right) dz$$

$$(Q_x, Q_y) = \int_{-H/2}^{H/2} \left(\tau_{xz}^{(k)}, \tau_{yz}^{(k)} \right) dz \tag{2.8}$$

$$(M_x, M_y, M_{xy}) = \int_{-H/2}^{H/2} \left(\sigma_x^{(k)}, \sigma_y^{(k)}, \tau_{xy}^{(k)} \right) z \; dz$$

where N and Q are the force resultants per unit length and M is the moment resultant per unit length . (See Figures 2.5 and 2.6)

To write the force and moment resultant, in term of strain, we have to write strain-displacement relations as follows:

$$\varepsilon_x = \varepsilon_x^0 + z\chi_x = \frac{\partial u_0}{\partial x} + z\frac{\partial \psi_x}{\partial x}$$

$$\varepsilon_y = \varepsilon_y^0 + z\chi_y = \frac{\partial v_0}{\partial y} + z\frac{\partial \psi_y}{\partial y} \qquad (2.9)$$

$$\varepsilon_z = 0$$

$$\gamma_{xy} = \varepsilon_{xy}^0 + z\chi_{xy} = \frac{\partial u_0}{\partial y} + \frac{\partial v_0}{\partial x} + z\left(\frac{\partial \psi_x}{\partial y} + \frac{\partial \psi_y}{\partial x}\right)$$

$$\gamma_{xz} = \psi_x + \frac{\partial w}{\partial x}$$

$$\gamma_{yz} = \psi_y + \frac{\partial w}{\partial y}$$

Using Equation (2.9) in conjunction with Equations (2.7) and (2.8) yields the following constitutive relations for the plate (in abbreviated notation):

$$\begin{bmatrix} \underline{N} \\ \underline{M} \end{bmatrix} = \begin{bmatrix} \underline{A} & \underline{B} \\ \underline{B} & \underline{D} \end{bmatrix} \begin{Bmatrix} \varepsilon^0 \\ \chi \end{Bmatrix} \qquad (2.10)$$

These constitutive relations are given in detail in Appendix I and the plate stiffness terms A_{ij}, B_{ij} and D_{ij} which appear in Equation (2.10) are defined by:

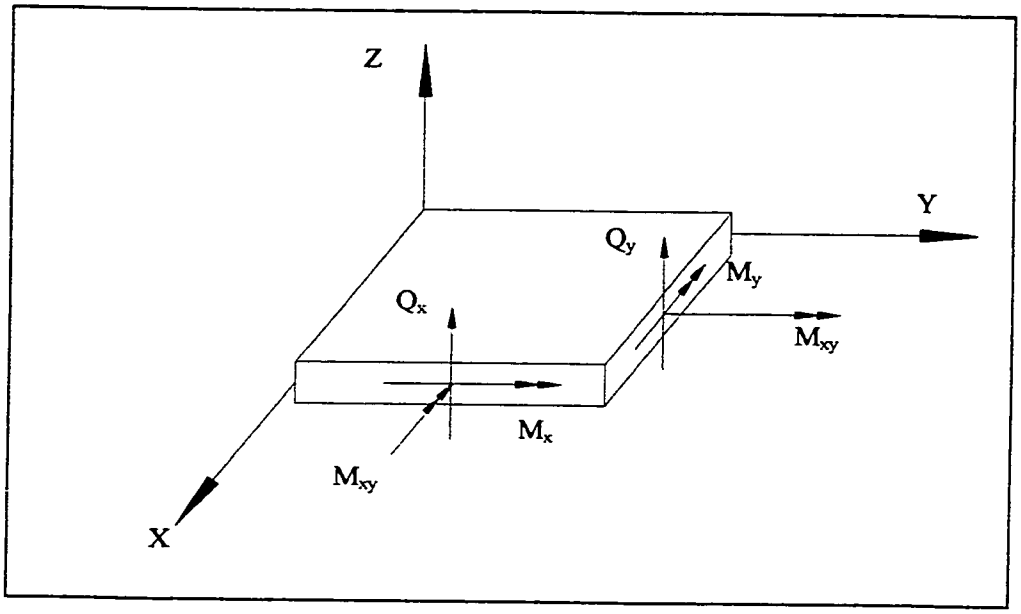

Figure 2.5: Moment and transverse shear resultant on a plate

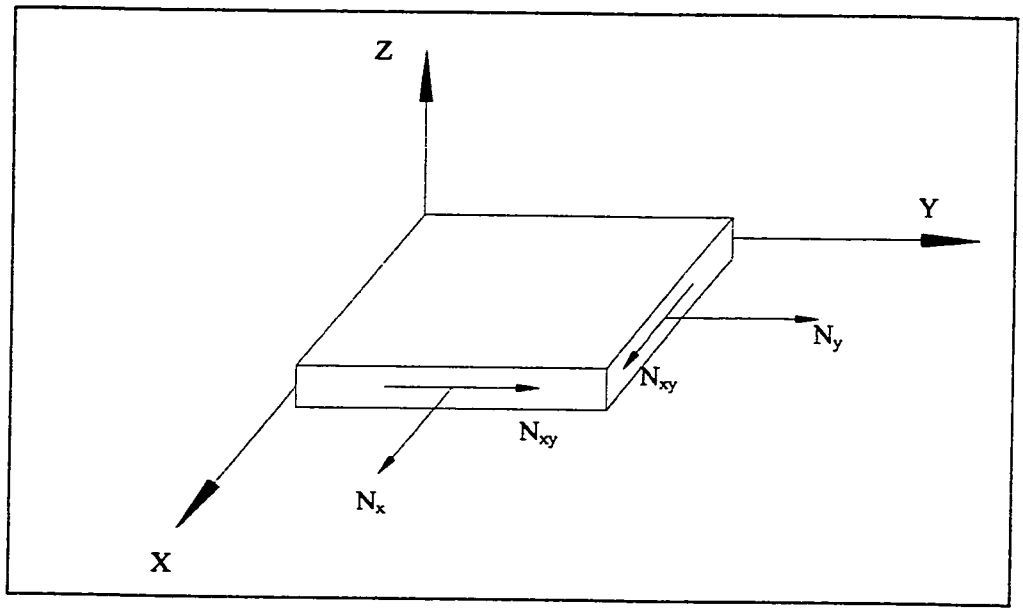

Figure 2.6: Resultant stress on a plate

$$(A_{ij}, B_{ij}, D_{ij}) = \int_{-H/2}^{H/2} Q_{ij}^{(K)}(1, z, z^2)dz \qquad i, j = 1,2,6 \tag{2.11}$$

From Equation (2.8), additional relations involving transverse shear are obtained as:

$$\begin{bmatrix} Q_y \\ Q_x \end{bmatrix} = \kappa \begin{bmatrix} A_{44} & A_{45} \\ A_{45} & A_{55} \end{bmatrix} \begin{Bmatrix} \gamma_{yz} \\ \gamma_{xz} \end{Bmatrix} \tag{2.12}$$

where

$$A_{ij} = \int_{-H/2}^{H/2} C_{ij}^{(k)} dz \quad (i, j = 4,5) \tag{2.13}$$

and κ is the shear correction factor and it is assumed to be 5/6. This factor is introduced to account for the fact that the transverse shear strain distributions are not uniform across the thickness of the plate. For symmetric laminates, the coupling between stretching and bending is eliminated and therefore $B_{ij}=0$. In addition, for orthotropic cross-ply laminates, we have $A_{16}= A_{26}= A_{45}=0$ and $D_{16}= D_{26}=0$.

Neglecting body forces, the equations of motion are:

$$\begin{aligned}
&\frac{\partial N_x}{\partial x} + \frac{\partial N_{xy}}{\partial y} = \rho^* \frac{\partial^2 u_0}{\partial t^2} + R\frac{\partial^2 \psi_x}{\partial t^2} \\
&\frac{\partial N_{xy}}{\partial x} + \frac{\partial N_y}{\partial y} = \rho^* \frac{\partial^2 v_0}{\partial t^2} + R\frac{\partial^2 \psi_y}{\partial t^2} \\
&\frac{\partial Q_x}{\partial x} + \frac{\partial Q_y}{\partial y} + F(x, y, z, t) + \rho_2 \frac{\partial \Phi_2}{\partial t}\bigg|_{z=-H/2} - \rho_1 \frac{\partial \Phi_1}{\partial t}\bigg|_{z=H/2} = \rho^* \frac{\partial^2 w_0}{\partial t^2} \\
&\frac{\partial M_x}{\partial x} + \frac{\partial M_{xy}}{\partial y} - Q_x = I\frac{\partial^2 \psi_x}{\partial t^2} + R\frac{\partial^2 u_0}{\partial t^2} \\
&\frac{\partial M_{xy}}{\partial x} + \frac{\partial M_y}{\partial y} - Q_y = I\frac{\partial^2 \psi_y}{\partial t^2} + R\frac{\partial^2 v_0}{\partial t^2}
\end{aligned} \tag{2.14}$$

where

$$I = \int_{-H/2}^{H/2} \rho z^2 dz,$$

$F(x,y,z,t)$ is the applied force, and ρ is the density of a single layer.

$\rho^* = \int_{-H/2}^{H/2} \rho dz$ is the plate density,

and,

$\rho_1 \frac{\partial \Phi_1}{\partial t}, \rho_2 \frac{\partial \Phi_2}{\partial t}$ are the liquid loading on both sides of the plate with ρ_1 and ρ_2 denoting the two liquid densities. The coupling normal-rotary inertia coefficient R is zero for the case of symmetric laminates or laminates constructed of the same unidirectional material. By substitution of Equations (2.6) and (2.12) into Equation (2.14), one can obtain the equations of motion in terms of the displacements and the rotations. The equations of motion decouples into two sets of equations governing the in-plane and the transverse (out-of-plate) motions.

The governing equations for the out-of-plane displacement can be expressed in the form:

$$\left.\begin{aligned}
&\kappa\left[A_{55}\frac{\partial\psi_x}{\partial x}+A_{55}\frac{\partial^2 w_0}{\partial x^2}+A_{44}\frac{\partial\psi_y}{\partial y}+A_{44}\frac{\partial^2 w_0}{\partial y^2}\right]-\rho_{L_1}\frac{\partial\Phi_1(x,y,\frac{H}{2},t)}{\partial t}+\\
&\rho_{L_2}\frac{\partial\Phi_2(x,y,\frac{-H}{2},t)}{\partial t}-\rho^{\bullet}\frac{\partial^2 w_0}{\partial t^2}=f(t)\delta(x)\delta(y)\\
&D_{11}\frac{\partial^2\psi_x}{\partial x^2}+D_{12}\frac{\partial^2\psi_y}{\partial x\partial y}+D_{66}\frac{\partial^2\psi_x}{\partial y^2}+D_{66}\frac{\partial^2\psi_y}{\partial x\partial y}-\kappa\left[A_{55}\psi_x+A_{55}\frac{\partial w_0}{\partial x}\right]-I\frac{\partial^2\psi_x}{\partial t^2}=0\\
&D_{66}\frac{\partial^2\psi_x}{\partial x\partial y}+D_{66}\frac{\partial^2\psi_y}{\partial x^2}+D_{12}\frac{\partial^2\psi_x}{\partial x\partial y}+D_{22}\frac{\partial^2\psi_y}{\partial y^2}-\kappa\left[A_{44}\psi_y+A_{44}\frac{\partial w_0}{\partial y}\right]-I\frac{\partial^2\psi_y}{\partial t^2}=0
\end{aligned}\right\} \quad (2.15)$$

where f (t) δ (x) δ (y) is the applied force.

- Elastic foundation: Stiffness of elastic foundation was taken into account in some cases, as we will see later. The stiffness is modeled as an ideal spring. The term Kw_o is added to the first equation of Equation (2.15) in order to incorporate the elastic foundation effect where K denotes the spring constant.

While the two governing equations for the in-plane motions are:

$$\left.\begin{aligned}
&A_{11}\frac{\partial^2 u_0}{\partial x^2}+A_{66}\frac{\partial^2 u_0}{\partial y^2}+(A_{12}+A_{66})\frac{\partial^2 v_0}{\partial x\partial y}-\rho^{\bullet}\frac{\partial^2 u_0}{\partial t^2}=0\\
&(A_{12}+A_{66})\frac{\partial^2 u_0}{\partial x\partial y}+A_{66}\frac{\partial^2 v_0}{\partial x^2}+A_{22}\frac{\partial^2 v_0}{\partial x\partial y}-\rho^{\bullet}\frac{\partial^2 v_0}{\partial t^2}=0
\end{aligned}\right\} \quad (2.16)$$

2.1.3.4 Solution Of The Model. The transient response (normal displacement) of the plate can be obtained by applying a triple Fourier Transform in space (x, y) and time to the out-of-plate equations. So, this leads to:

$$\hat{\psi}_x(x,y,\omega) = \frac{1}{4\pi^2}\int_{-\infty}^{\infty}\int_{-\infty}^{\infty}\Psi_x(\xi_1,\xi_2,\omega)e^{i(\xi_1 x+\xi_2 y)}d\xi_1 d\xi_2$$

$$\hat{\psi}_y(x,y,\omega) = \frac{1}{4\pi^2}\int_{-\infty}^{\infty}\int_{-\infty}^{\infty}\Psi_y(\xi_1,\xi_2,\omega)e^{i(\xi_1 x+\xi_2 y)}d\xi_1 d\xi_2 \qquad (2.17)$$

$$\hat{w}_0(x,y,\omega) = \frac{1}{4\pi^2}\int_{-\infty}^{\infty}\int_{-\infty}^{\infty}W_0(\xi_1,\xi_2,\omega)e^{i(\xi_1 x+\xi_2 y)}d\xi_1 d\xi_2$$

where $\hat{\psi}_x(x,y,\omega)$, $\hat{\psi}_y(x,y,\omega)$, and $\hat{w}_0(x,y,\omega)$ are the Fourier time transforms of $\psi_x(x,y,t)$, $\psi_y(x,y,t)$ and $w_0(x,y,t)$ respectively. Here, ξ_1 and ξ_2 represents the wavenumbers along the x and y directions respectively. The unknown functions Ψ_x, Ψ_y ,and W_0 satisfy the system of linear equations:

$$[M]\{V\} = \{F\}$$

where [M] is a 3×3 symmetric matrix given in Appendix I.

$$\{V\}^T = \{W_0 \quad \Psi_x \quad \Psi_y\}$$
$$\{F\}^T = \{f(\omega) \quad 0 \quad 0\}$$

Therefore, to recover the normal physical displacement *w(x,y,z,t)*, we have to obtain the inverse Fourier transform of $\hat{w}_0(x,y,\omega)$.

2.1.3.5 Dispersion Relations. The determinant of the matrix [M] gives the characteristic equation for flexural wave propagation (first anti-symmetric mode). The characteristic equation has more than

one root. However, only one root approaches $\omega = 0$ as the wave number ξ approaches zero, and this is the root corresponding to the lowest anti-symmetric mode.

For the extensional and in-plane waves, we consider plane waves of the type:

$$u_o = Ue^{i\xi(\alpha - ct)}, \qquad v_o = Ve^{i\xi(\alpha - ct)}, \tag{2.18}$$

where U and V are constant amplitudes, ξ is the wavenumber, c is the phase velocity $(c = \omega/\xi)$, and α is given by:

$$\alpha = x\cos(\varphi) + y\sin(\varphi)$$

where φ is the angle between the direction of wave propagation and the x-axis.

By substituting Equation (2.18) into Equation (2.16), a system of two homogeneous equations for the two constants U and V can be written. For nontrivial solutions, the determinant of the resulting coefficients matrix is set equal to zero:

$$\begin{vmatrix} A_{11}\cos\varphi + A_{66}\sin^2\varphi - \rho Hc^2 & (A_{12} + A_{66})\cos\varphi\sin\varphi \\ (A_{12} + A_{66})\cos\varphi\sin\varphi & A_{66}\cos^2\varphi + A_{22}\sin^2\varphi - \rho Hc^2 \end{vmatrix} = 0 \tag{2.19}$$

By expanding, we obtain a quadratic equation in c^2 as

$$c^4 - \beta_1 c^2 + \beta_2 = 0$$

where,

$$\beta_1 = (A_{11}\cos^2\varphi + A_{22}\sin^2\varphi + A_{66})/\rho H$$

$$\beta_2 = \frac{1}{(\rho H)^2}\begin{vmatrix} A_{11}\cos\varphi + A_{66}\sin^2\varphi & (A_{12}+A_{66})\cos\varphi\sin\varphi \\ (A_{12}+A_{66})\cos\varphi\sin\varphi & A_{66}\cos^2\varphi + A_{22}\sin^2\varphi \end{vmatrix}$$

It is noted that the phase velocity c does not depend on the wavenumber ξ, thus these waves are nondispersive. It is evident that there exist two-phase velocities corresponding to two modes of wave propagation. Although the two waves involve both in-plane extensional deformation as well as in-plane shear, we are able to tell from the eigenvectors which one is dominant. Thus, we label the two waves as extensional wave and in-plane shear wave accordingly.

Extensional and shear waves:

1. For waves propagating in the x-direction ($\varphi = 0^0$), the phase velocity of the extensional mode is

$$c_e = \sqrt{\frac{A_{11}}{\rho H}}$$

while the phase velocity of the in-plane shear mode is

$$c_s = \sqrt{\frac{A_{66}}{\rho H}}$$

Both modes propagating in this direction are pure modes (uncoupled).

2. For waves propagating in the y-direction ($\varphi = 90^0$), then

$$c_e = \sqrt{\frac{A_{22}}{\rho H}}$$

and

$$c_s = \sqrt{\frac{A_{66}}{\rho H}}$$

Since this is also a symmetry axis of the orthotropic laminates, both modes propagating in this direction are also pure modes. However, for propagation at ($\varphi = 45^0$), both modes become quasi-modes (coupled).

2.1.3.6 Evaluation Of The Double Integrals. The major task in the calculation of the normal displacement is the evaluation of the double integrals of Equation (2.17). The flow chart of the computer code used to find the displacement is shown in Figure 2.7. The integrand $W_0(\xi_1, \xi_2, \omega)$ has special properties that make the evaluation of the integral a difficult job. It has a singularity of $O(\omega^{-2})$ at $\omega = 0$. Thus, we should start the integration at frequencies away from zero. This presents a big problem if the low-frequency end of the forcing function *f(t)* is not band limited. Moreover, the integrand has extremely irregular behavior, which gets worse at higher frequencies. It has irregular oscillations and sharp spikes at isolated points. This can be confirmed by plotting the real part of $W_0(\xi_1, 0, \omega)$ for a

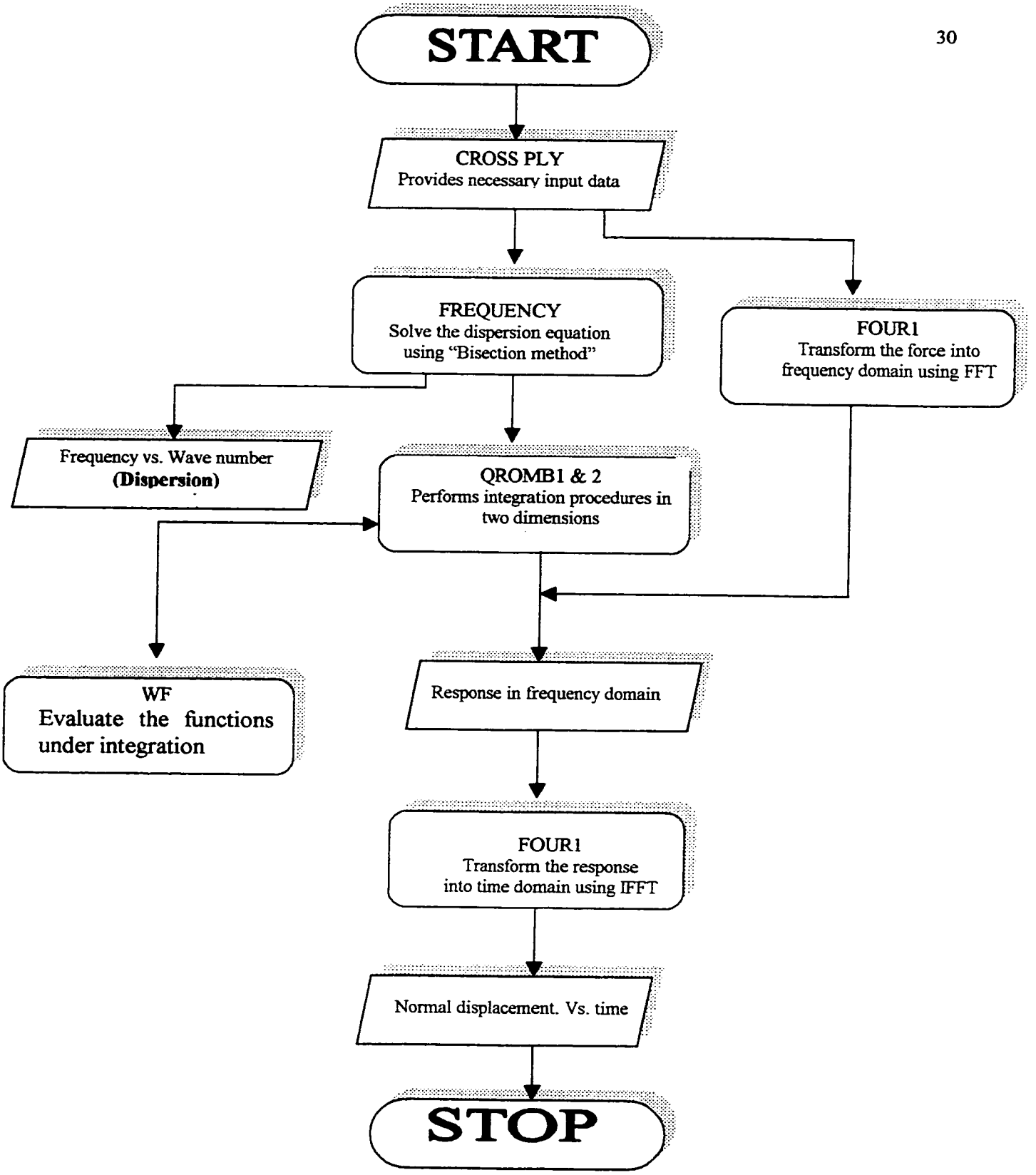

Figure 2.7: Flow chart of the computer code

plate against ξ_1 for different frequencies and this is shown in Figure 2.8.The locations of these sharp spikes represent the roots of the flexural dispersion equation. Since standard integration algorithms will not be practical to evaluate the double integrals of such an extremely ill-behaved function, an efficient algorithm with good accuracy must be implemented. Based on the one-dimensional Romberg's method for numerical integration, a modified computer code was written to calculate the normal displacement. Basically, the integration domain in one direction , i.e. ξ_1-direction divided into a number of rough sub-domains by choosing an initial step-size. For each one of these upper sub-domains, the integration domain in the other direction, i.e. ξ_2-direction, is similarly divided into lower rough sub-domains. Then, the function under integration is evaluated before the step-size in the ξ_2-direction is decreased by a factor of ½ to calculate the relative error. If the relative error is within the required accuracy, the next lower sub-domain (in ξ_2-direction) is considered. Otherwise, the relative step-size will be refined until this accuracy is achieved. The step-size for the upper sub-domain (ξ_1-direction) will also be refined if the specified accuracy in that direction is not satisfied. The fractional accuracy used in our computations was 1.0×10^{-3} (in both directions).

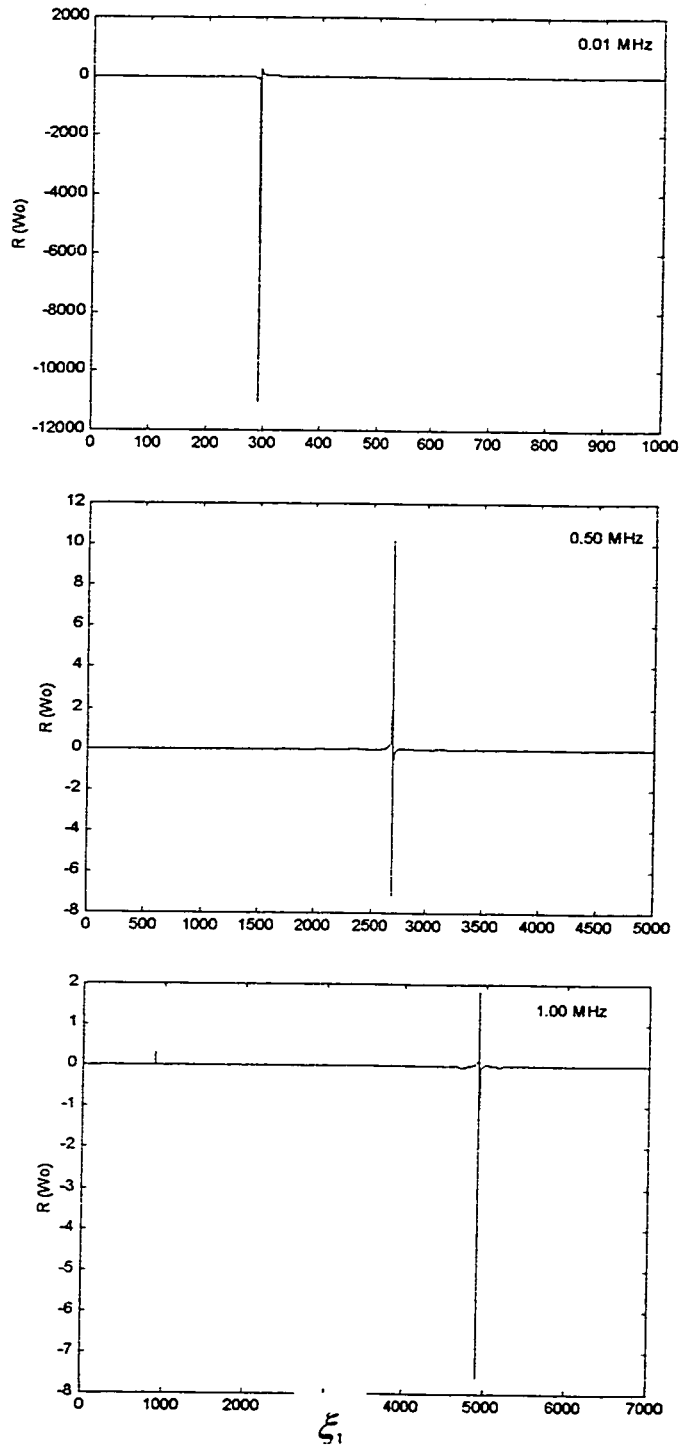

Figure 2.8 : $\mathbf{R\{W_o(\xi_1, 0, \omega)\}}$ for a laminated plate for several frequencies

2.2 SINGLE MOVING LOAD

For moving loads, we will write equations of motion of the problem described in Figure 2.9 in term of the moving coordinate system (η , ζ , z) , where (η,ζ) is a moving coordinate system defined by [(x-V_xt),(y-V_yt)]. The load moves with a constant speed V. V_x and V_y are the components of V in x and y directions respectively.

2.2.1 UPPER AND LOWER LIQUID

Equtions for both liquids are written as:

$$\nabla^2 \Phi_i = 0, \tag{2.20}$$

where $\Phi_i = \Phi_i(\eta,\zeta,z,t)$ is a velocity potential and i is 1 and 2 for the upper and lower liquids, respectively.

The boundary condition is similar to those mentioned in the fixed coordinates (x,y,z,t). They can be summarized as follows:

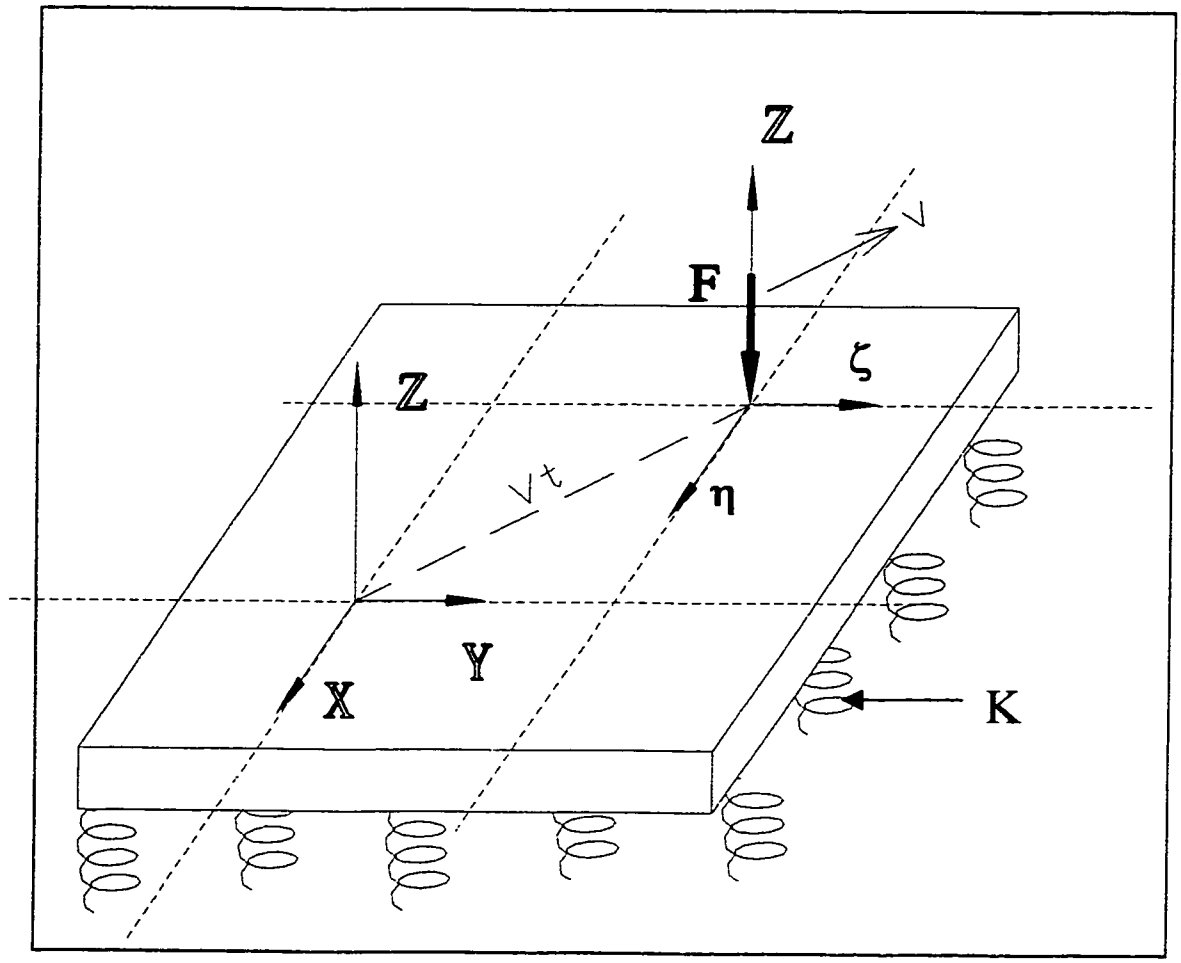

Figure 2.9: Geometric representation of a plate exposed to a moving load on elastic foundation

$$\rho_1 \left.\frac{\partial \Phi_1}{\partial t}\right|_{z=H_1+\frac{H}{2}} = 0$$

$$\left.\frac{\partial \Phi_1}{\partial z}\right|_{z=\frac{H}{2}} = \frac{\partial w_0}{\partial t} \qquad (2.21)$$

$$\left.\frac{\partial \Phi_2}{\partial z}\right|_{z=-(H_2+\frac{H}{2})} = 0$$

$$\left.\frac{\partial \Phi_2}{\partial z}\right|_{z=-\frac{H}{2}} = \frac{\partial w_0}{\partial t} \qquad (2.22)$$

2.2.2 PLATE

Equations of motion of the plate are written in terms of the new moving coordinate as well. For out-of-plane motion:

$$\left.\begin{aligned}
&\kappa\left[A_{55}\frac{\partial \psi_\eta}{\partial \eta} + A_{55}\frac{\partial^2 w_0}{\partial \eta^2} + A_{44}\frac{\partial \psi_\zeta}{\partial \zeta} + A_{44}\frac{\partial^2 w_0}{\partial \zeta^2}\right] - \rho_1 \frac{\partial \Phi_1(\eta,\zeta,\frac{H}{2},t)}{\partial t} + \\
&\rho_2 \frac{\partial \Phi_2(\eta,\zeta,\frac{-H}{2},t)}{\partial t} - Kw_o - \rho^* \frac{\partial^2 w_0}{\partial t^2} = f(t)\delta(\eta)\delta(\zeta) \\
&D_{11}\frac{\partial^2 \psi_\eta}{\partial \eta^2} + D_{12}\frac{\partial^2 \psi_\zeta}{\partial \eta \partial \zeta} + D_{66}\frac{\partial^2 \psi_\eta}{\partial \zeta^2} + D_{66}\frac{\partial^2 \psi_\zeta}{\partial \eta \partial \zeta} - \kappa\left[A_{55}\psi_\eta + A_{55}\frac{\partial w_0}{\partial \eta}\right] - I\frac{\partial^2 \psi_\eta}{\partial t^2} = 0 \\
&D_{66}\frac{\partial^2 \psi_\eta}{\partial \eta \partial \zeta} + D_{66}\frac{\partial^2 \psi_\zeta}{\partial \eta^2} + D_{12}\frac{\partial^2 \psi_\eta}{\partial \eta \partial \zeta} + D_{22}\frac{\partial^2 \psi_\zeta}{\partial \zeta^2} - \kappa\left[A_{44}\psi_\zeta + A_{44}\frac{\partial w_0}{\partial \zeta}\right] - I\frac{\partial^2 \psi_\zeta}{\partial t^2} = 0
\end{aligned}\right\} \qquad (2.23)$$

Note the appearance of the parameter K in the previous equations. It stands for the stiffness of the foundation, which is taken into account in this type of problem.

For the in-plane motion, one can write:

$$\left.\begin{aligned} A_1\frac{\partial^2 u_0}{\partial\eta^2}+A_{66}\frac{\partial^2 u_0}{\partial\zeta^2}+(A_{12}+A_{66})\frac{\partial^2 u_0}{\partial\eta\partial\zeta}-\rho^*\frac{\partial^2 u_0}{\partial t^2}=0 \\ (A_{12}+A_{66})\frac{\partial^2 v_0}{\partial\eta\partial\zeta}+A_{66}\frac{\partial^2 v_0}{\partial\eta^2}+A_{22}\frac{\partial^2 v_0}{\partial\eta\partial\zeta}-\rho^*\frac{\partial^2 v_0}{\partial t^2}=0 \end{aligned}\right\} \quad (2.24)$$

- *Applying Fourier Transformations for Moving Coordinate Systems:*

Now, we will describe how to take the Fourier transform of a given function $G(\eta,\zeta,z,t)$, where the moving coordinate system (η,ζ,z) is related to the stationary coordinate system as:

$$\begin{aligned} \eta &= x-V_x t \\ \zeta &= y-V_y t \\ z &= z \end{aligned} \quad (2.25)$$

First, let us define the Fourier as :

$$\Im[G(\eta,\zeta,z,t)]=\hat{G}(\bar{\xi}_1,\bar{\xi}_2,z,\bar{\omega})$$

where $\bar{\xi}_i$ is the wavenumber and $\bar{\omega}$ is the frequency related to the new moving coordinate system.

$$\dot{G}=\frac{\partial G}{\partial\eta}\bullet\frac{\partial\eta}{\partial t}+\frac{\partial G}{\partial\zeta}\bullet\frac{\partial\zeta}{\partial t}+\frac{dG}{dt} \text{ (chain rule)}$$

but,

$\eta = x - V_x t$ and $\zeta = y - V_y t$. Therefore, one can write:

$$\frac{\partial \eta}{\partial t} = -V_x \quad \text{, and} \quad \frac{\partial \zeta}{\partial t} = -V_y$$

$$\Rightarrow \quad \dot{G} = -V_x \frac{\partial G}{\partial \eta} - V_y \frac{\partial G}{\partial \zeta} + \frac{\partial G}{\partial t}$$

$$\Rightarrow \quad \Im(\dot{G}) = -V_x i\bar{\xi}_1 \hat{G} - V_y i\bar{\xi}_2 \hat{G} + i\bar{\omega}\hat{G}$$

$$= (\bar{\omega} i - V_x i\bar{\xi}_1 - V_y i\bar{\xi}_2)\hat{G}$$

$$= i(\bar{\omega} - V_x\bar{\xi}_1 - V_y\bar{\xi}_2)\hat{G}$$

And for $\ddot{G}$:

$$\Im(\ddot{G}) = \Im\left(\frac{\partial \dot{G}}{\partial t}\right) = i(\bar{\omega} - V_x\bar{\xi}_1 - V_y\bar{\xi}_2)\Im(\dot{G})$$

$$= -(\bar{\omega} - V_x\bar{\xi}_1 - V_y\bar{\xi}_2)^2 G$$

- *POST TRANSFORMATION:*

After performing the Fourier Transformation to equations of motion for liquids and plate, one can write the governing equation in this form:

$$[\bar{M}]\{\bar{V}\} = \{\bar{F}\}$$

where $\{\bar{V}\}^T = \{W_\circ \quad \Psi_\eta \quad \Psi_\zeta\}$, $\{\bar{F}\}^T = \{f(\bar{\omega}) \quad 0 \quad 0\}$

and $[\bar{M}]$ is a 3×3 symmetric matrix given in Appendix II.

2.2.3 SOLUTION:

In general, the dynamic displacement can be obtained using the triple inverse Fourier transforms as:

$$w(\eta,\zeta,t)=\frac{1}{(2\pi)^3}\int_{-\infty}^{\infty}\int_{-\infty}^{\infty}\int_{-\infty}^{\infty}W_{\circ}(\bar{\xi}_1,\bar{\xi}_2,\bar{\omega})e^{i\bar{\xi}_1\eta}e^{i\bar{\xi}_2\zeta}e^{i\bar{\omega}t}d\bar{\xi}_1d\bar{\xi}_2d\bar{\omega}.$$

If the moving load has a harmonic variation of the amplitude as in our case and only the steady case response is of interest, the displacement

$$w(\eta,\zeta,t)=\frac{1}{(2\pi)^2}\int_{-\infty}^{\infty}\int_{-\infty}^{\infty}W_{\circ}(\bar{\xi}_1,\bar{\xi}_2)e^{i\bar{\xi}_1\eta}e^{i\bar{\xi}_2\zeta}d\bar{\xi}_1d\bar{\xi}_2$$

hence $W_{\circ}(\bar{\xi}_1,\bar{\xi}_2) \propto fn\{[M(\bar{\xi}_1,\bar{\xi}_2,\bar{\Omega})],F\}$

where $\bar{\Omega}$ is the load frequency.

The transformed force F is evaluated by

$$F(\xi_1,\xi_2,t)=|f|e^{i\bar{\Omega}t}\int_{-\infty}^{\infty}\int_{-\infty}^{\infty}f(\eta,\zeta)e^{i\bar{\xi}_1\eta}e^{i\bar{\xi}_2\zeta}d\eta d\zeta$$

2.3 TWO MOVING LOADS

The effect of two-force loading (Figure 2.10) on the response is investigated here. L_η and L_ζ are the center-to-center distances of the loads in the η- and ζ-directions, and θ

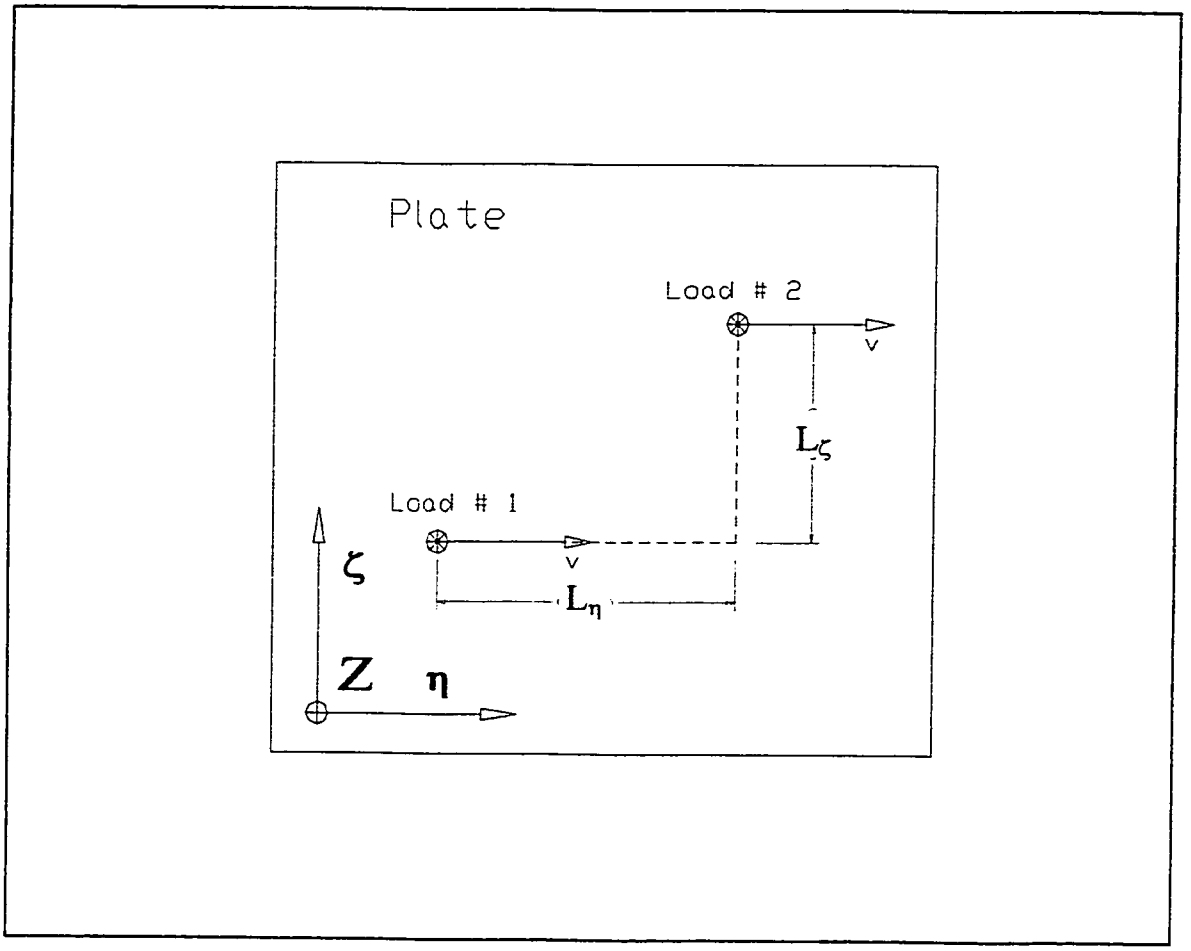

Figure 2.10: Geometric Representation of a plate exposed to two moving loads

is the phase between the loads. The approach followed here is the same approach used by Kim *[14]*.

Tow harmonic loads, namely, $\sin\overline{\Omega}t$ and $\sin(\overline{\Omega}t+\theta)$ are applied on the plate. The amplitude of the normal response of the plate can be obtained as:

$$\sqrt{a_1^2+b_1^2+a_2^2+b_2^2+2[(a_1a_2+b_1b_2)\cos\theta-(a_1b_2-b_1a_2)\sin\theta]}$$

where a_1, b_1, a_2 and b_2 denote $a_1(\eta,\zeta), b_1(\eta,\zeta), a_2(\eta-L_\eta,\zeta-L_\zeta)$ and $b_2(\eta-L_\eta,\zeta-L_\zeta)$, respectively. These terms are extracted from the following two expressions:

$$a_1(\eta,\zeta)+ib_1(\eta,\zeta)=\frac{1}{(2\pi)^2}\int_{-\infty}^{\infty}\int_{-\infty}^{\infty}W_o(\overline{\xi}_1,\overline{\xi}_2)e^{i\overline{\xi}_1\eta}e^{i\overline{\xi}_2\zeta}d\overline{\xi}_1d\overline{\xi}_2$$

and,

$$a_2(\eta-L_\eta,\zeta-L_\zeta)+ib_2(\eta-L_\eta,\zeta-L_\zeta)=\frac{1}{(2\pi)^2}\int_{-\infty}^{\infty}\int_{-\infty}^{\infty}W_o(\overline{\xi}_1,\overline{\xi}_2)e^{i\overline{\xi}_1(\eta-L_\eta)}e^{i\overline{\xi}_2(\zeta-L_\zeta)}d\overline{\xi}_1d\overline{\xi}_2$$

For multiple forces (more than two), the response can be obtained similarly using the above approach.

CHAPTER 3

RESULTS AND DISCUSSIONS

Four types of elastic plates, namely, isotropic; and 3-plys, 6-plys, and 12-plys laminated plates were investigated in this work. These plates were exposed to different loading conditions e.g. stationary loads, liquid loadings, and a single or multiple moving loads.

As shown in Figure 2.1, the plate was loaded by liquids on both sides. Dispersion curves were calculated for plates under those mentioned conditions. Effects of both liquids on dispersion curves were investigated as well.

Normal transient responses were also computed for the plates along three main directions, namely, 0°, 45°, and 90° directions. We studied the effects of the liquid loading on these responses. Furthermore, group velocities were calculated and compared with each other under different circumstances and along different directions.

Finally, two types of plates, namely, an isotropic plate, and the 6-ply laminated plates were studied under moving harmonic loads. Critical velocities were computed for both plates under different load velocities. Moreover, the two plates were subjected to two moving harmonic loads. Effects of phase differences between the two forces and their velocities were investigated for both plates.

Throughout this chapter, the following notations are used to define the important parameters for the present work:

H	:	plate thickness
H_1	:	the upper liquid depth
H_2	:	the lower liquid depth
ρ	:	the plate density
ρ_1	:	the upper liquid density
ρ_2	:	the lower liquid density

3.1 STATIONARY LOADS

In this section, the plates are investigated under a harmonic stationary load. First, dispersion curves are computed for the 3-ply laminated plate along the three main directions and under different liquid load conditions. The properties of the 3-ply E-glass/epoxy fiber reinforced plate are given in Table 3.1.

TABLE 3.1: Properties of the Composite Plates

ρ	1857 Kg/m^3
H	0.762×10^{-3} m
$C_{11}^{(K)}$	38.0×10^9 N/m^2
$C_{12}^{(K)}$	3.10×10^9 N/m^2
$C_{22}^{(K)}$	11.75×10^9 N/m^2
$C_{23}^{(K)}$	5.30×10^9 N/m^2
$C_{55}^{(K)}$	4.60×10^9 N/m^2

3.1.1 DISPERSION CURVES FOR WATER/PLATE/MERCURY SYSTEM ALONG THE 45° DIRECTION

Dispersion curves were calculated for the 3-ply composite plate when loaded by water on the upper side and mercury on the lower side. They are shown in Figures 3.1 and 3.2 for high and low depth of mercury respectively. In these two figures, changes in dispersion curves due to the change of H_1, observed for high and low H_2, are not noticeable. This is because of the following:

- Effects of boundary conditions
- Effects of density

First: Effects of boundary conditions:

By studying the dispersion relation we notice that it is affected by the term $\rho_i \omega^2 \Lambda_i \Gamma_i$ (defined earlier in chapter 2), where i is equal to 1 and 2 for the upper and lower liquid, respectively. This term, which is by definition a function of liquid depths, is always greater for the lower liquid. Subsequently, the influence of changing the lower liquid's depth on dispersion curves is greater.

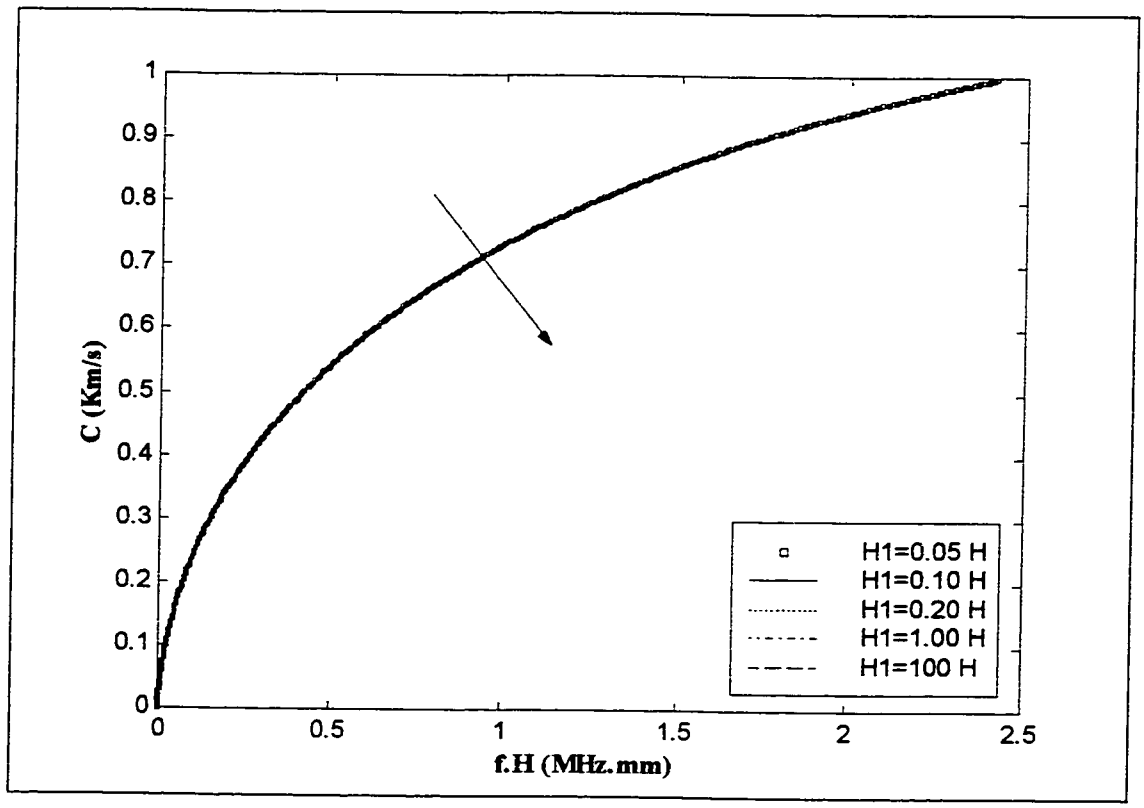

Figure 3.1: Dispersion curves for the 3-ply laminated plate along 45° direction for water/plate/mercury system, H_2 = 0.05H, for various water depths.

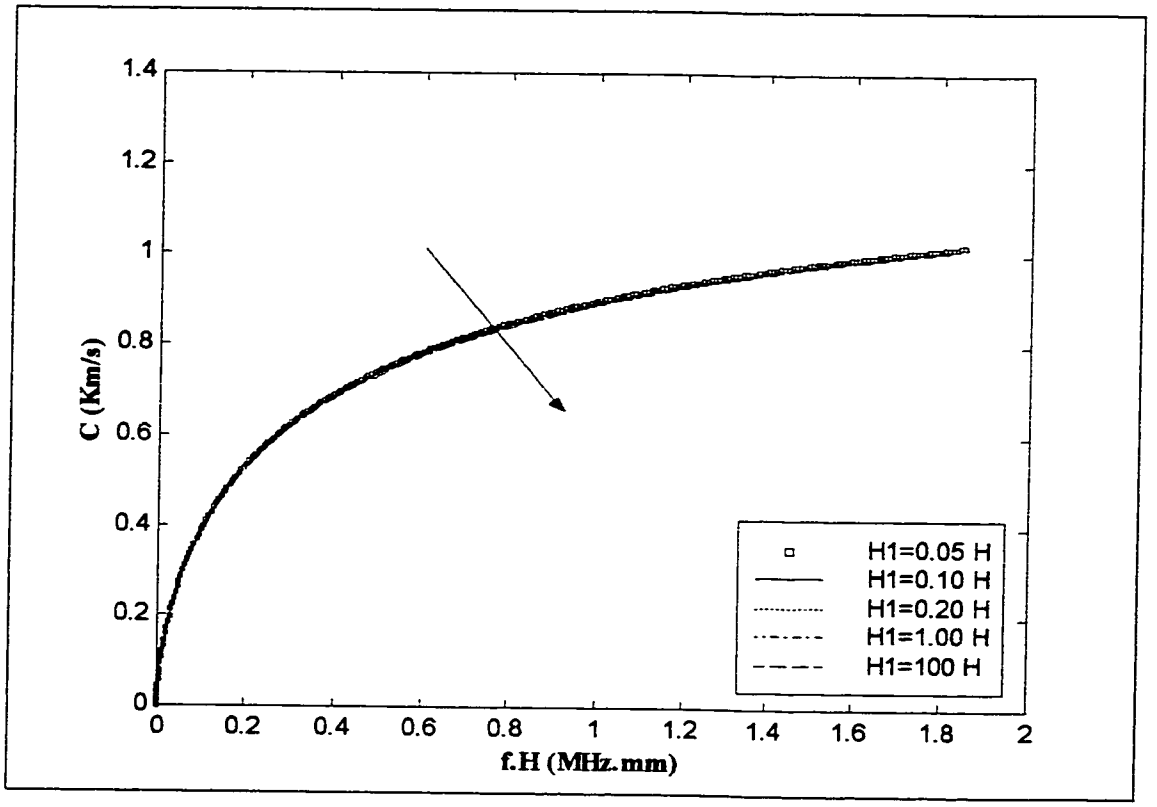

Figure 3.2: Dispersion curves for the 3-ply laminated plate along 45° direction for water/plate/mercury system, H_2 = 100H, for various water depths

Second: Effects of density

The term mentioned above is a function of the densities of the two liquids and so is the dispersion relation. Therefore, the effect of the denser liquid on the dispersion curves will be more pronounced.

By comparing dispersion curves in Figure 3.1 with those in Figure 3.2, one can clearly see the effect of the depth of the lower liquid i.e. mercury on dispersion curves. For a given frequency, the phase velocity is larger for higher depth of mercury than that of a lower depth. For instance, with H_1 equal to 0.05 H, the phase velocity is about 0.8 *km/s* at 1.2 *MHz.mm* for the lower depth case and almost equal to 0.94 *km/s* for the higher depth case at the same frequency.

However, when the depth of the lower liquid i.e. mercury is varied, dispersion curves change considerably. By looking at Figures 3.3 and 3.4, the phase velocity changes from about 0.7 *km/s*, with H_2 equal to 0.05 H, to almost 0.9 *km/s*, with H_2 equal to 0.05 H, at 1 *MHz.mm*. This considerable change (29 %) is again due the reasons stated earlier.

In both figures, it is noted that at low frequencies (less than 4.5 *MHz.mm*), the effect of the liquid depth is more pronounced than at higher frequencies. Furthermore, for higher frequencies, as the mercury depth increases beyond 0.30 H, its effect on dispersion curves becomes less pronounced.

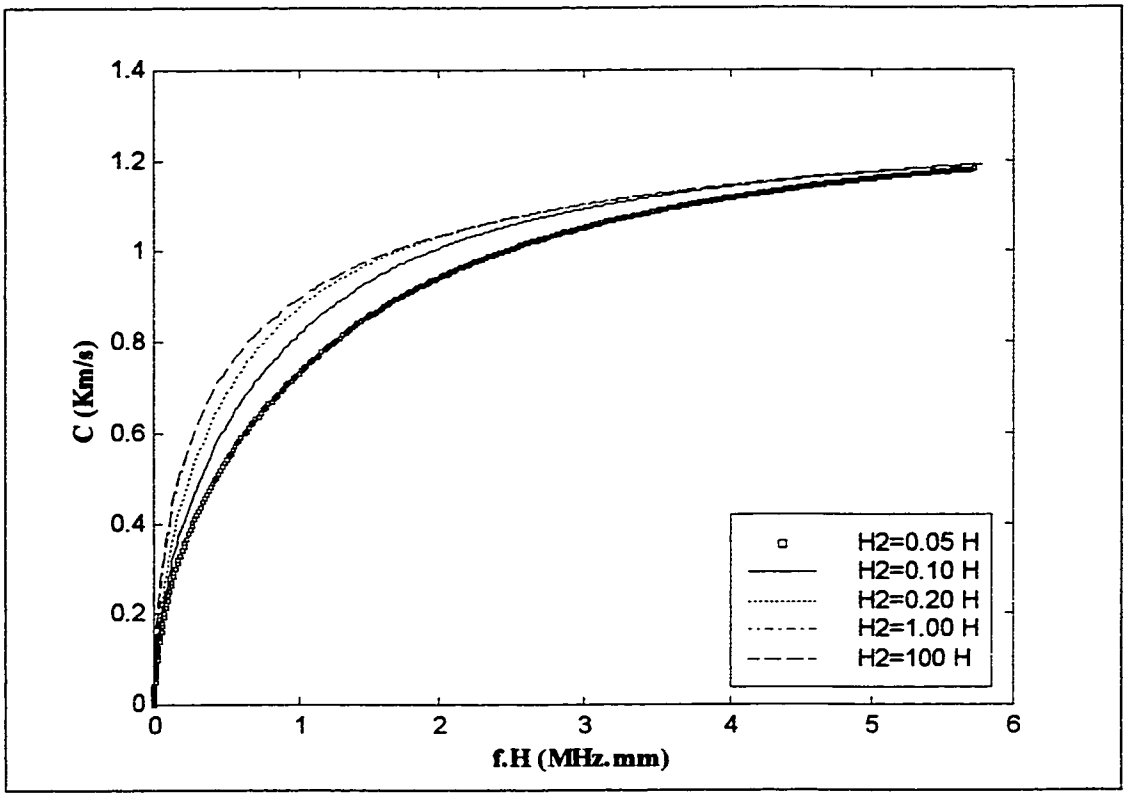

Figure 3.3: Dispersion curves for the 3-ply laminated plate along 45° direction for water/plate/mercury system, H_1 = 0.05H, for various mercury depths

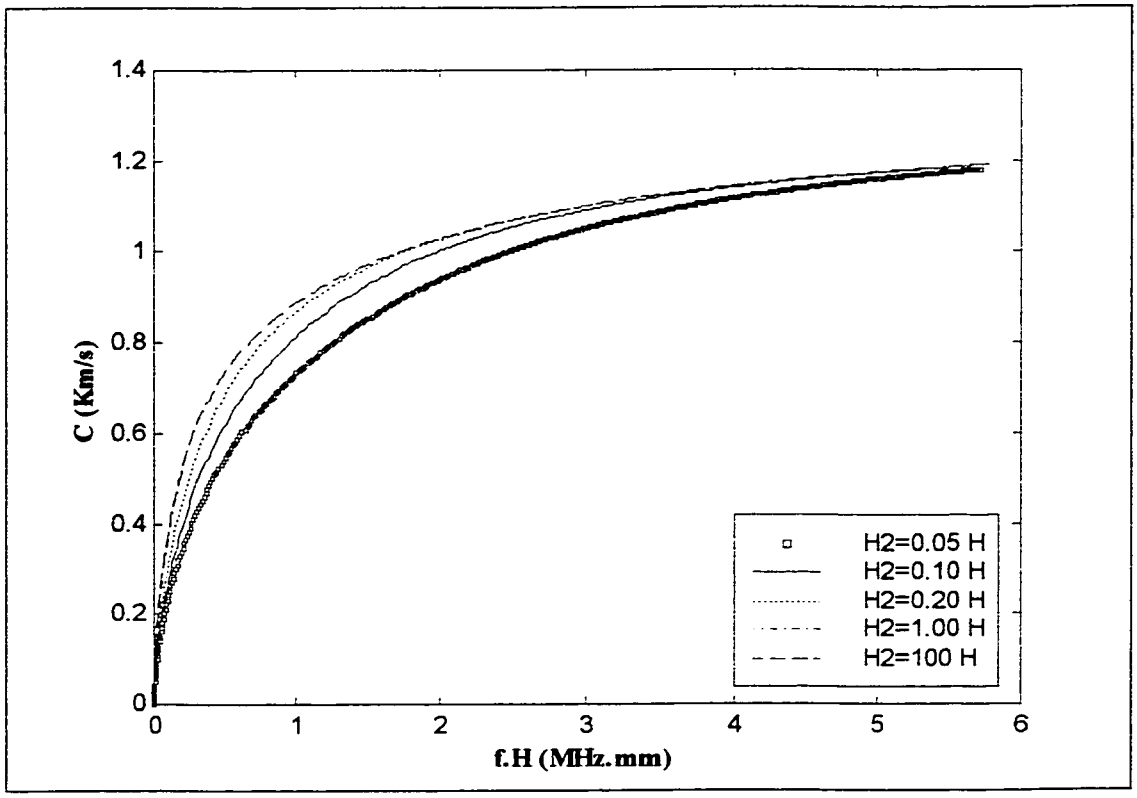

Figure 3.4: Dispersion curves for the 3-ply laminated plate along 45° direction for water/plate/mercury system, H_1 = 100H, for various mercury depths

By comparing the dispersion curves in Figure 3.3 (where the water depth is lower) to those in Figure 3.4 (where the water depth is higher), it is easy to see that both sets of curves show almost identical behavior for the whole frequency range.

3.1.2 DISPERSION CURVES FOR MERCURY/PLATE/WATER SYSTEM ALONG THE 45^{O} DIRECTION

In this section, dispersion curves were studied when the two liquids were switched i.e. the mercury occupies the upper and the water occupies the lower portion of the system. Dispersion curves for this system are plotted in Figures 3.5 and 3. 6 for high and low values of H_2 respectively.

In both figures, at a given frequency, it is noted that as the mercury depth increases, the phase velocity decreases significantly e.g., it drops from 0.95 to 0.74 *km/s* as H_1 increases from 0.05H to 100H at 0.5 *MHz.mm* for H_2 equal to 100H. Moreover, the phase velocity of the flexural wave tends to converge to higher values as the mercury depth decreases.

Although the two sets of curves behave similarly, they differ noticeably in phase velocity values at a given frequency. Numerically, in Figure 3.5, as stated earlier, the phase velocity is 0.95 ,for H_1 equal to 0.05H, and 0.74 *km/s*, for H_1 equal to 100 H, at 0.50 *MHz.mm*, where as in Figure 3.6, it is 0.85 and 0.70 *km/s* respectively, at the same conditions.

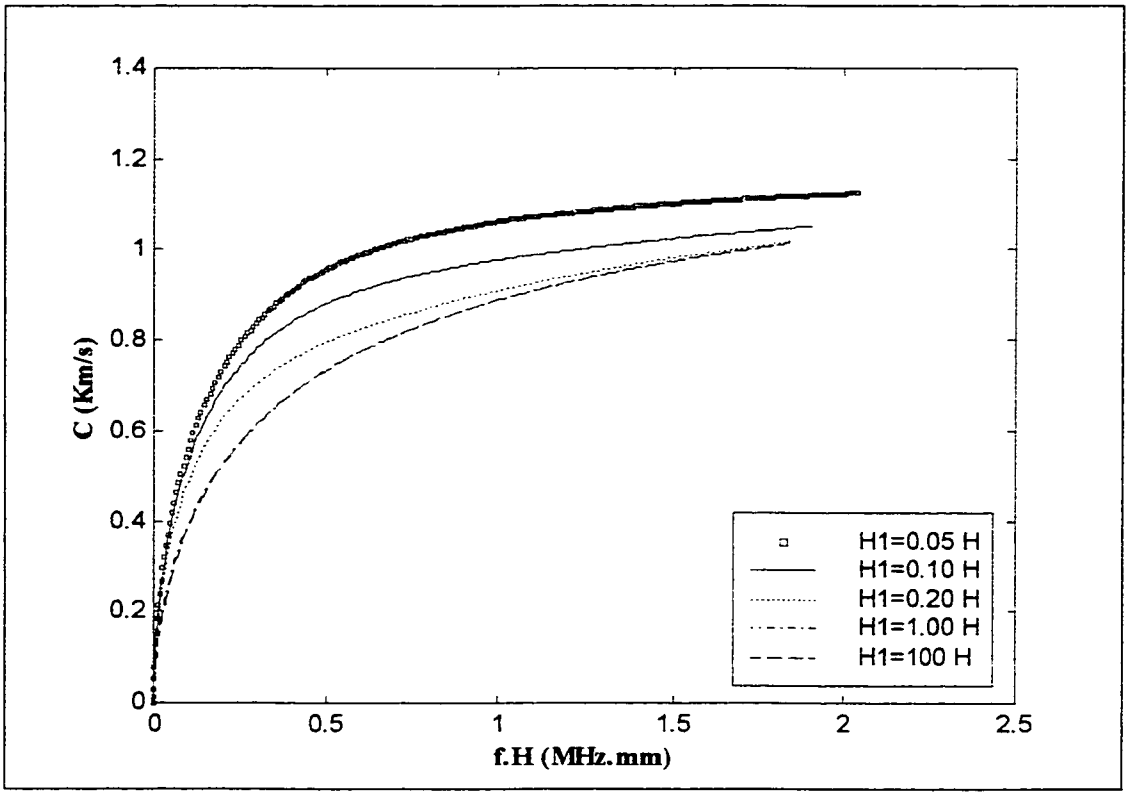

Figure 3.5: Dispersion curves for the 3-ply laminated plate along 45° direction for mercury/plate/water system, H_2 = 100H, for various mercury depths

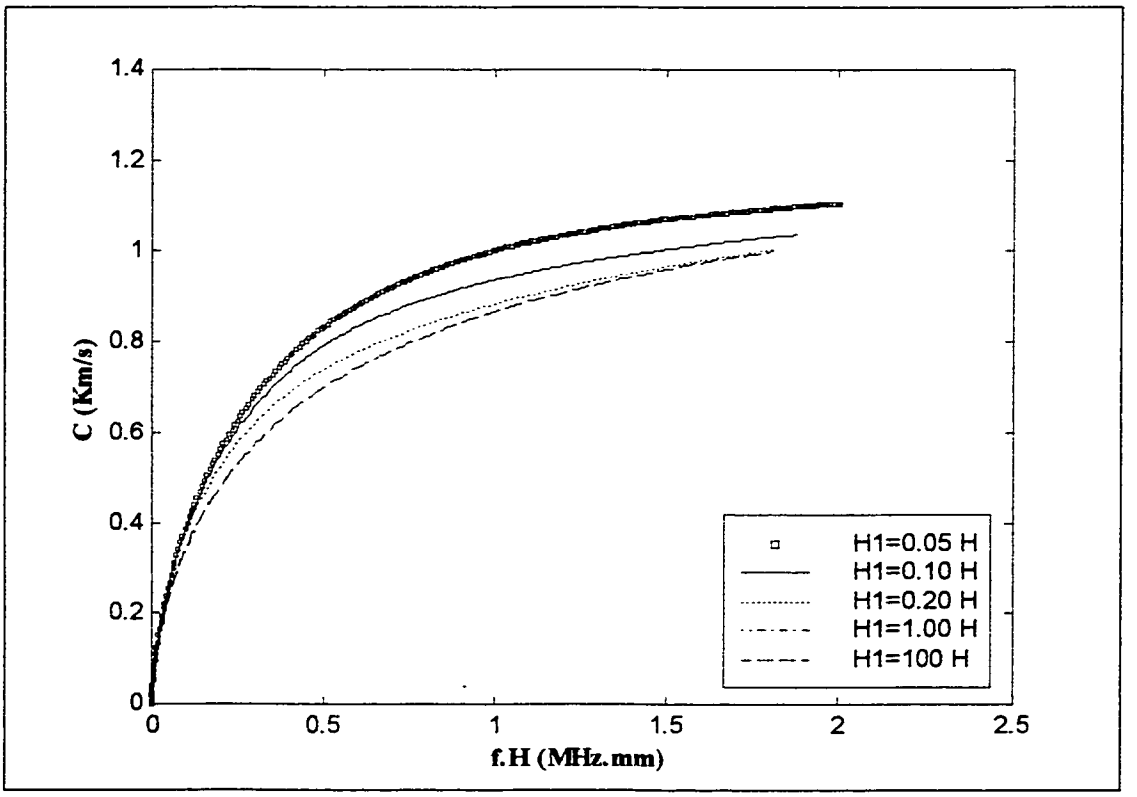

Figure 3.6: Dispersion curves for the 3-ply laminated plate along 45° direction for mercury/plate/water system, $H_2 = 0.05H$, for various mercury depths

In contrast to the previous case, the effect of changing the water depth is studied for high and low depth of mercury. The effects on the dispersion curves are relatively less noticeable for higher H_1 value as shown in Figure 3.7. Phase velocity changes with 4.60% from 0.70 to 0.67 *km/s* for H_2 equal to 100H and 0.05 H respectively at 0.40 *MHz.mm*. However, as H_1 i.e. mercury depth becomes small the effect of water depth is more pronounced. The percentage increases up to 14.0% at the same conditions. (See Figure 3. 8).

3.1.3 DISPERSION CURVES FOR WATER/PLATE/WATER SYSTEM ALONG 0-DIRECTION

In the previous systems, dispersion curves were calculated when the two liquids were different. However, in the present system both liquids were water. Dispersion curves were calculated along the 0°-direction, and shown in Figure 3.9. H_1 value was varied from 0.05H to 100H while H_2 value was kept low at 0.05H. No significant change in phase velocity, less than 1.50% between 0.05H and 100H at 1 *MHz.mm*, is observed. This is due to the boundary condition effects described earlier. It can be also noted that at low frequencies, less than 0.40 *MHz.mm*, dispersion curves almost coincide. However, at higher frequencies, greater than 0.75 *MHz.mm* dispersion curves tend to diverge.

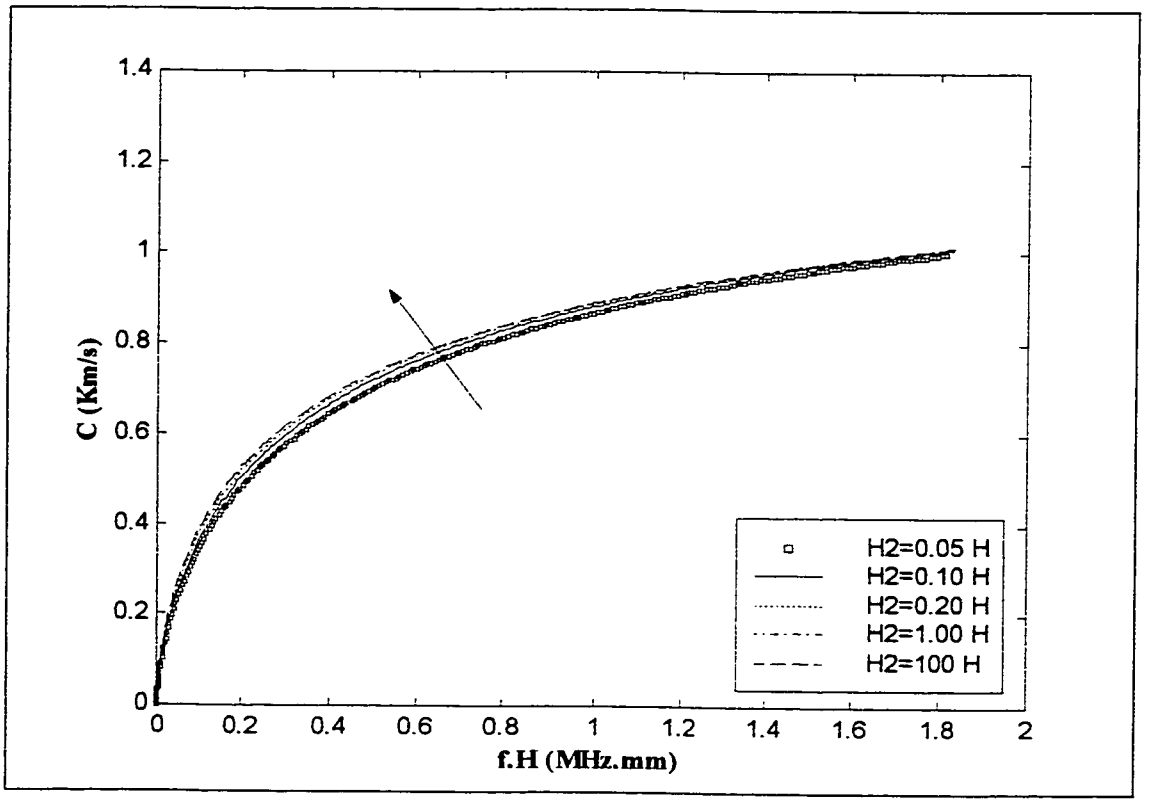

Figure 3.7: Dispersion curves for the 3-ply laminated plate along 45° direction for mercury/plate/water system, H_1 = 100H, for various water depths

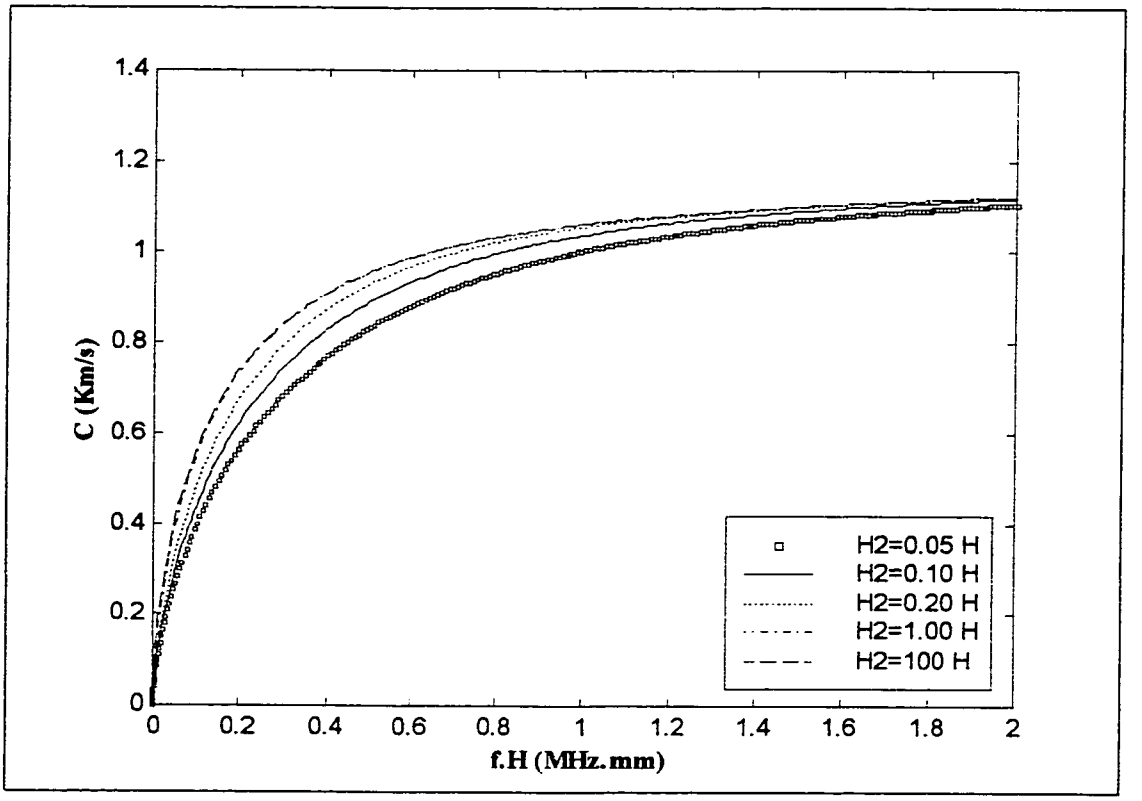

Figure 3.8: Dispersion curves for the 3-ply laminated plate along 45° direction for mercury/plate/water system, H_1 = 0.05H, for various water depths

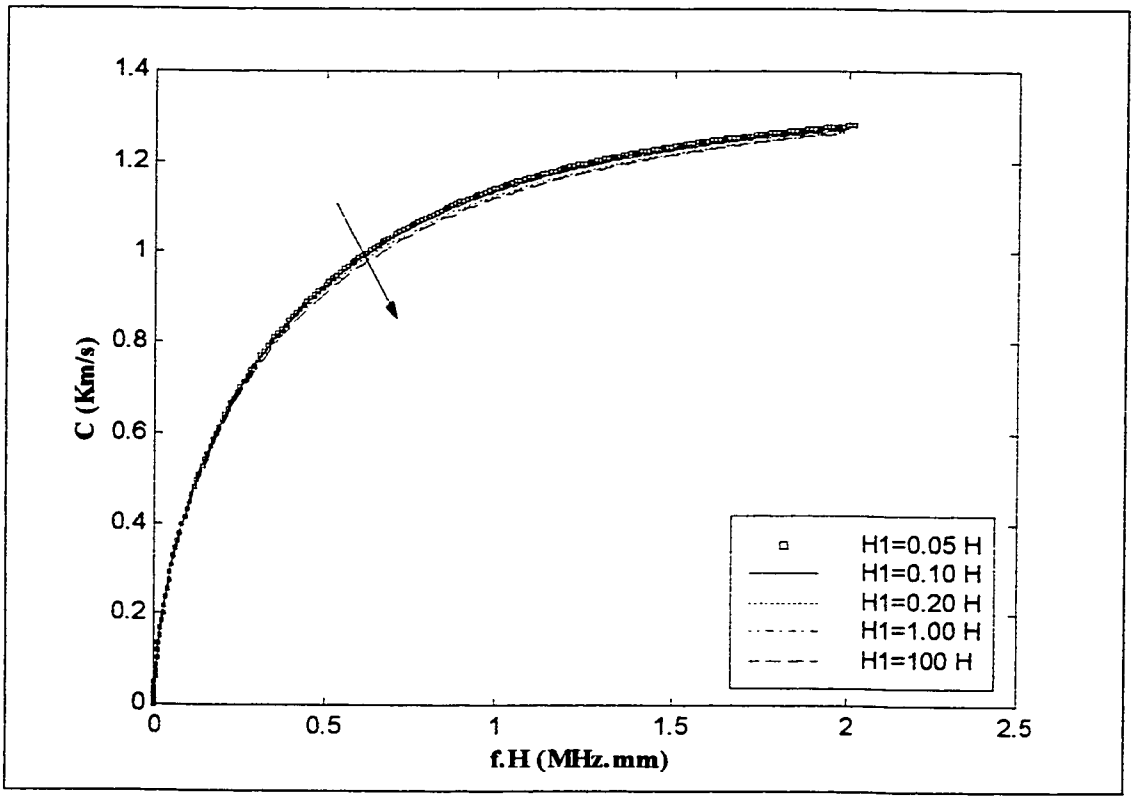

Figure 3.9: Dispersion curves for the 3-ply laminated plate along 0° direction for water/plate/water system, $H_2 = 0.05H$, for various values of H_1

In Figure 3.10, dispersion curves were calculated when the value of H_2 was increased to 100H. The percentage change in the phase velocity increases to almost 5%. However, both groups of curves in Figures 3.9 and 3.10 converge to the same phase velocity (almost 1.30 *km/s*).

The effect of the lower water on dispersion curves was studied along the same direction and the results are presented in Figures 3.11 and 3.12 for low and high value of H_1, respectively. It can be easily noticed for both sets of dispersion curves that as H_2 increases, the phase velocity increases.

In Figure 3.11, where H_1 was kept low at 0.05H, the dispersion curves diverge considerably for frequencies between 0.20 and 1.50 *MHZ.mm*, as H_2 changes (with the exception of H_2 equal to H and 100H). At 0.5 *MHz.mm*, the phase velocity increases from 0.96 to 1.17 *km/s* (22% increase) as the H_2 increases from 0.05H to 100H. However, the percentage drops to (5.20%) at 1.50 *MHz.mm*, where the phase velocities tend thereafter to converge to a constant value of almost 1.32 *km/s*.

In Figure 3.12, H_2 value is increased to 100 H. Dispersion curves here exhibit similar characteristics to those of Figure 3.11. However, by comparing the two figures, one can find that there are some slight differences in dispersion curves. For example, the percentage change of the phase velocity drops slightly to 20% at 0.5 *MHz.mm* and to 4.63% at 1.50 *MHz.mm*. This slight change is due to the weaker effect of changing H_1 value.

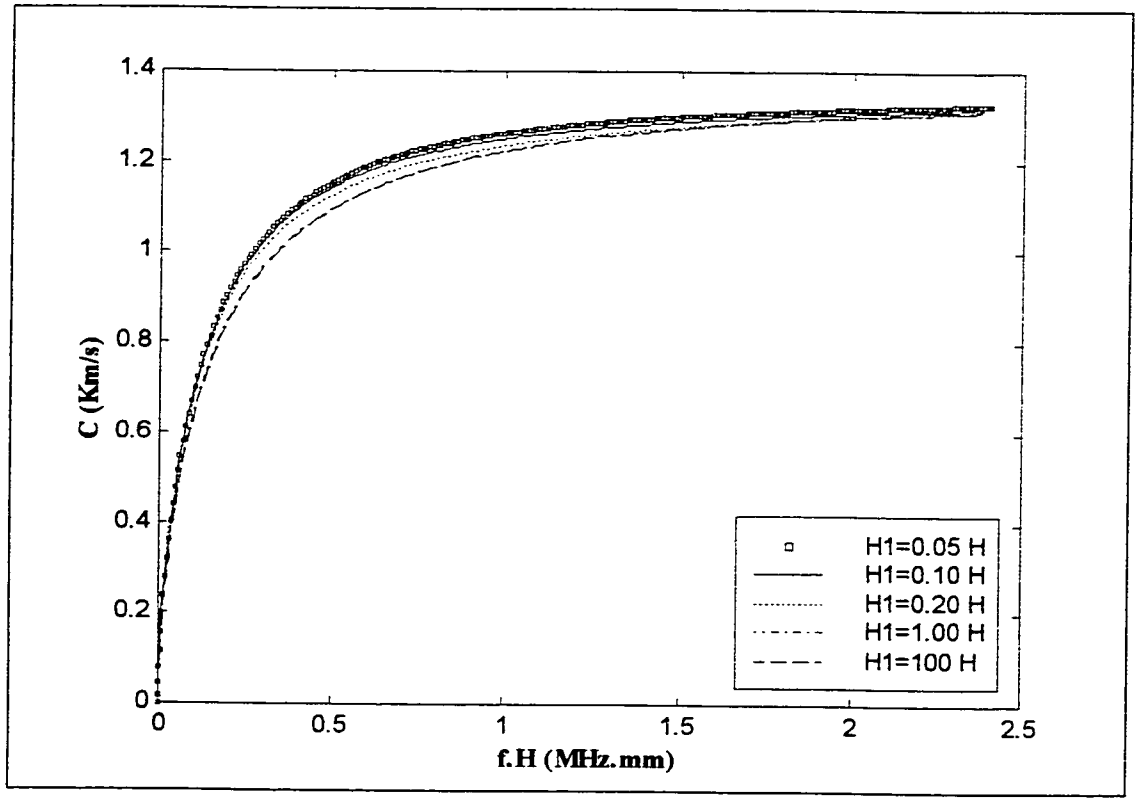

Figure 3.10: Dispersion curves for the 3-ply laminated plate along 0° direction for water/plate/water system, $H_2 = 100H$, for various values of H_1

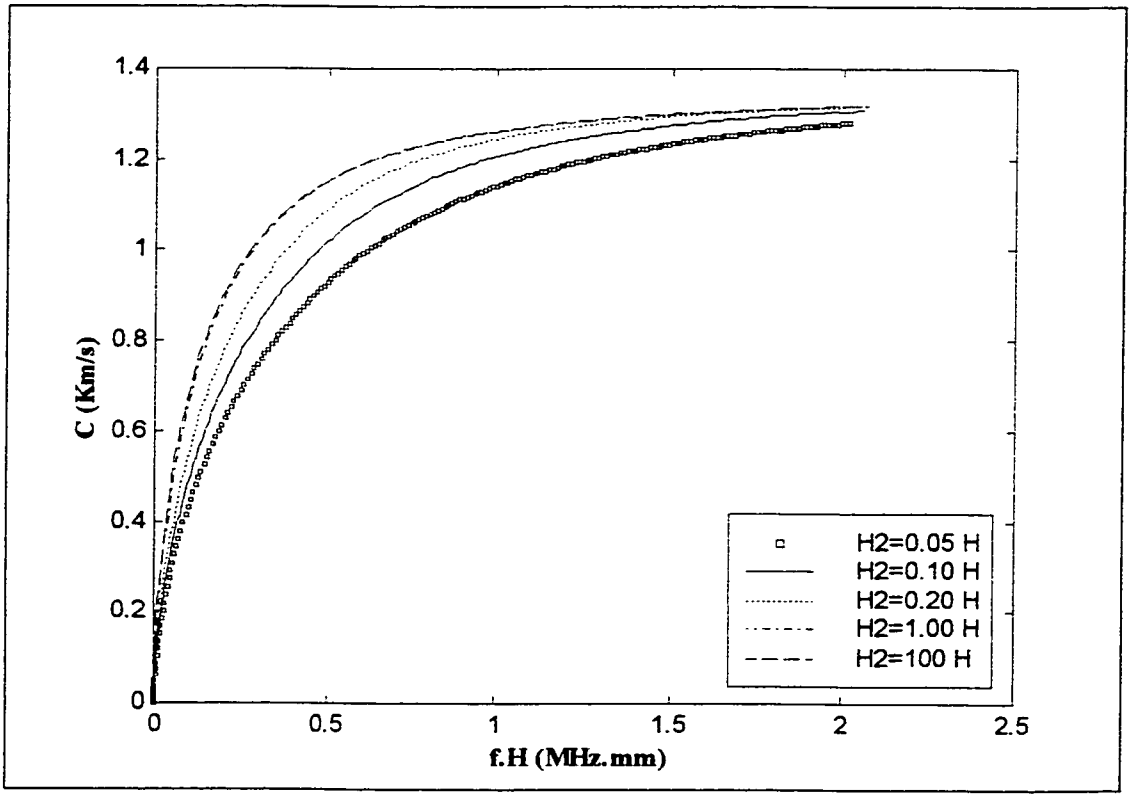

Figure 3.11: Dispersion curves for the 3-ply laminated plate along 0° direction for water/plate/water system, $H_1 = 0.05H$, for various values of H_2

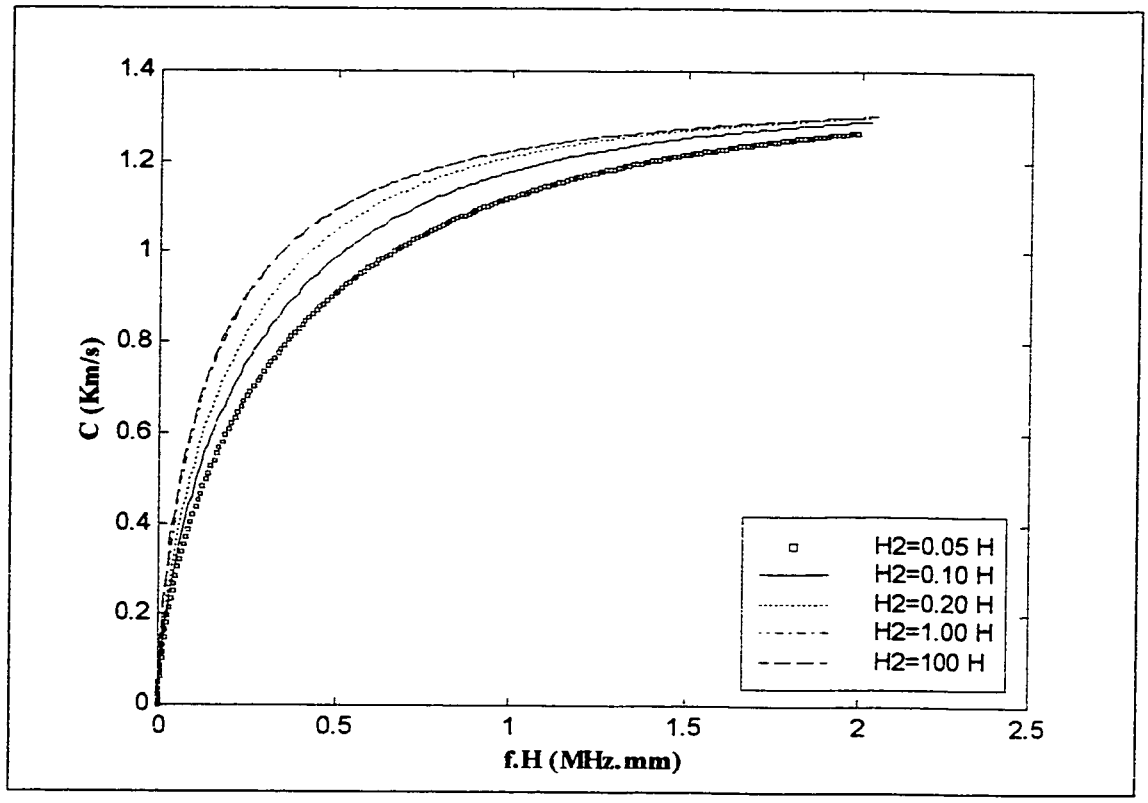

Figure 3.12: Dispersion curves for the 3-ply laminated plate along 0° direction for water/plate/water system, $H_1 = 100H$, for various values of H_2

3.1.4 DISPERSION CURVES FOR WATER/PLATE/WATER SYSTEM ALONG 90^{O} DIRECTION

The effects of the upper liquid depth on dispersion curves along the 90° direction are shown in Figures 3.13 and 3.14, for low and high depth of the lower liquid. Furthermore, the effects of the lower liquid along the same direction are also shown in Figures 3.15 and 3.16 respectively. Similar effects, due to the change of parameters studied along the 0°-dirction, can be observed here as well. However, under all circumstances, the phase velocity values are greater along the 0°-direction than those along the 90°direction. For instance, the phase velocity is 1.27 *km/s* in Figure 3.11 versus 1.10 *km/s* in Figure 3.15 at a frequency of 1 *MHz.mm* provided that the plate is under the same loading conditions for both cases. This observation is expected because more fibers are oriented along the 0°-dirction, which means that the rigidity is greater along this direction for 0°/90°/0° composite plate.

3.1.5 EFFECTS OF LIQUID DENSITY ON DISPERSION CURVES

The next step was to study the density effects of both liquids on the associated dispersion curves. The 3-ply composite plate was loaded with liquids on both sides with depths equal to 100 H.

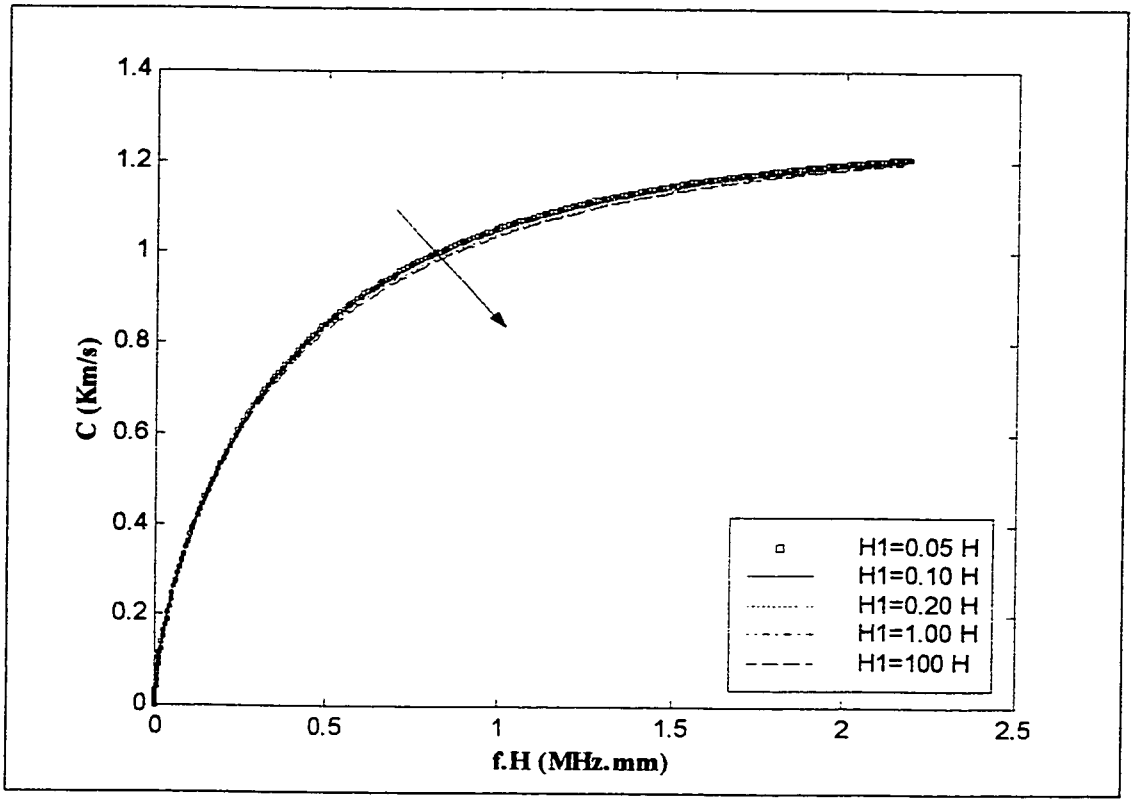

Figure 3.13: Dispersion curves for the 3-ply laminated plate along 90° direction for water/plate/water system, $H_2 = 0.05H$, , for various values of H_1

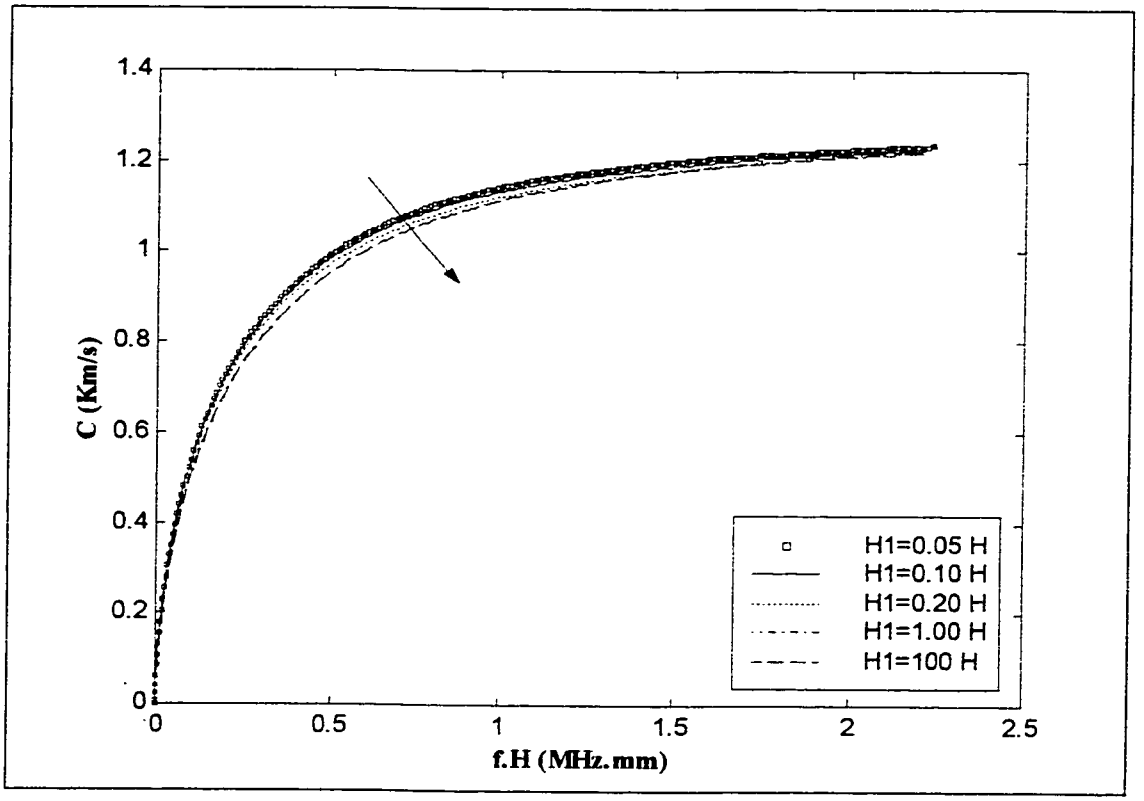

Figure 3.14: Dispersion curves for the 3-ply laminated plate along 90° direction for water/plate/water system, H_2=100H, for various values of H_1

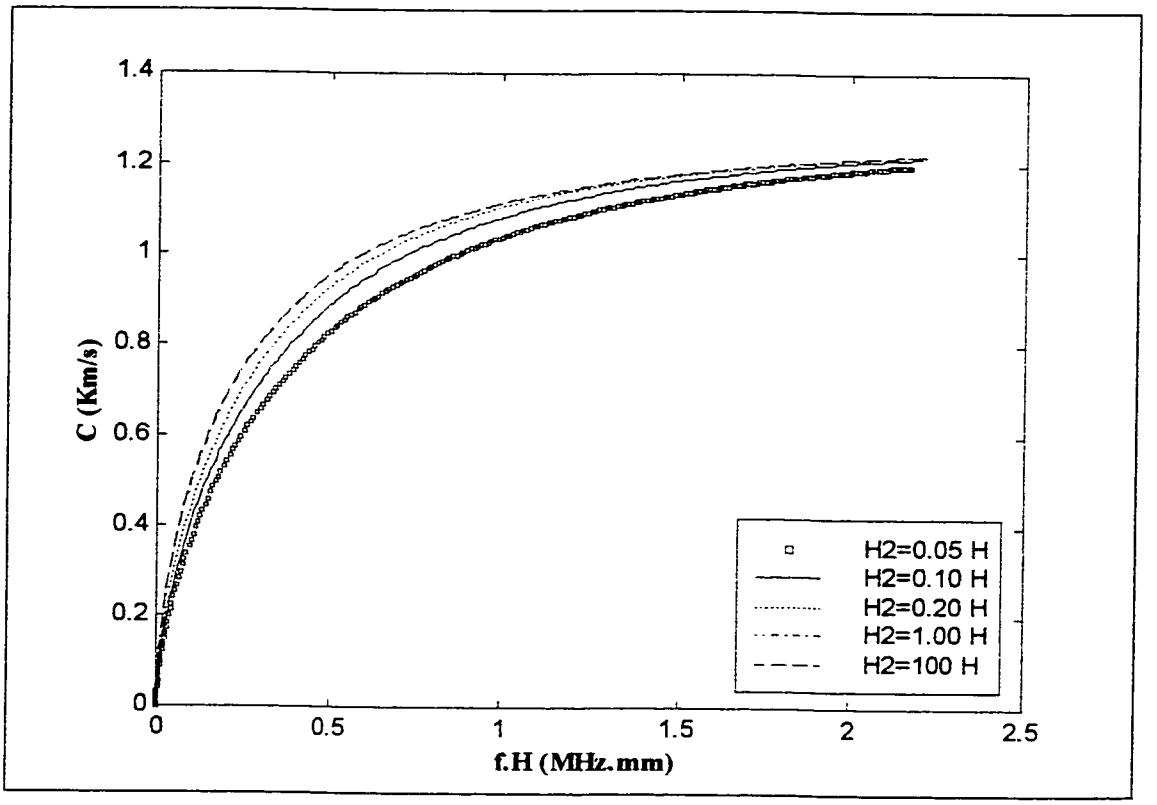

Figure 3.15: Dispersion curves for the 3-ply laminated plate along 90° direction for water/plate/water system, $H_1 = 100H$, for various values of H_2

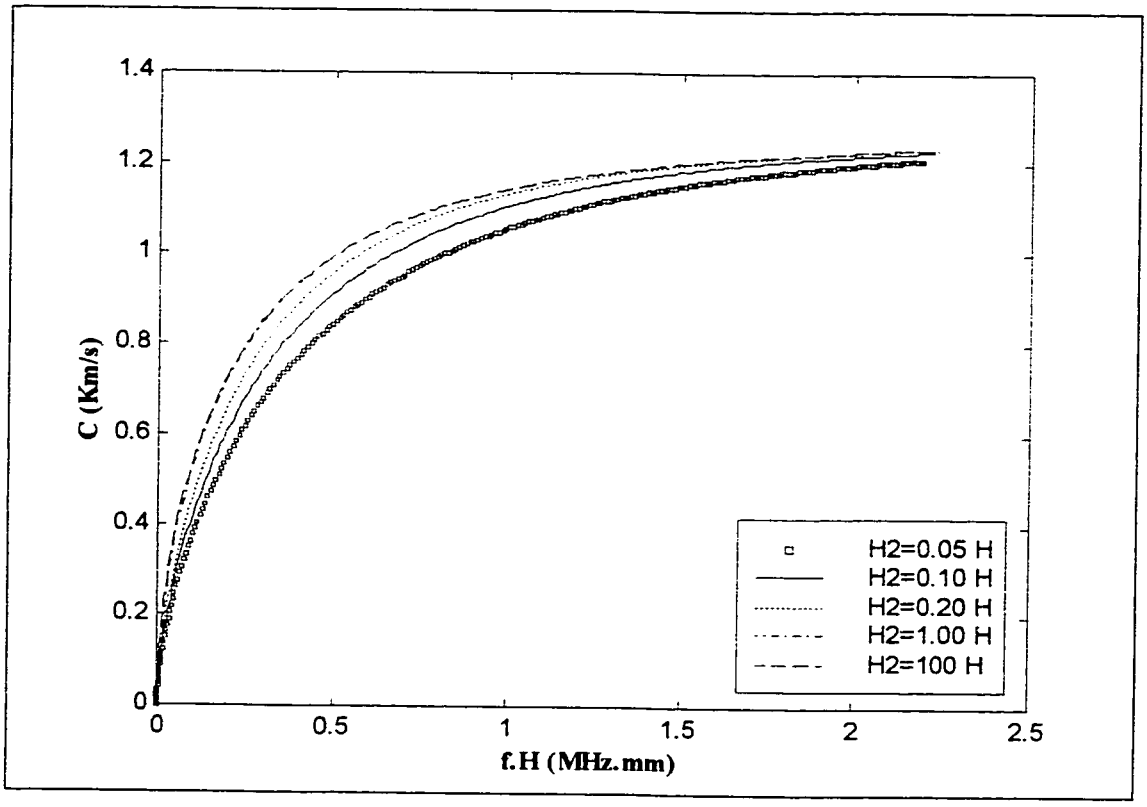

Figure 3.16: Dispersion curves for the 3-ply laminated plate along 90° direction for water/plate/water system, $H_1 = 0.05H$, for various values of H_2

First, dispersion curves were calculated for several values of ρ_1 ,with low and high values of ρ_2, and they are shown in Figures 3.17 and 3.18, respectively. In Figure 3.17, ρ_2 was kept as low as 800 kg/m^3, whereas ρ_1 was varied from 800 up to 13,570 kg/m^3. It can be easily seen that the phase velocity decreases as ρ_1 increases at a given frequency. For instance, at 0.2 *MHz.mm*, it drops from around 0.864 to 0.573 *km/s* (51 % decrease) as ρ_1 increases from 800 kg/m^3 to 13,570 kg/m^3.

In Figure 3.18, ρ_2 was kept as high as 13,570 kg/m^3. Dispersion curves exhibit the same general characteristics as those of Figure 3.17. However, it can be noted that the phase velocity is smaller here. Numerically, the phase velocity at 0.2 *MHz.mm* is around 0.568 *km/s* compared to 0.864 *km/s* of Figure 3.17 for ρ_1 equal to 800 kg/m^3. Moreover, by comparing closely Figure 3.17 with Figure 3.18, we can notice that the change in phase velocity with respect to the change in density is less in Figure 3.18. For example, at 0.25 *Mhz.mm*, the percentage change in phase velocity is 15.0% in Figure 3.18 compared to 33.0 % in Figure 3.17.

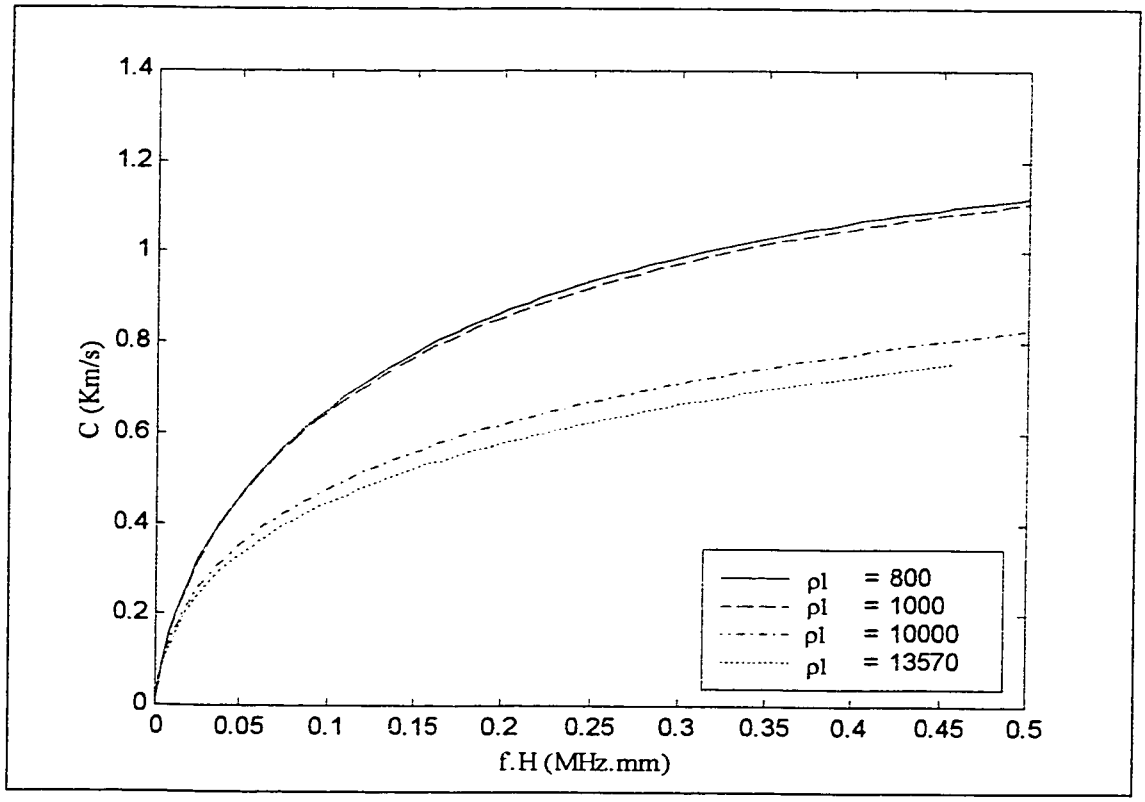

Figure 3.17: Dispersion curves for the 3-ply laminated plate along 0° direction for various ρ_1 values ($\rho_2 = 800\ Kg/m^3$)

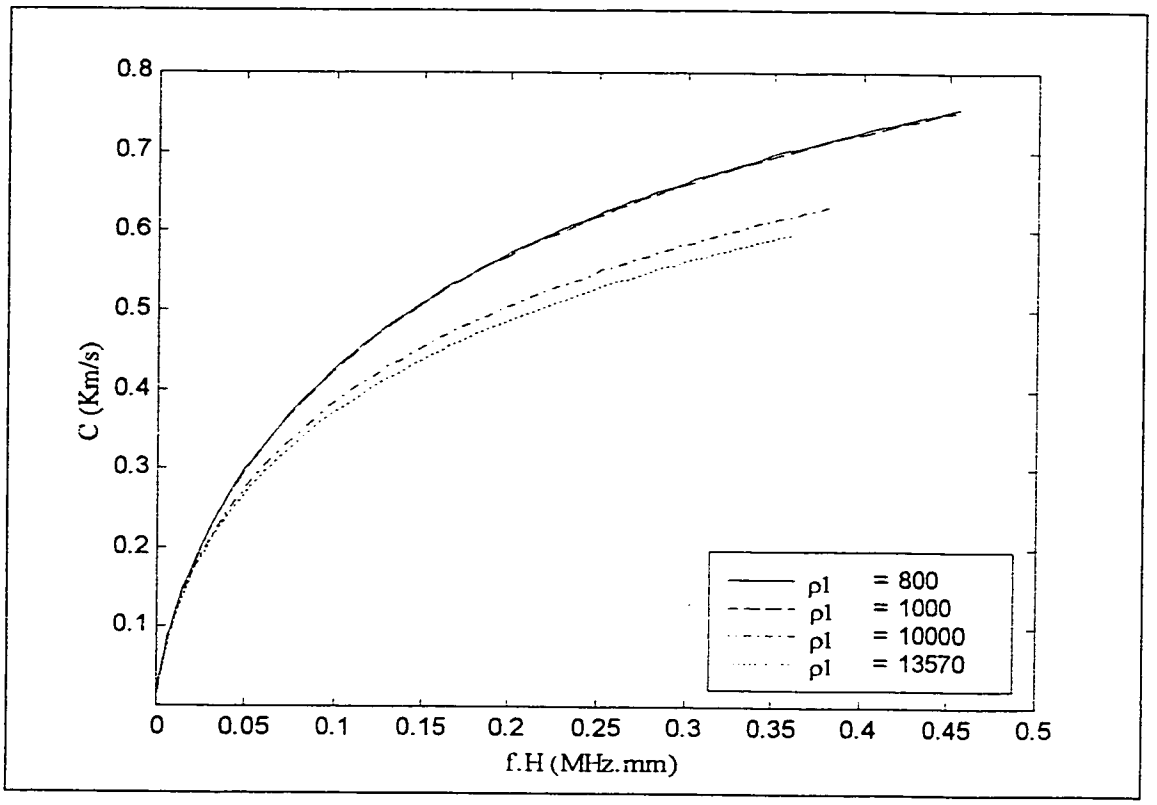

Figure 3.18: Dispersion curves for the 3-ply laminated plate along 0° direction for various ρ_1 values ($\rho_2 = 13{,}570\ Kg/m^3$)

The effect of varying ρ_2 was also studied. Again, the dispersion curves were produced for the two cases of low and high values of ρ_1 and they are shown in Figures 3.19 and 3.20, respectively.

In Figure 3.19, ρ_1 was kept low at 800 kg/m^3, whereas ρ_2 was varied from 800 to 13,570 kg/m^3. Similar observations are noticed here. The phase velocity decreases as ρ_2 increases, e.g. it drops from 0.983 to 0.659 *km/s* (32.0 % decrease) as ρ_2 increases from 800 to 13,570 kg/m^3 at 0.3 *MHz.mm*.

In Figure 3.20, ρ_1 is kept as high as 13,570 kg/m^3. The same behavior of dispersion curves is found. Once more, it can be noted that the phase velocity values are smaller than those of Figure 3.19. This can be checked at, for instance, 0.30 *MHz.mm*., where the phase velocity is 0.559 *km/s*, for ρ_1 equal to 13,570 kg/m^3, and 0.662 *km/s* for ρ_1 equal to 800 kg/m^3. Similar to Figures 3.17 and 3.18, it can be noticed that dispersion curves are more compact in Figure 3.20 than those in Figure 3.19.

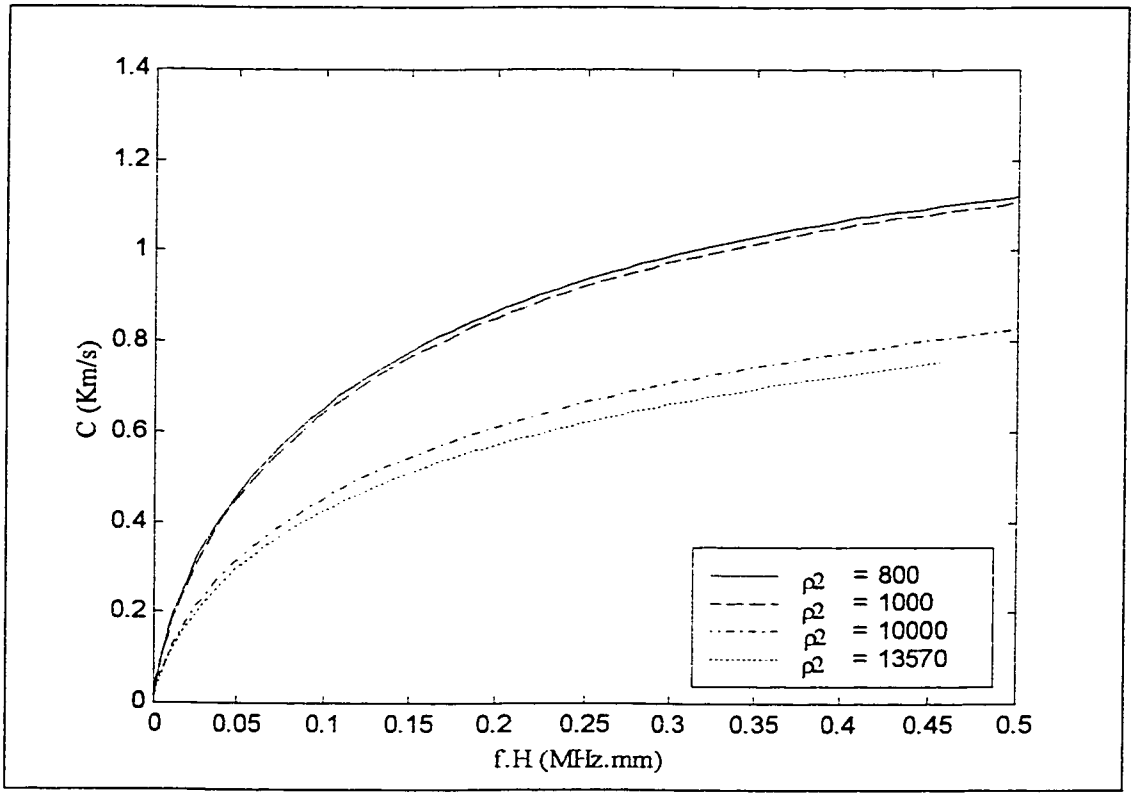

Figure 3.19: Dispersion curves for the 3-ply laminated plate along 0° direction for various ρ_2 values ($\rho_1 = 800\ Kg/m^3$)

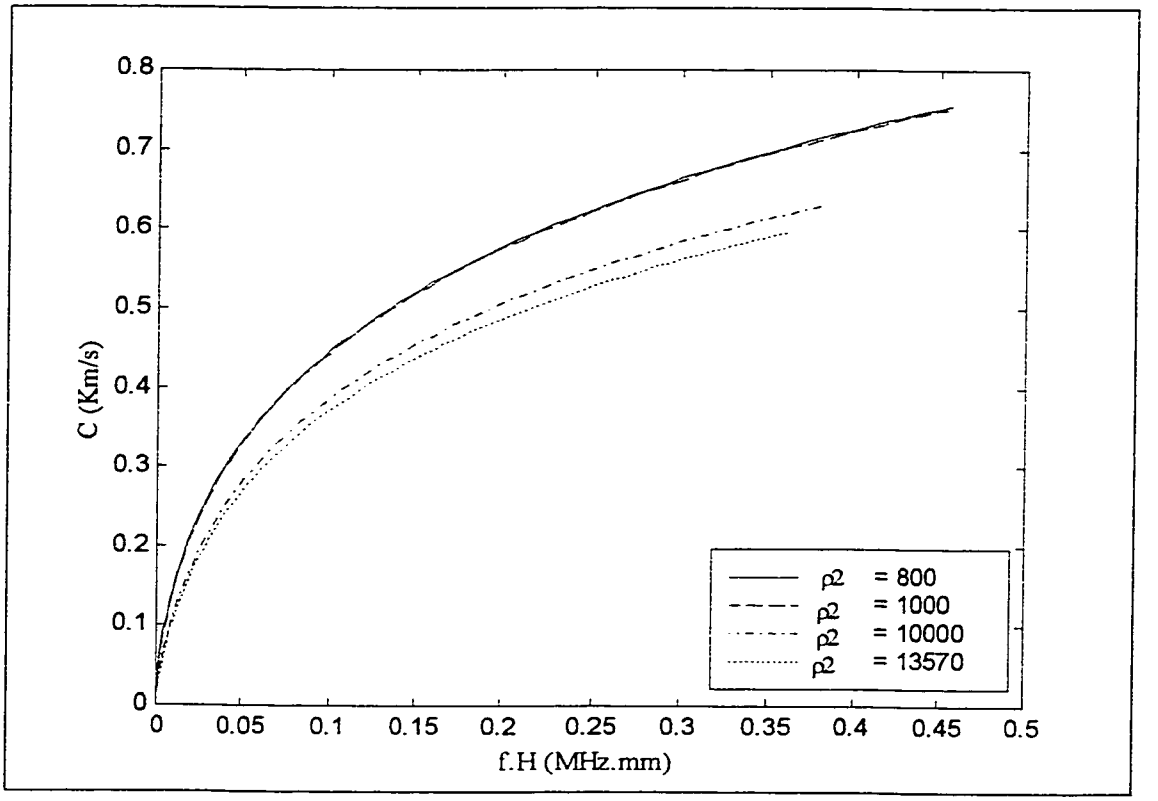

Figure 3.20: Dispersion curves for the 3-ply laminated plate along 0° direction for various ρ_2 values ($\rho_1 = 13{,}570\ Kg/m^3$)

3.1.6 THE NORMAL TRANSIENT RESPONSE OF 3-PLY COMPOSITE PLATES

The first investigation set to study the normal transient was done on the 3-ply composite plate. This plate is 3-ply symmetric plate, where the plys stacking order is [0°/90°/0°]. The properties of the plate are given in Table 3.1.

The plate was loaded on both sides by water with water depths and density given in Table 3.2.

TABLE 3.2: Properties of the Upper and Lower Water

Property	Value
H_1	100 H
H_2	100 H
ρ_1	1000.0 kg/m^3
ρ_2	1000.0 kg/m^3

The plate was excited by an amplitude modulated 0.20 *MHz* central frequency force. This excitation force and its power spectrum are shown on Figure 3.21. The frequency of this force is bounded between 0.13 *MHz* as a low end and 0.26 *MHz* as a high end. The transient responses for the plate were computed along three axial directions, namely, 0°-,45°-,and 90°-direction, at three different locations: 10H, 20H, and 40H.

Figure 3.22 shows the normal transient responses of the plate along the 0°-direction at the three locations. It can be seen that the amplitude of the wave decreases as the location distance increases. This attenuation is expected because the attenuation effect was introduced in the numerical model for the composite plate to account for the fact that most composite plates are made of highly attenuating materials. An attenuation of approximately 59% is observed on the wave as it travels from the first to the third location. Furthermore, its shape is distorted because the propagating mode exhibits some dispersion as it travels along the plate. One can notice that the wave is broadened as it gets far from the force source.

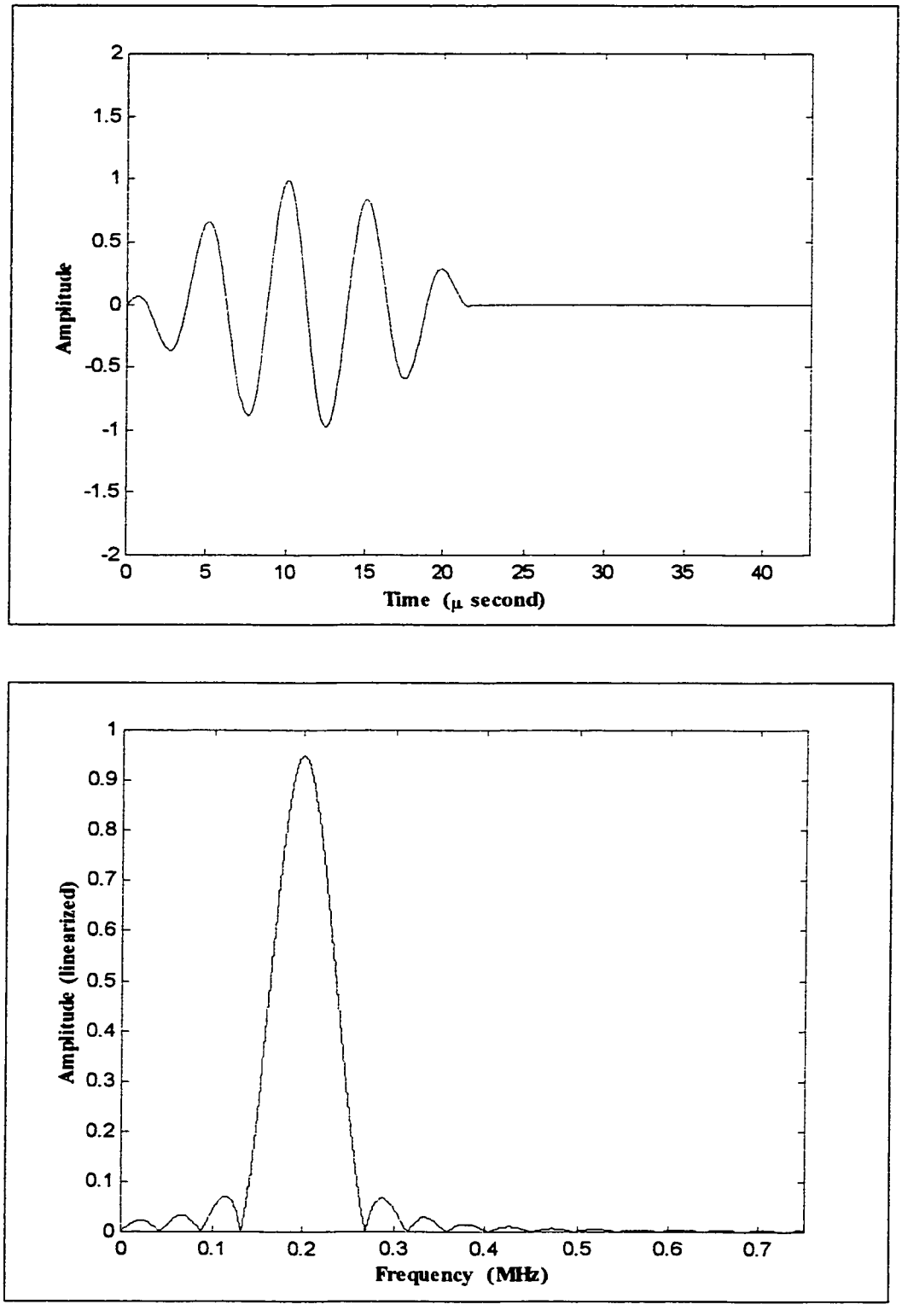

Figure 3.21: The excitation force used with its power spectrum

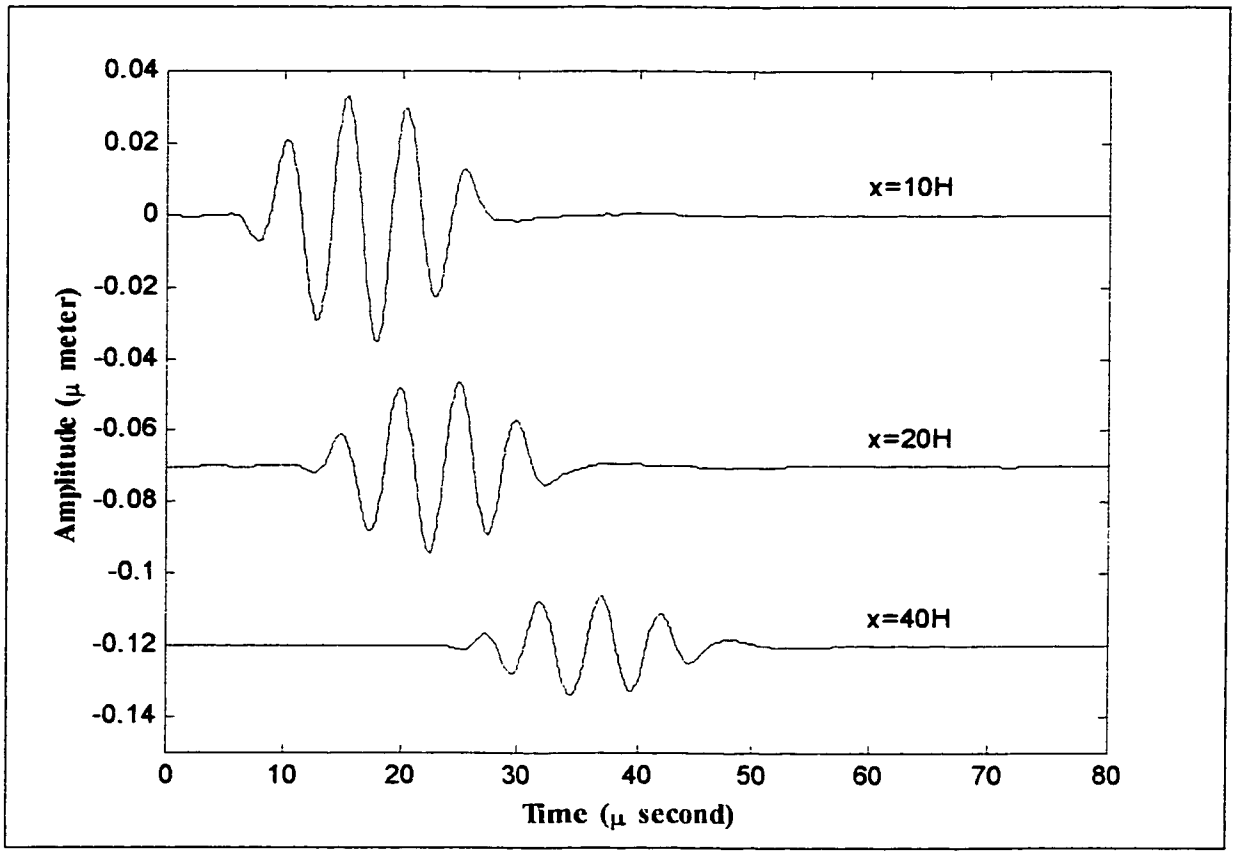

Figure 3.22: The transient response of the 3-ply plate along the 0° direction, at three different locations

Figures 3.23 and 3.24 show the normal transient response of the plate along 45°-, and 90°-direction, respectively. Attenuation and distortion of the wave are observed along these directions as well.

Group Velocity:

The group velocity is defined as:

$$C_{group} = \frac{d\omega}{d\xi}$$

where ω is the frequency and ξ is the wavenumber. The group velocity has been computed along the 0°-, and 90°-dirction, and plotted in Figure 3.25. We can see that the group velocity along the 0°-dirction is greater than its value along the other directions. Its value for this plate is around 1300 *m/s* along the 0°-dirction and 1209 *m/s* along the 90°-dirction at 0.20 *MHz*. Figures 3.22, 3.23 and 3.24, can also verify this result. The difference in the group velocity was due to the fact that more fibers were oriented along the 0°-dirction i.e. the plate is more rigid along the 0°-direction. In the 45°-dirction, the effect of the fibers would be in the middle between the two extreme cases.

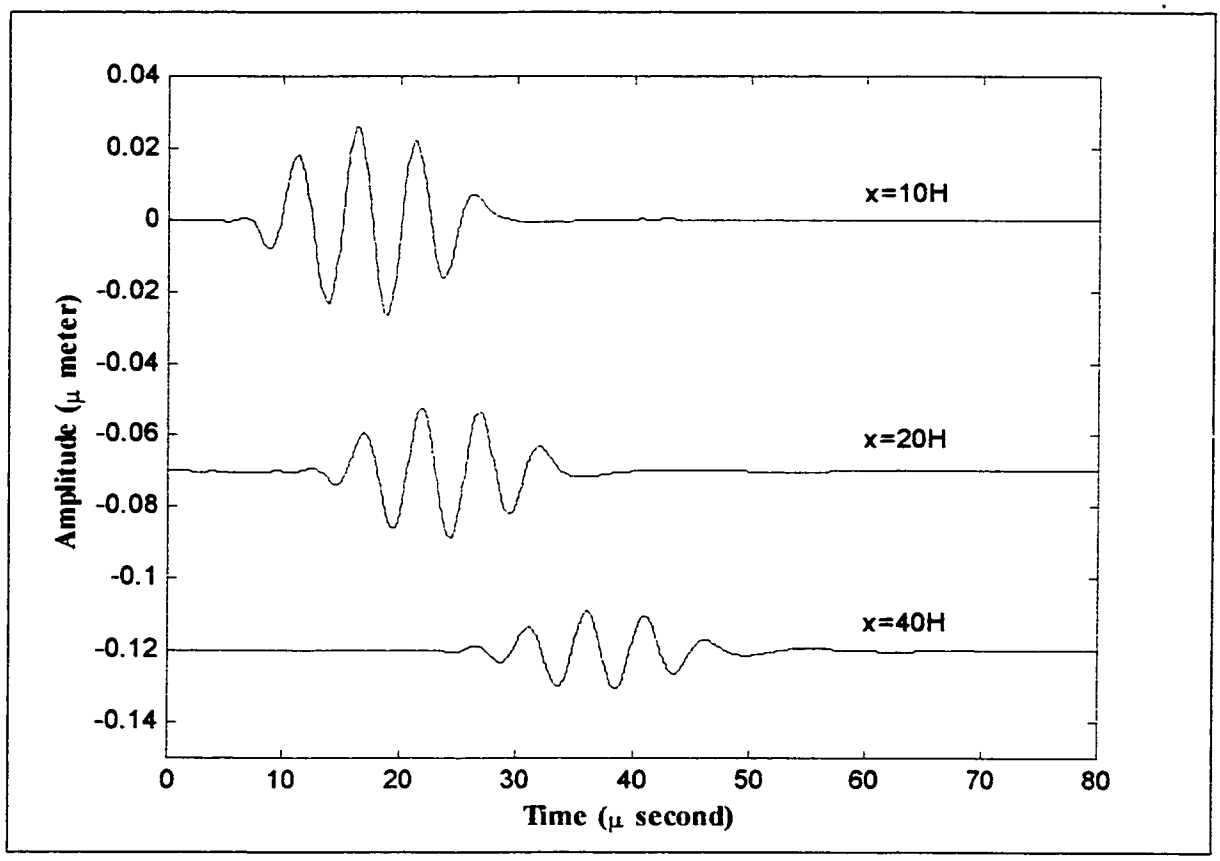

Figure 3.23: The transient response of the 3-ply plate along the 45° direction, at three different locations

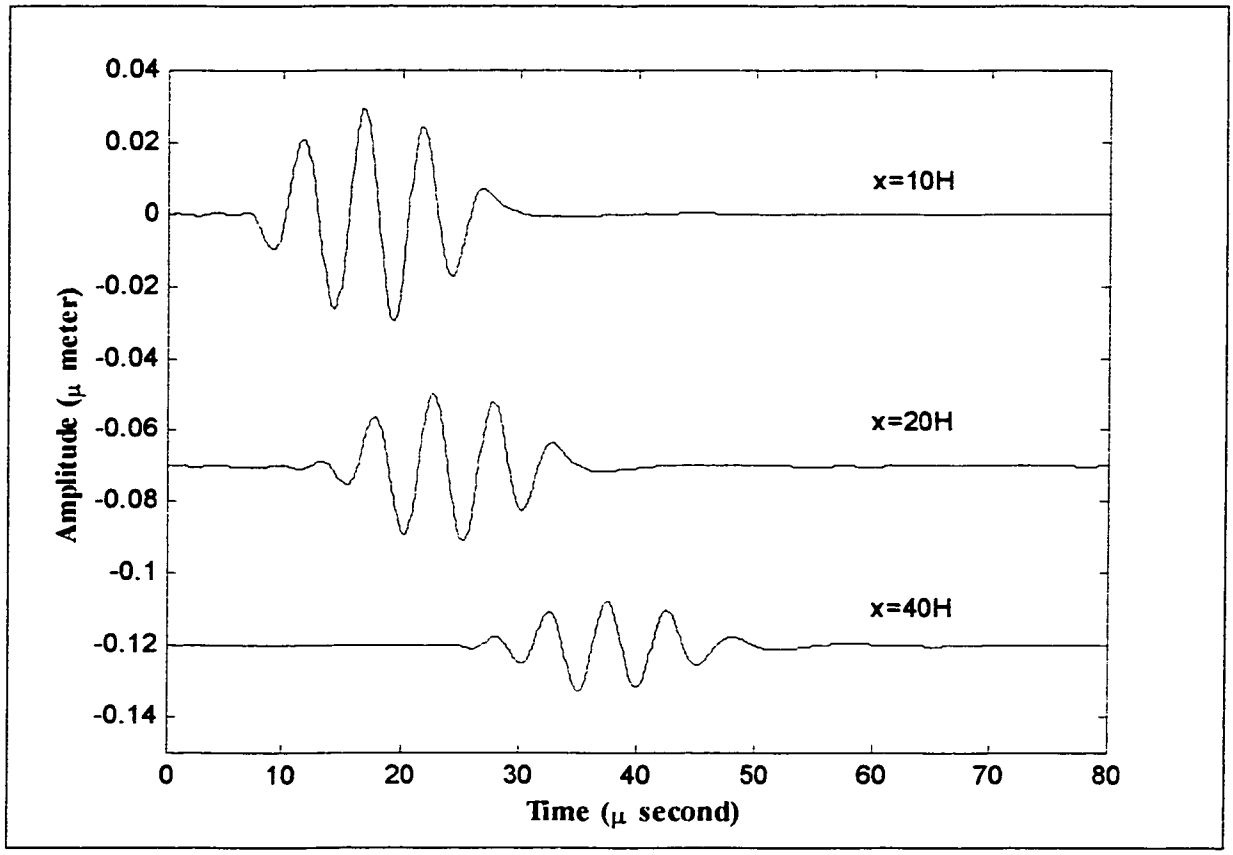

Figure 3.24: The transient response of the 3-ply plate along the 90° direction, at three different locations

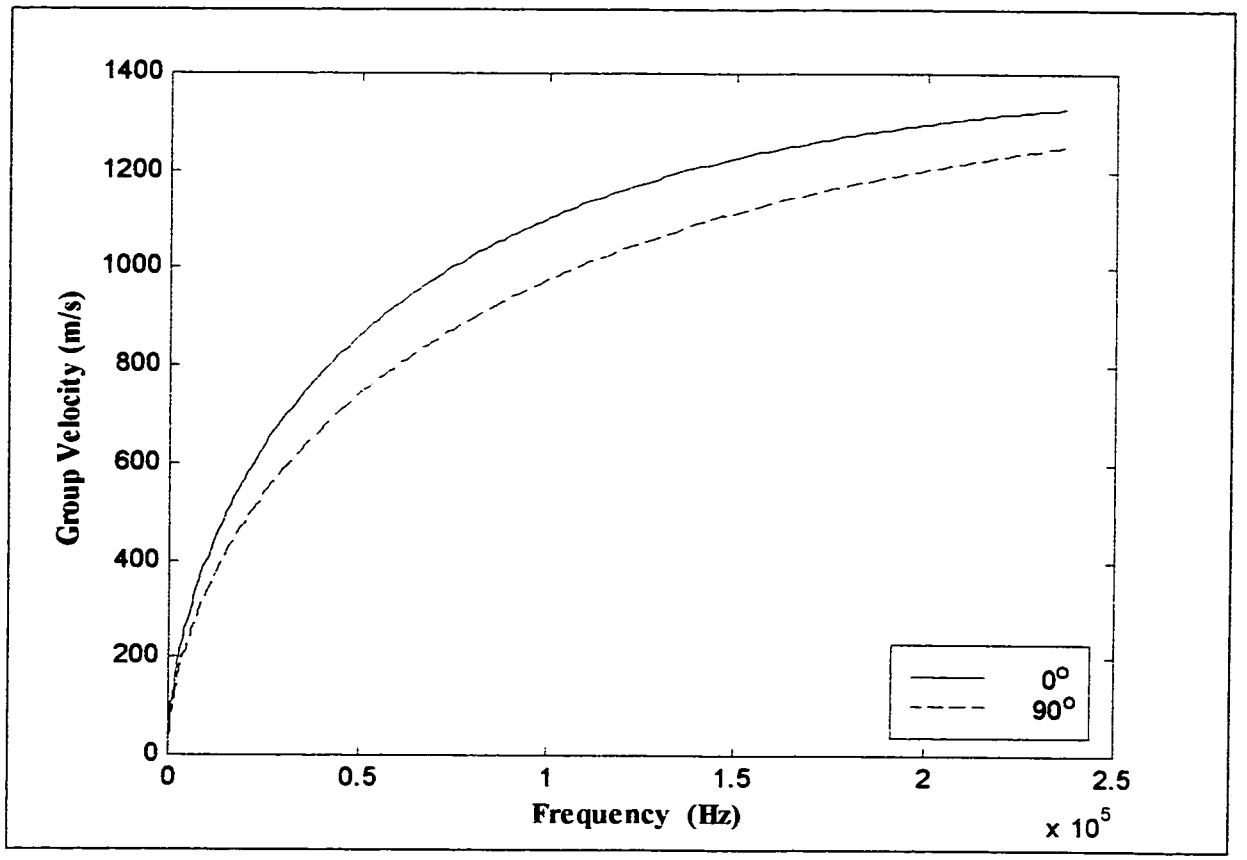

Figure 3.25: The group velocity of the 3-ply plate along the 0° and the 90° directions

3.1.7 THE NORMAL TRANSIENT RESPONSES OF 6-PLY COMPOSITE PLATES

The second task was to compute the normal transient responses of 6-ply laminated plate. This plate is 6-ply E-glass/epoxy fiber reinforced plate with a thickness of 1.524 mm and a stacking order of [0°/90°/0°/0°/90°/0°]. Its properties are given in Table 3.3.

TABLE 3.3: Properties of the 6-Ply Composite Plate

ρ	1857 Kg/m^3
H	1.524×10^{-3} m
$C_{11}^{(K)}$	38.0×10^9 N/m^2
$C_{12}^{(K)}$	3.10×10^9 N/m^2
$C_{22}^{(K)}$	11.75×10^9 N/m^2
$C_{23}^{(K)}$	5.30×10^9 N/m^2
$C_{55}^{(K)}$	4.60×10^9 N/m^2

The plate was loaded by water on both sides with the same parameters given in Table 3.2. The plate was excited by the same 0.20 *MHz* central frequency force shown in Figure 3.21. Its normal transient responses were calculated along the three main directions, i.e. 0°, 45°, and 90° directions at three different locations, namely, 10H, 20H, and 40H. These responses are shown in Figures 3.26, 3.27 and 3.28, along the three directions, respectively.

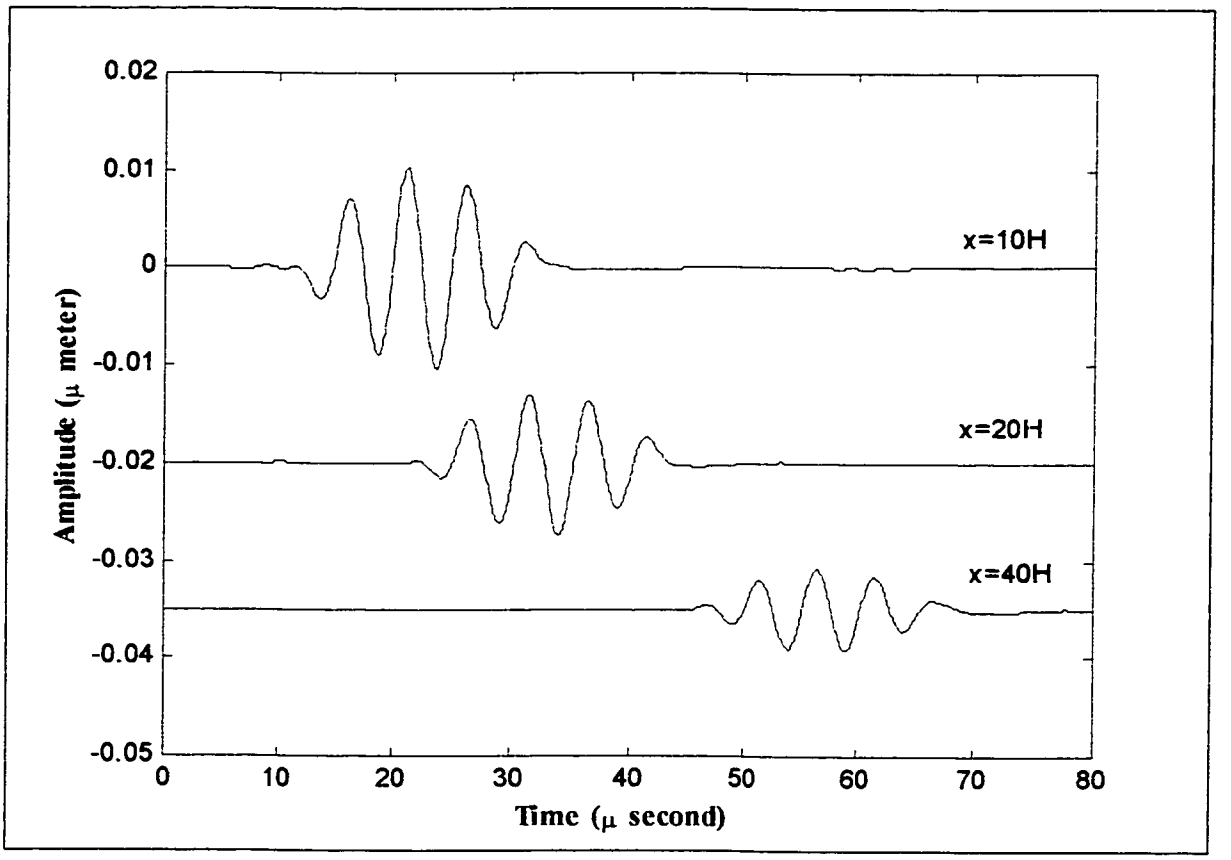

Figure 3.26: The transient response of the 6-ply plate along the 0° direction, at three different locations

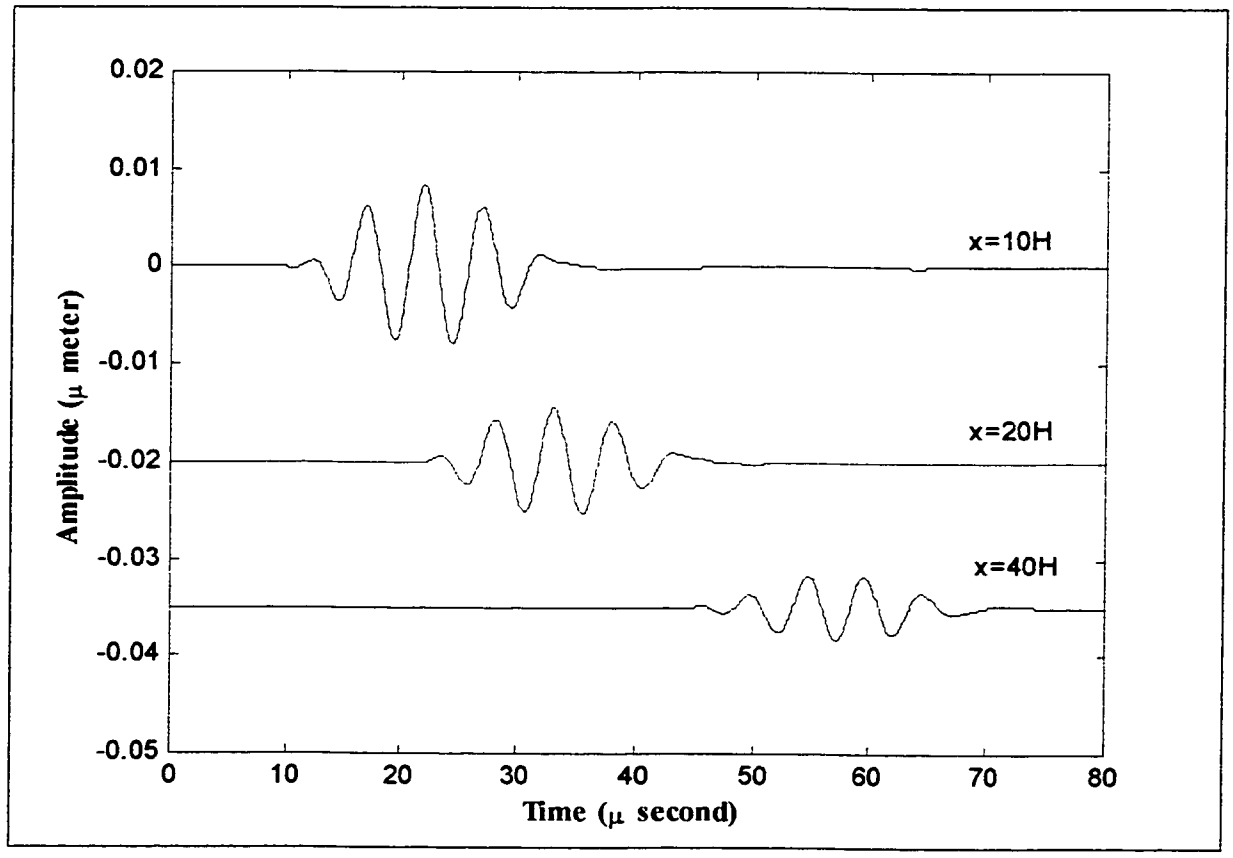

Figure 3.27: The transient response of the 6-ply plate along the 45° direction, at three different locations

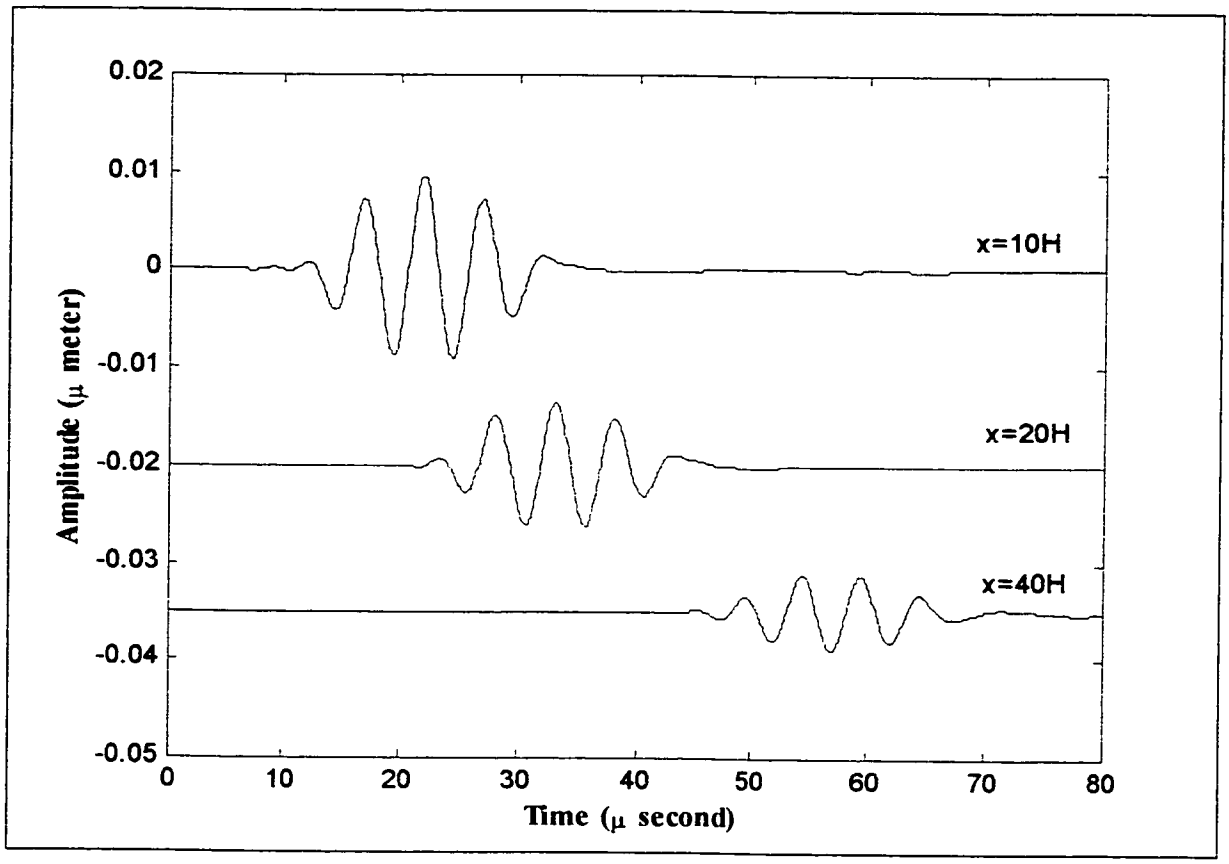

Figure 3.28: The transient response of the 6-ply plate along the 90° direction, at three different locations

Similar to the 3-ply laminated plate, the attenuation and dispersion behavior of the flexural waves can be observed along the three directions. Differences in group velocity along the three directions can be seen as well. The group velocity was estimated along the 0° direction and was found to be approximately 1418 *m/s*, and 1406 *m/s* along the 90° direction at 0.20 *MHz*.

If the response of the 6-ply plate is compared to that of the 3-ply pate, differences in wave behavior and group velocity can be seen clearly. Distortion in the wave shape is more pronounced in the 6-ply laminated composite plate. This is due to the fact that the 6-ply laminated plate is more dispersive than the 3-ply one. Moreover, the amplitude of the normal response is less in the 6-ply laminated plate. We can also notice that the group velocity is greater for the 6-ply plate. This difference in group velocity is due to the existence of more fibers in the 6-ply laminated plates, which subsequently increase the rigidity of such plates.

3.1.8 THE NORMAL TRANSIENT RESPONSES OF 12-PLY COMPOSITE PLATES

In this section, the normal transient response of a 12-ply E-glass/epoxy fiber reinforced plate, with a stacking order of $[0°/90°/0°/0°/90°/0°]_{sym}$, was computed. The properties of this plate are given in Table 3.4.

TABLE 3.4: Properties of the 12-Ply Composite Plate	
ρ	1857 Kg/m^3
H	3.048×10^{-3} m
$C_{11}^{(K)}$	38.0×10^9 N/m^2
$C_{12}^{(K)}$	3.10×10^9 N/m^2
$C_{22}^{(K)}$	11.75×10^9 N/m^2
$C_{23}^{(K)}$	5.30×10^9 N/m^2
$C_{55}^{(K)}$	4.60×10^9 N/m^2

It was exposed to the same loading conditions mentioned in the previous two sections. The 0.20 MHz central frequency, shown in Figure 3.21 along with its spectrum, was used to excite the plate. Again, the normal transient response of the plate was computed along the three main directions i.e. 0°,45°, and 90° directions, at three different locations, namely 10H, 20H, and 40H. These responses are shown in Figures 3.29, 3.30 and 3.31.

The computed flexural wave exhibit similar behavior as observed in the previous 3 and 6-ply plates. The group velocity can be estimated along the 0° direction to be 1470 *m/s*.

3.1.9 THE NORMAL TRANSIENT RESPONSE OF THE ISOTROPIC PLATE

An isotropic plate is also investigated. An aluminum plate with the following specifications was selected:

$\rho = 2800\ Kg/m^3$, $E = 72 \times 10^9\ N/m^2$,

$\mu = 27 \times 10^9\ N/m^2$, $H = 1.524\ mm$,

Hence, from these data, it can be found that:

$\nu = 0.33$, $C_S = 3100\ m/s$,

$r = C_L/C_S = 1.985$

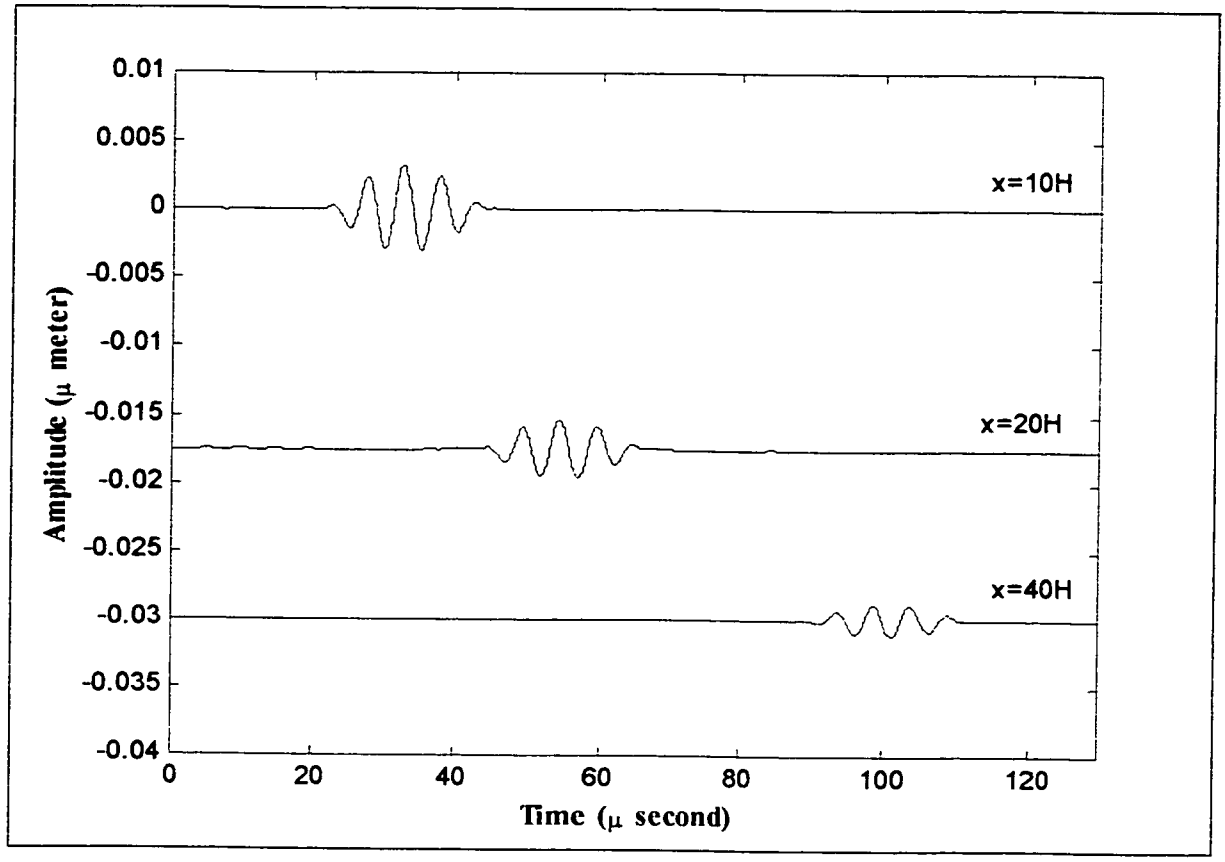

Figure 3.29: The transient response of the 12-ply plate along the 0° direction, at three different locations

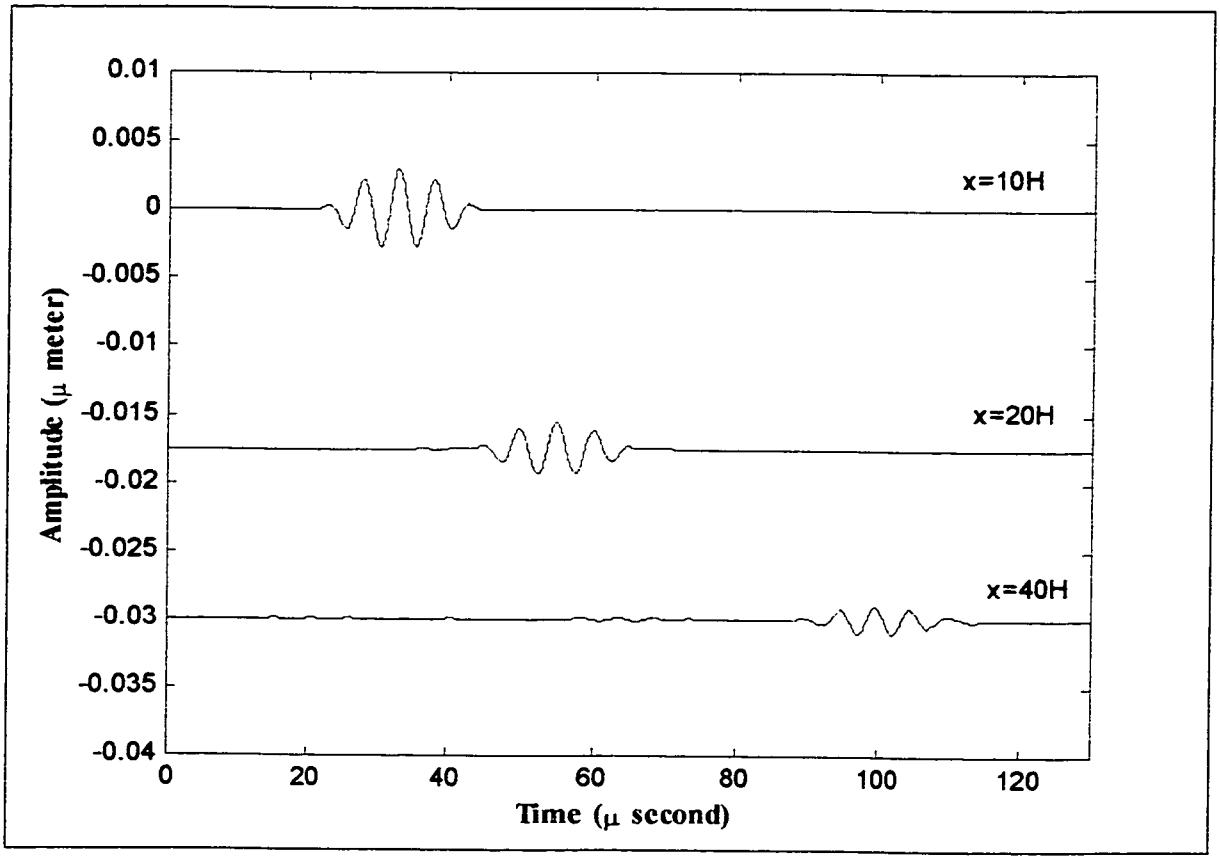

Figure 3.30: The transient response of the 12-ply plate along the 45° direction, at three different locations

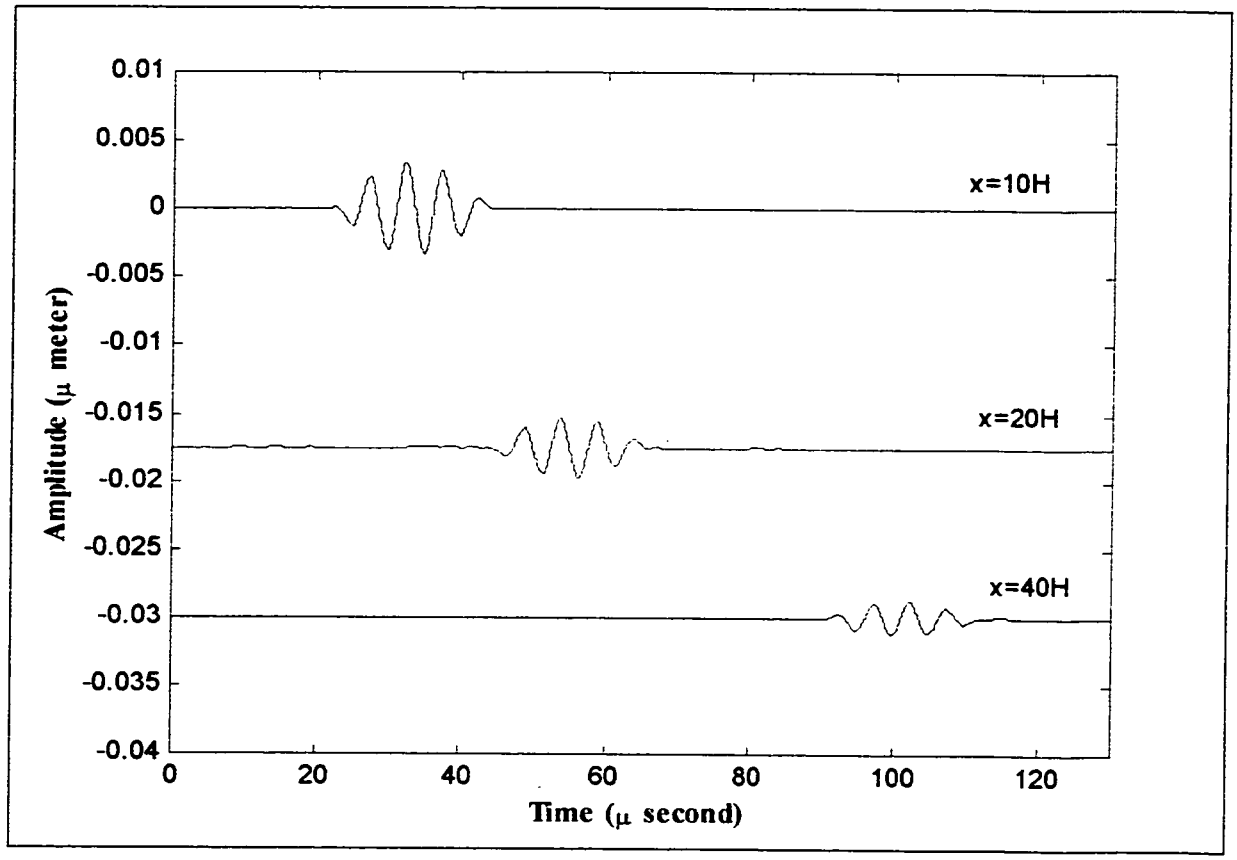

Figure 3.31: The transient response of the 12-ply plate along the 90° direction, at three different locations

The same 0.20 *MHz* central frequency amplitude modulated force was used to excite this plate. The plate is loaded by the liquid on both sides with same loading conditions given in Table 3.2.

In Figure 3.32, the transient normal displacement of the aluminum plate is plotted at three different locations, namely 10H, 20H, and 40H. It is clear that as the location gets far from the force source, the amplitude of the displacement gets smaller.

If the displacement of the isotropic plate of a given thickness, were compared to that of the composite plate of the same thickness, we would find that the amplitude of the displacement of the isotropic plate is greater. Furthermore, the wave suffers less distortion in its shape. This refers to the fact that the isotropic plate is composed of less dispersive materials. The group velocity was calculated for the aluminum plate and shown in Figure 3.33. Obviously, the group velocity of the isotropic plate is greater than that of the laminated composite plate. It is estimated to be approximately equal to 2528 *m/s* for the aluminum plate versus 1418 *m/s* for the 6-ply laminated plate under the same circumstances.

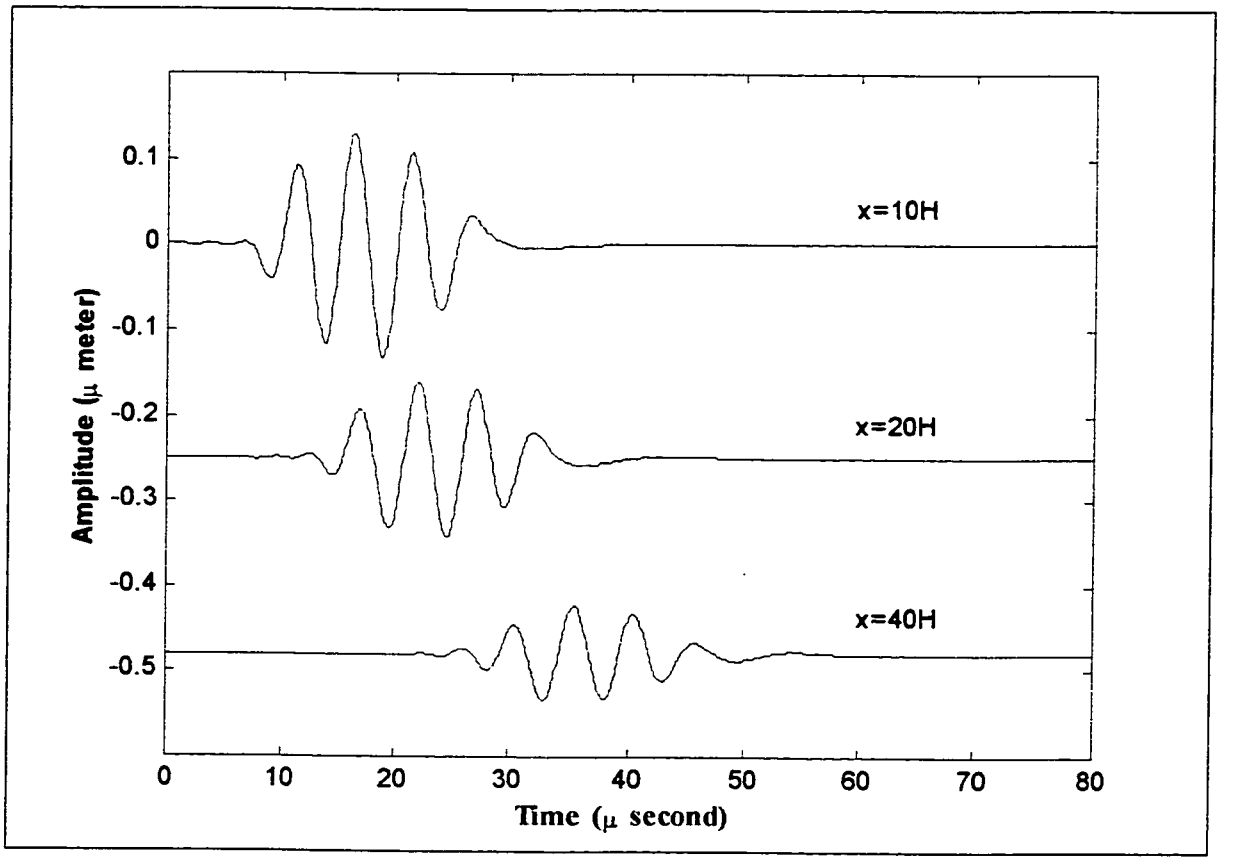

Figure 3.32: The transient response of the isotropic plate at three different locations

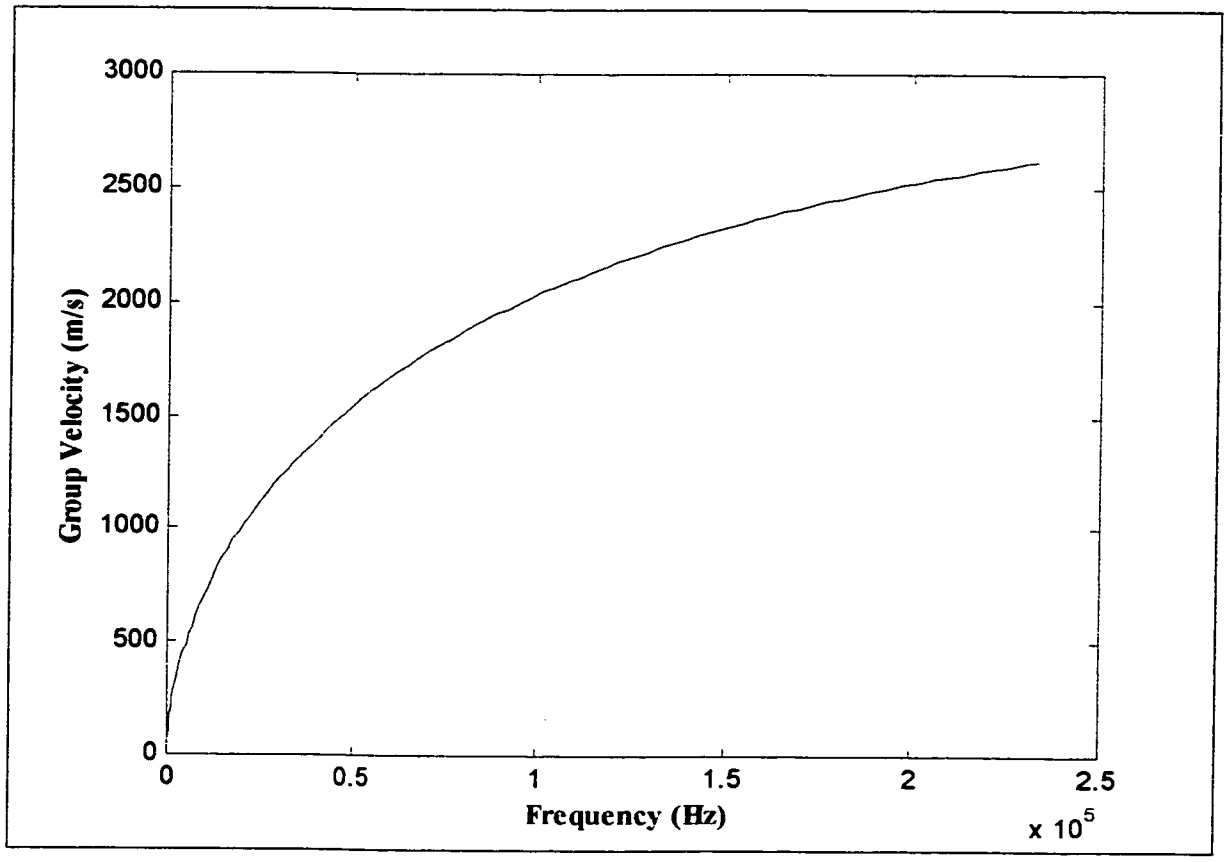

Figure 3.33: The group velocity of the isotropic plate

3.1.10 RESPONSE OF THE 6-PLY LAMINATED PLATE WITH AND WITHOUT LIQUID LOADING

The lower liquid effect on the normal transient response of the 6-ply laminated plate was investigated. First, we computed the normal response of the plate without the liquid loading. Then, we compared it with the response of the plate when the lower liquid loading was present. Both responses were calculated along the 0° direction at a location of 10H from the source. The two responses are shown in Figure 3.34. It is clear from the figure that the amplitude of the normal transient response of the plate is greater when the liquid is absent.

The group velocity for both cases were calculated and shown in Figure 3.35. It is clear that this group velocity when the liquid loading is absent is higher than its value when the liquid is present for all frequencies.

Next, the effect of changing the lower water liquid depth was investigated at a distance of 20H. The depth was varied from 0.05H up to 100H and the resulted responses are shown in Figure 3.36. We see that as the liquid depth increases, the amplitude of the normal transient response decreases. Figure 3.37 gives a closer look at the normal responses when the liquid depth is 0.05H and 100H. Clearer differences in the amplitude, signal phase and the group velocity of the wave are observed. The amplitude is reduced by a percentage of 12.50 and the group velocity drops from approximately 1354 *m/s* to 1332 *m/s*, as the depth increases from 0.05H to 100H. (See Figure 3.38)

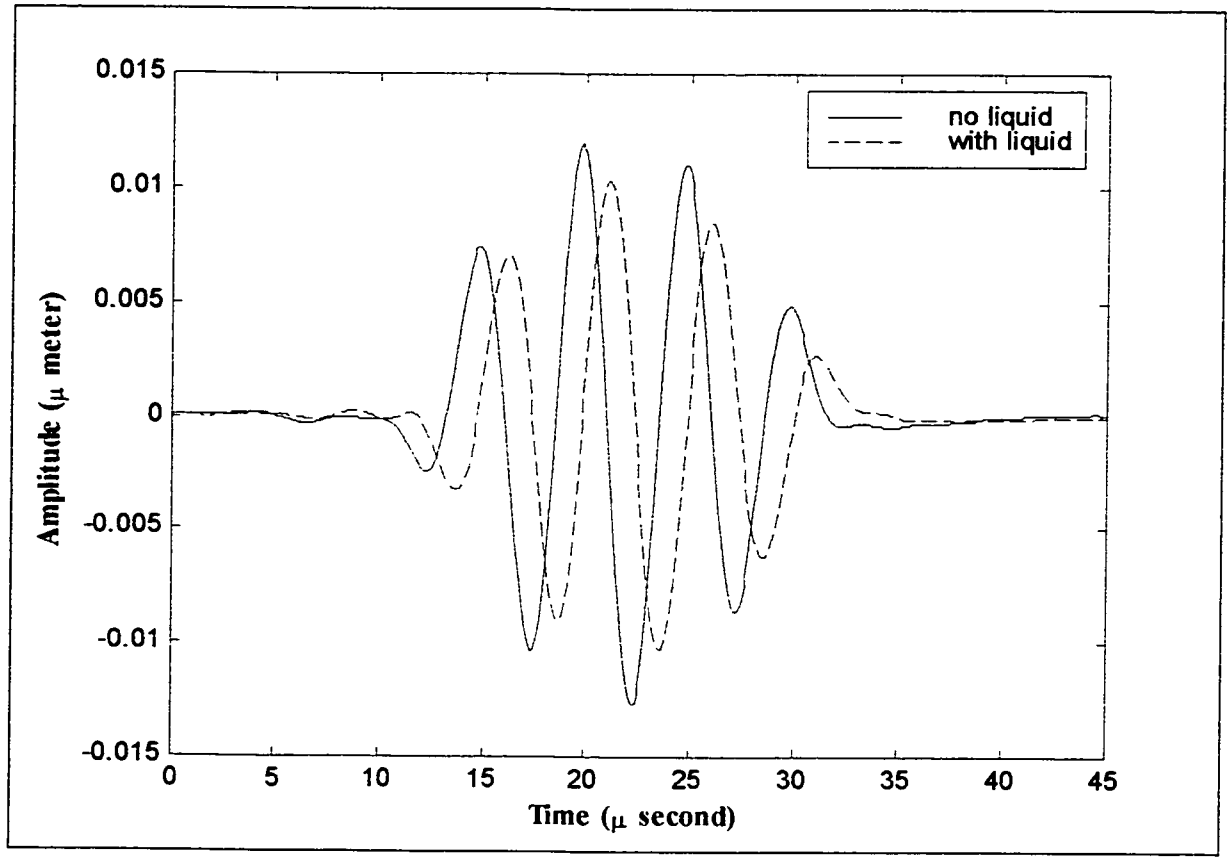

Figure 3.34: The transient response of the 6-ply plate along the 0° direction, with and without the liquid loading

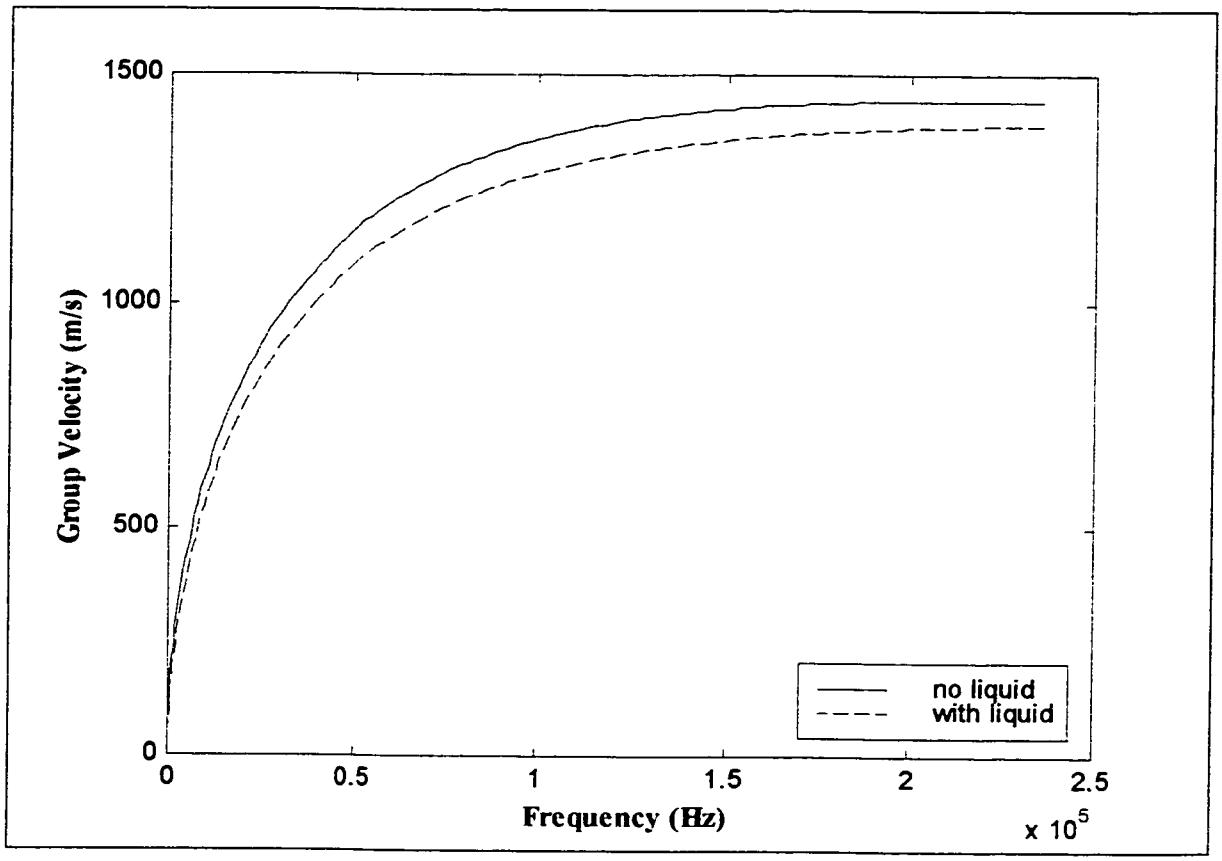

Figure 3.35: The group velocity of the 6-ply plate along the 0° direction with and without the liquid loading

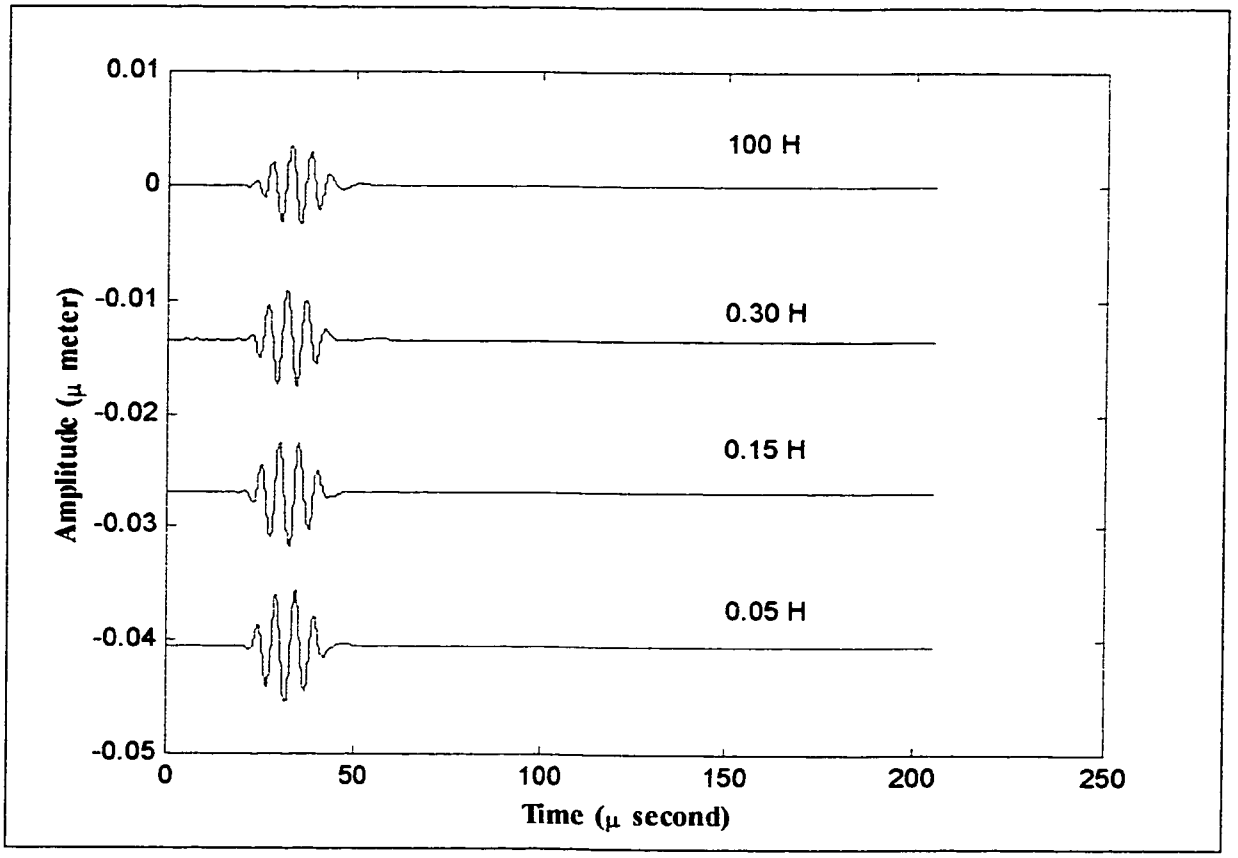

Figure 3.36: The transient response of the 6-ply plate along the 45° direction, with several H_2

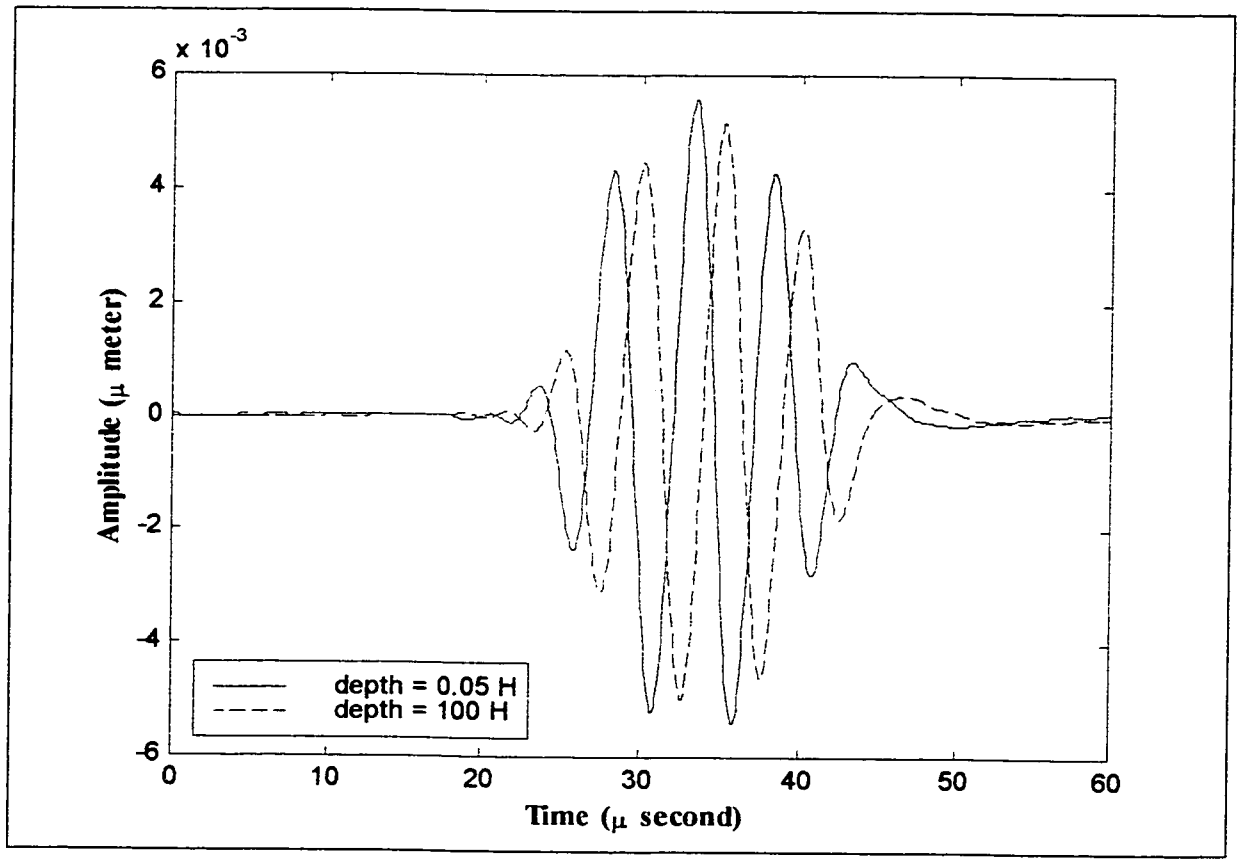

Figure 3.37: A closer look for H_2=0.05H and H_2=100H

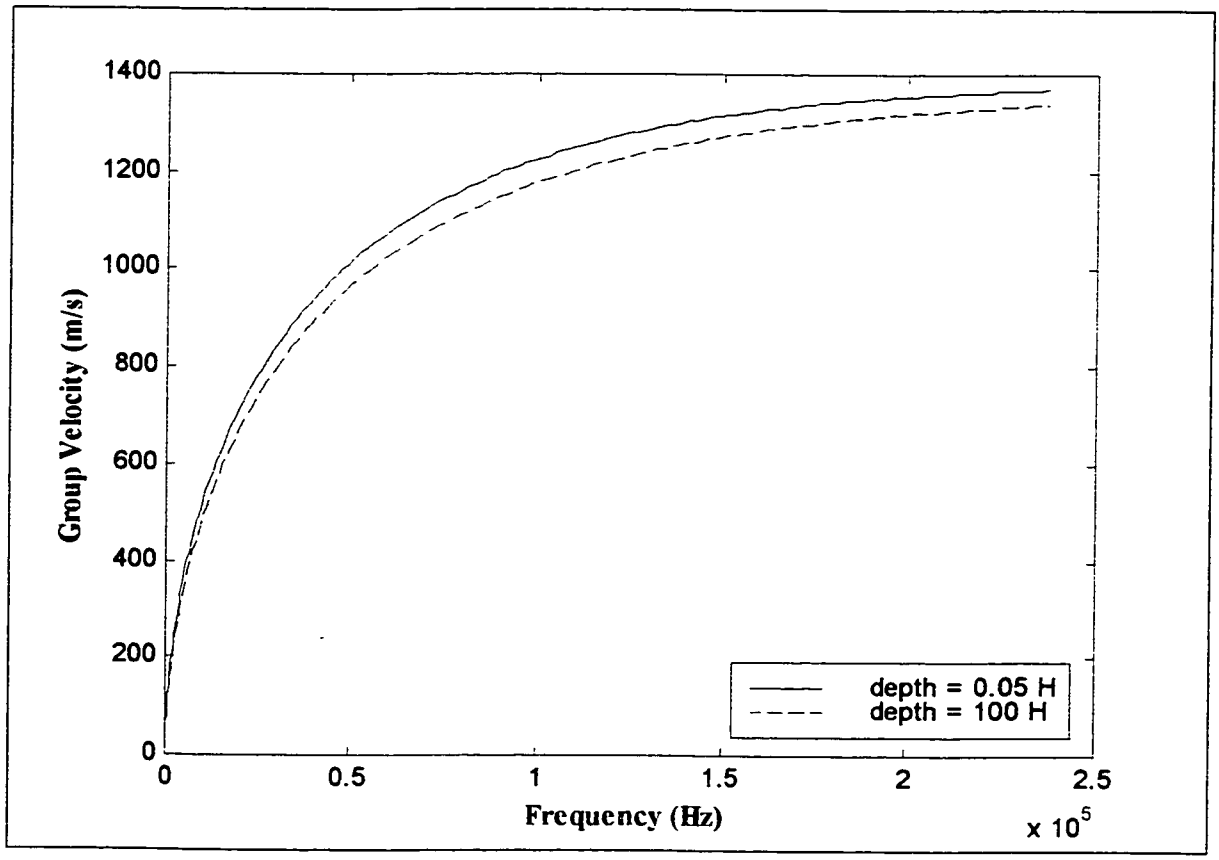

Figure 3.38: The group velocity of the 6-ply plate for H_2=0.05H, and H_2=100H

3.2 SINGLE MOVING LOAD

The second part of the present work was to investigate the plates under moving point loads with and without liquid loadings. The plates were excited by a moving harmonic point load having a magnitude of unity. Two types of plates were tested, namely, an isotropic plate and a 6-ply laminated composite plate. The properties of the isotropic and the 6-ply laminated plates are given in Tables 3.5 and 3.3, respectively. The plates were subjected to moving loads with continuous harmonic waveforms.

TABLE 3.5: Properties of the Isotropic Plate

ρ	366 kg/m^3
ν	0.35
λ	1.310×10^9 N/m^2
μ	5.615×10^9 N/m^2

An important term called the critical velocity of the moving load was investigated for both types of plate at two values of frequency, namely, 5 *Hz* and 50 *Hz*. The critical velocity of a moving load is defined as the velocity at which the maximum normal displacement of the plate occurs. The effects of both the liquid loadings and the foundation stiffness on the critical velocity were studied. Furthermore, the effect of the liquid depth on the critical velocity was investigated as well.

3.2.1 RELATION BETWEEN THE PLATE THICKNESS AND THE CRITICAL VELOCITY

First, the relation between the critical velocity and the plate thickness was investigated at a low frequency value of 3 *Hz*. Typically, the isotropic plate was studied in this case.

Initially, a 150 mm thick isotropic plate, was considered. The load speed was varied, and the maximum displacement of the plate was calculated at every speed and then plotted as in Figure 3.39. From the figure, the critical velocity (the velocity where the maximum normal displacement peak occurs) can be found to be approximately 193 *m/s*.

Similar figures were generated for other values of thickness at the same frequency. For instance, for a plate thickness of 4 mm, the critical velocity was approximately 13.0 *m/s*. (See Figure 3.40)

Critical velocities were calculated for several values of plate thickness and the results are shown in Figure 3.41. The plot shows the proportionality between the critical velocity of the moving load and the plate thickness at 3 *Hz*. It is clear that the critical velocity decreases as the plate thickness decreases. It drops from 193 *m/s* to 13 *m/s* as the thickness decreases from 150 *mm* to 4 *mm*.

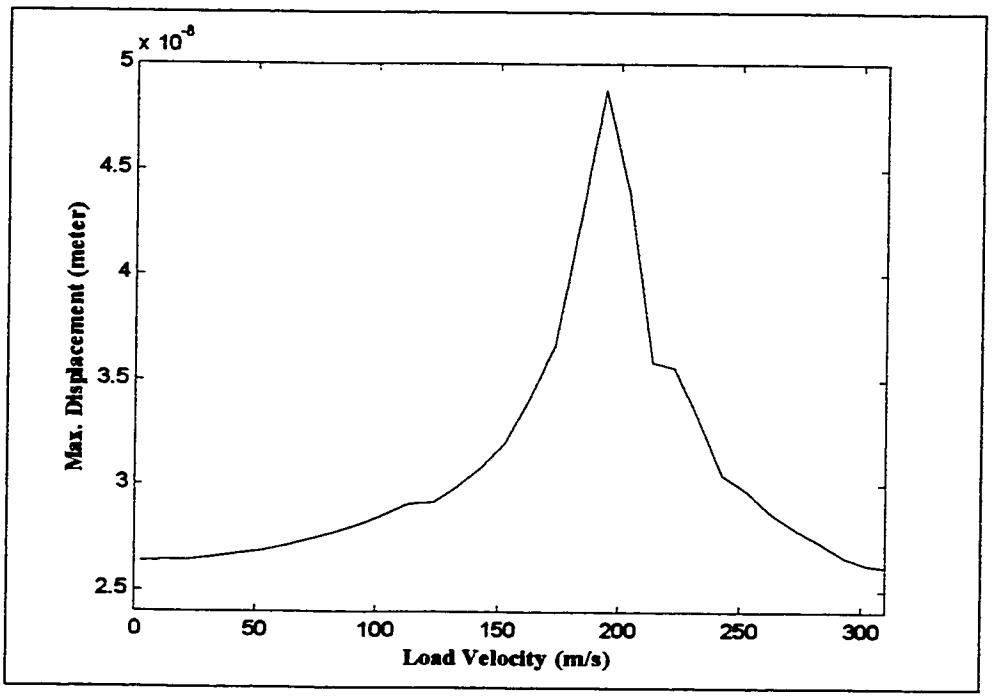

Figure 3.39: Maximum displacement versus load velocity for 150 mm thick plate

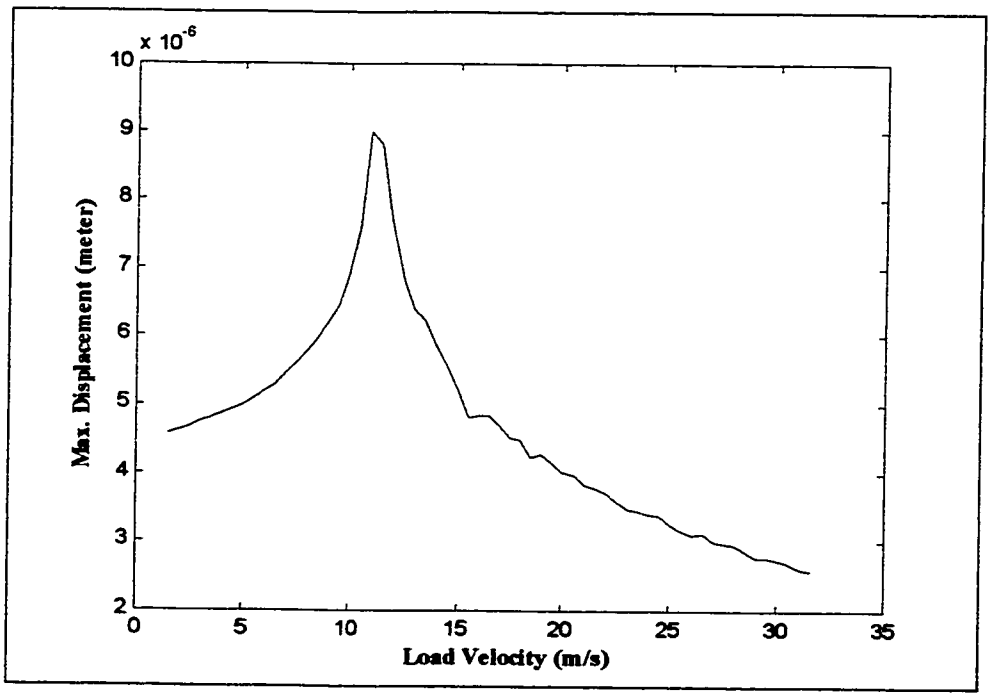

Figure 3.40: Maximum displacement versus load velocity for 4 mm thick plate

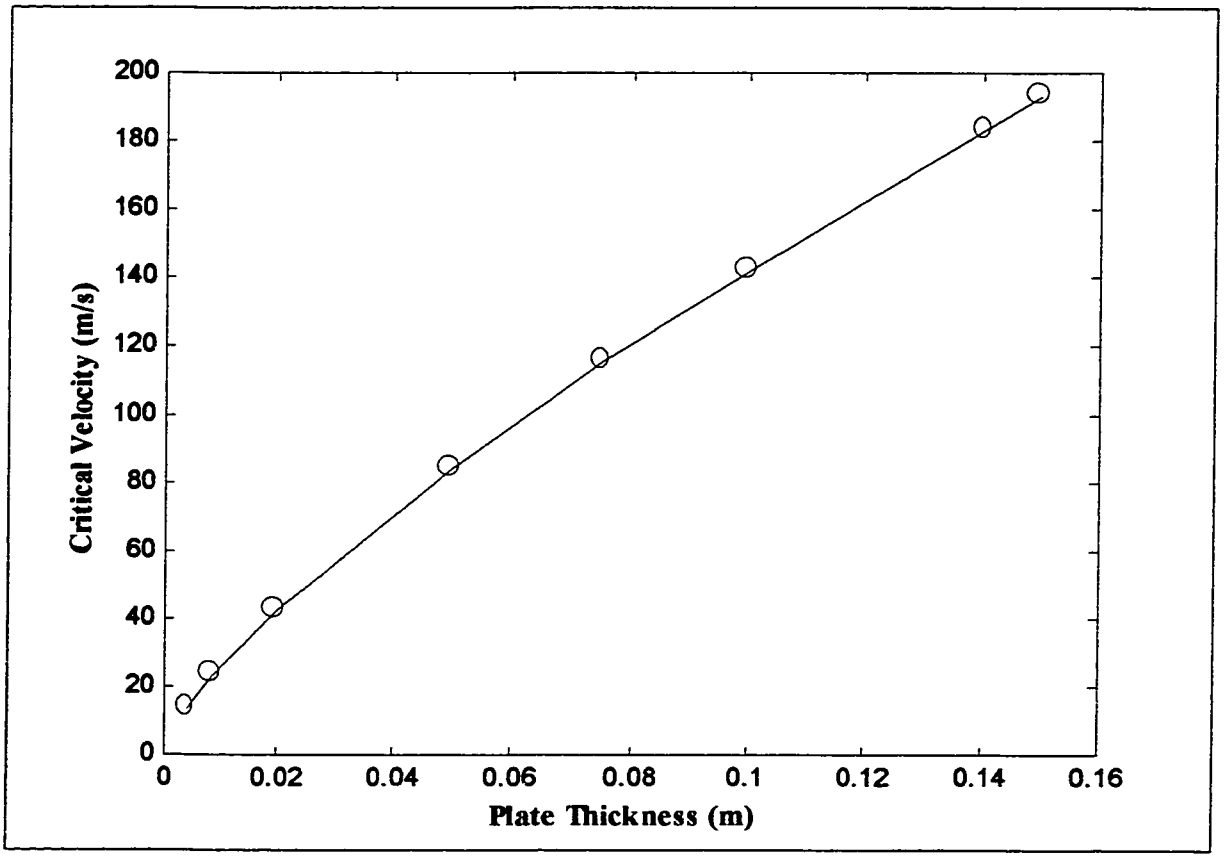

Figure 3.41: Critical velocity versus plate thickness

3.2.2 ISOTROPIC PLATES UNDER A MOVING LOAD OF 5 HZ FREQUENCY

The 4 *mm* thick isotropic plate having the properties of Table 3.5 was investigated under three different conditions for a low load-frequency of 5 *Hz*. First, no water loading on the plate was present whereas the stiffness of the elastic foundation was taken into account and was assumed to be 0.095×10^9 N/m^2. The maximum normal displacement of the plate was computed for various load velocities and shown in Figure 3.42. It can be seen from the figure that there exists a critical velocity ≈ 13.0 *m/s*.

Second, the maximum normal displacement was calculated when the lower liquid loading, with a depth of H, was present. The stiffness of the foundation was ignored in this case. The result is shown in Figure 3.43. From the figure, one can notice that the critical velocity is shifted toward zero. Moreover, a sharp drop in the maximum displacement is observed, once the force velocity increases beyond the zero.

Finally, the maximum normal displacement was computed when both the lower liquid loading and the foundation stiffness were taken into considerations. The result is shown in Figure 3.44. We notice that the curve is smoother than those of Figures 3.42 and 3.43 and more broadened than that of Figure 3.43. The critical velocity is still zero.

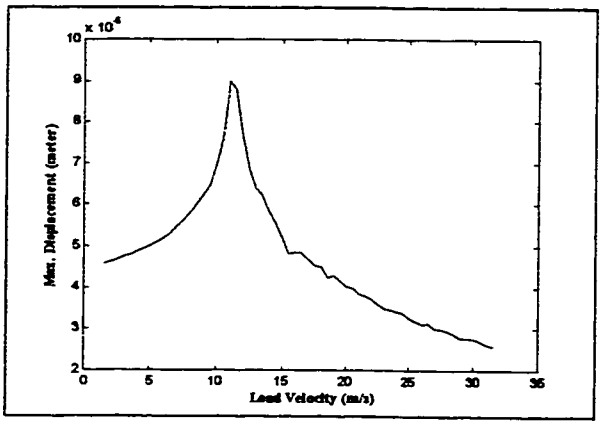

Figure 3.42: Maximum displacement versus the 5 Hz load velocity for the isotropic plate, with elastic foundation stiffness

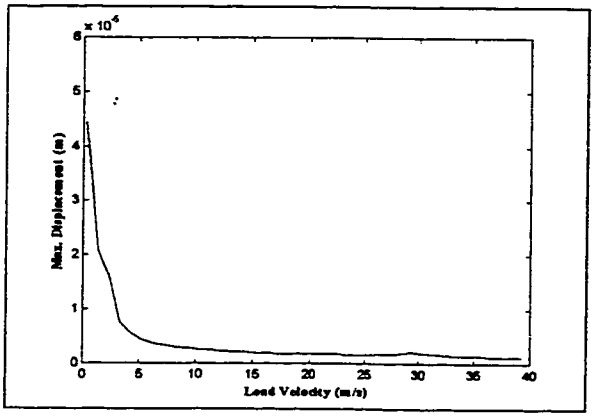

Figure 3.43: Maximum displacement versus the 5 Hz load velocity for the isotropic plate, with the lower water loading, without foundation stiffness

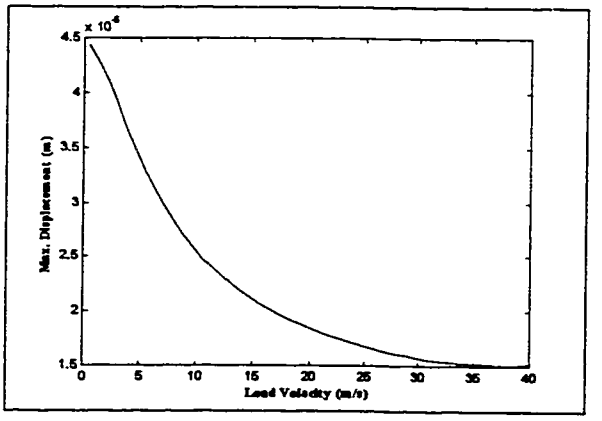

Figure 3.44: Maximum displacement versus the 5 Hz load velocity for the isotropic plate, with both foundation stiffness and water loading

3.2.3 ISOTROPIC PLATES UNDER A MOVING LOAD OF 50 HZ FREQUENCY

The previous investigations were repeated for the isotropic plate but under a moving load with a relatively higher frequency of 50 *Hz*. For the first case, where only the foundation stiffness was taken into consideration, the result is shown in Figure 3.45. It is notably clear that there are two critical velocities as the frequency is increased to 50 *Hz*. By comparing the current figure to Figure 3.42, it can be concluded that, for a low frequency load (near to zero), only one critical velocity will appear. However, for relatively higher load frequencies (around 50 *Hz*), another critical velocity was expected. The two critical velocities for this case are 11.0 *m/s* and 13.5 *m/s*.

Figure 3.46 presents the result for the case where only water loading exists. The curve rises to a peak value at a relatively low velocity (3.50 *m/s*), then drops steeply, and thereafter fluctuates as the velocity becomes higher. Therefore, it can be concluded that with the absence of the foundation stiffness, fluctuation in the maximum displacement are more pronounced, especially with higher frequency loads. This can be demonstrated by comparing the curve Figure 3.46, where the frequency is 50 *Hz*, with that of Figure 3.43, where the frequency is 5 *Hz*.

For the last case, when both lower water loading and foundation stiffness are considered, the effects of the water loading and foundation stiffness add. The critical velocity shifts to zero due to the presence of water and the curve is quite smooth with no fluctuations due to the presence of foundation as shown in Figure 3.47.

3.2.4 6-PLY LAMINATED PLATES UNDER A MOVING LOAD OF 5 HZ FREQUENCY

The 6-ply laminated plate was investigated under a moving load with a low frequency of 5 *Hz* for the three cases mentioned earlier. Similar to the isotropic plate, one critical velocity was found for the first case but with a higher value of approximately 90.0 *m/s* as shown in Figure 3.48. If this figure were compared to the corresponding one of the isotropic plate Figure 3.42, we can see that the magnitude of the critical velocity is higher for the laminated plate.

In the second case, as shown in Figure 3.49, similar to what has been noticed for the isotropic plate, the critical velocity is shifted toward zero with a maximum value of displacement, then the curve drops steeply and converges to a constant value of displacement as the velocity increases.

In the last case, where both lower liquid loading and foundation stiffness were considered, the critical speed was shifted towards zero and the curve is quite smoother and more broadened (See Figure 3.50).

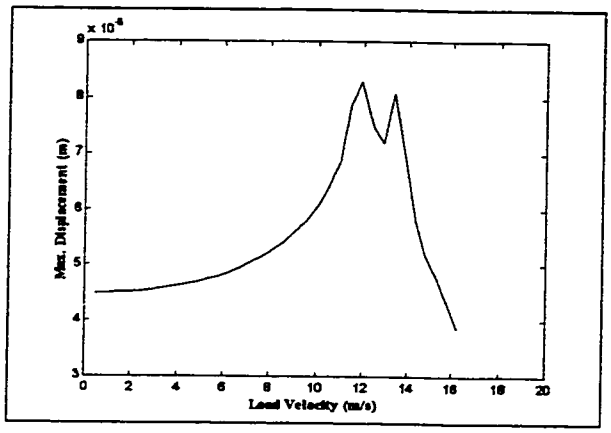

Figure 3.45: Maximum displacement versus the 50 Hz load velocity for the isotropic plate, with foundation stiffness

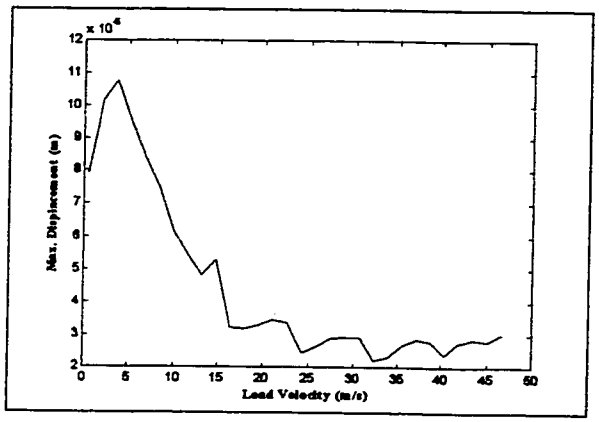

Figure 3.46: Maximum displacement versus the 50 Hz load velocity for the isotropic plate, with the lower water loading, without foundation stiffness

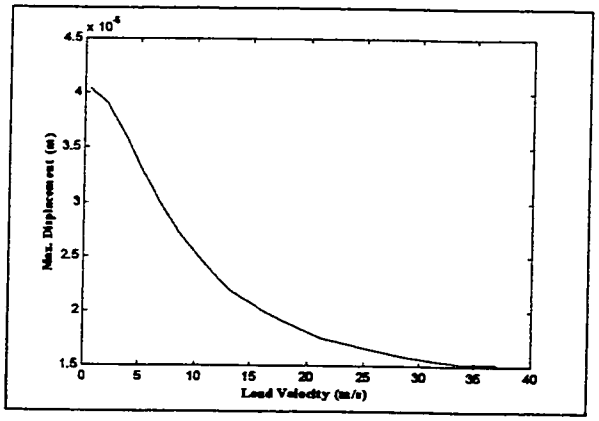

Figure 3.47: Maximum displacement versus the 50 Hz load velocity for the isotropic plate, with both foundation stiffness and water loading

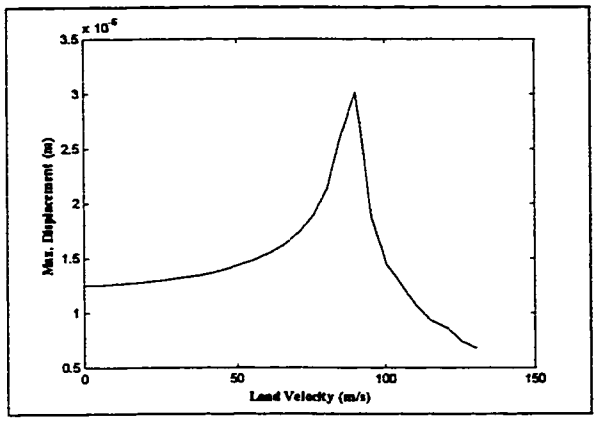

Figure 3.48: Maximum displacement versus the 5 Hz load velocity for the 6-ply laminated plate, with foundation stiffness

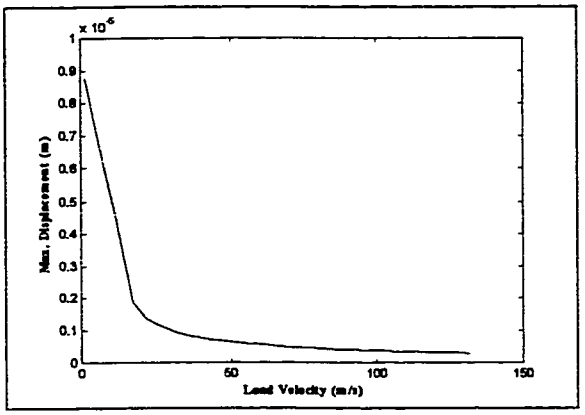

Figure 3.49: Maximum displacement versus the 5 Hz load velocity for the 6-ply laminated plate, with the lower water loading, without foundation stiffness

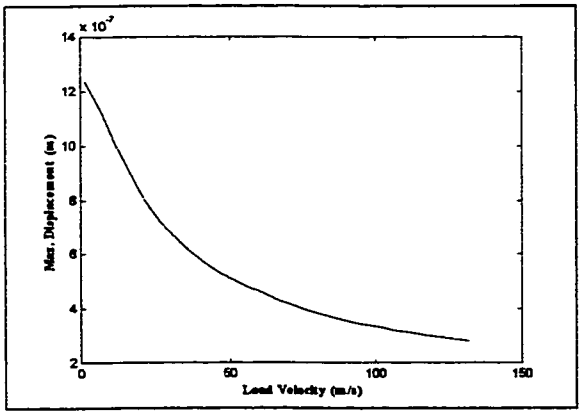

Figure 3.50: Maximum displacement versus the 5 Hz load velocity for the 6-ply laminated plate, with both foundation stiffness and water loading

3.2.5 6-PLY LAMINATED PLATES UNDER A MOVING LOAD OF 50 HZ FREQUENCY

Here, the 50 *Hz* moving load is applied to the 6-ply laminated plate under the three cases mentioned earlier. Dissimilar in the first case to the low frequency force, two peaks corresponding to the two critical velocities can be observed at approximately 92.0 *m/s* and 105 *m/s*, as shown in Figure 3.51. Thereafter, fluctuations in the maximum displacement curve start to appear for higher velocities (beyond the second critical velocity).

In the second case, where only water loading was considered, the curve starts smoothly rising to its maximum peak clearly, at a speed of 17.0 *m/s* (See Figure 3.52). Only one critical velocity can be seen. For higher velocities, fluctuations are more pronounced in contrast to the low frequency case where they were almost absent.

Figure 3.53 shows the results when both the water loading and the stiffness of the foundation were considered. The critical velocity is shifted to zero, and the curve exhibits smooth characteristics without noticeable fluctuations. It is also worth mentioning here that the curve is a little bit more broadened in the vicinity of zero velocity when compared to the corresponding low frequency case (See Figure 3.49).

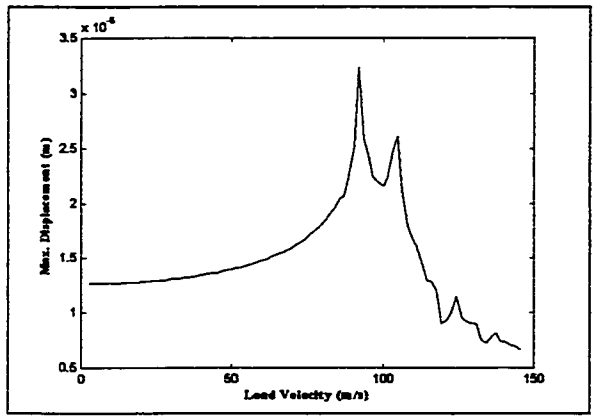

Figure 3.51: Maximum displacement versus the 50 Hz load velocity for the 6-ply laminated plate, with foundation stiffness

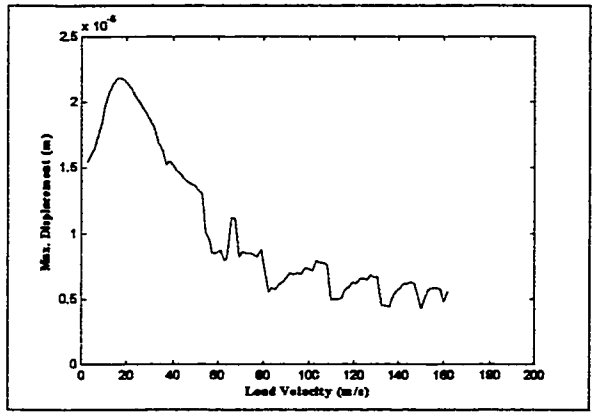

Figure 3.52: Maximum displacement versus the 50 Hz load velocity for the 6-ply laminated plate, with the lower water loading, without foundation stiffness

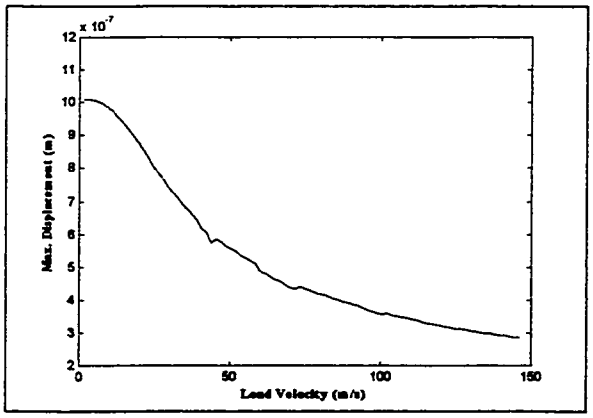

Figure 3.53: Maximum displacement versus the 50 Hz load velocity for the 6-ply laminated plate, with both foundation stiffness and water loading

3.2.6 EFFECT OF THE UPPER LIQUID DEPTH ON BOTH PLATES

In this section, the maximum displacement was calculated against various load velocities for three depths of the upper liquid, namely, 0.05H, H, and 100H while the lower liquid depth was kept constant at 100H. The 50 *Hz* moving load was applied to both the isotropic and the 6-ply plates and the results are shown in Figures 3.54 and 3.55. In both figures, as the depth increases, the critical velocity is shifted to the right and the maximum displacement magnitude becomes larger. Moreover, it should be noted that the fluctuations in the composite plate is more pronounced here.

3.2.7 EFFECT OF THE LOWER LIQUID DEPTH ON BOTH PLATES

The same calculations were performed for both plates again to see the effect of the lower liquid depth as well. In contrast to the last case, as the depth increases the critical velocity is shifted to the left, while the maximum displacement curve is reduced as shown in Figures 3.56 and 3.57. Moreover, the fluctuations are observed to be more pronounced in this case.

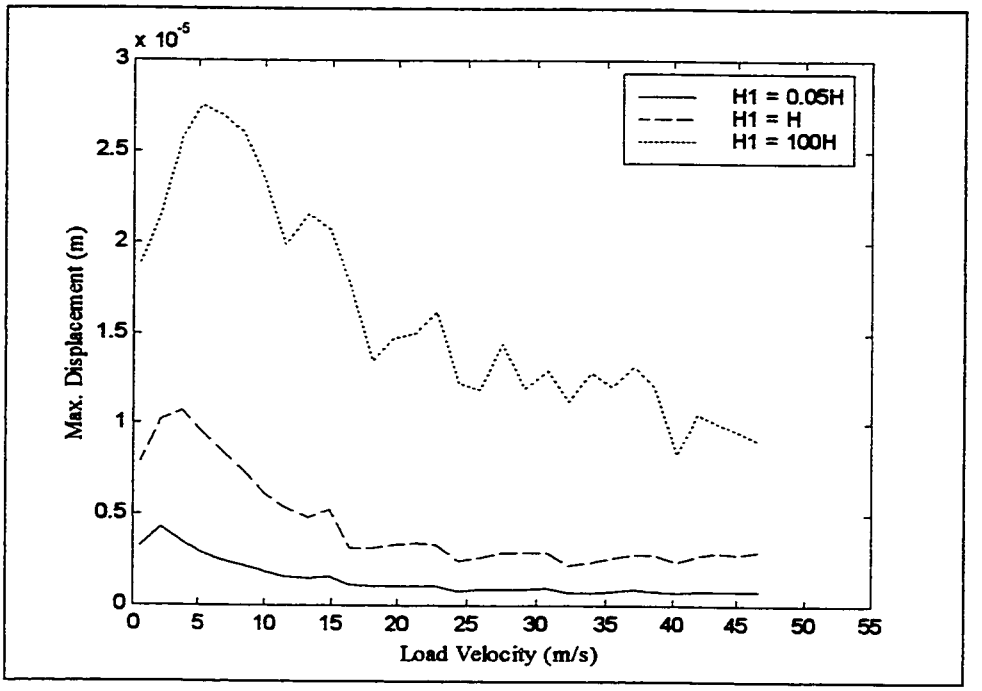

Figure 3.54: The upper liquid depth (H_1) effect on the maximum displacement versus load velocity curve for the isotropic plate

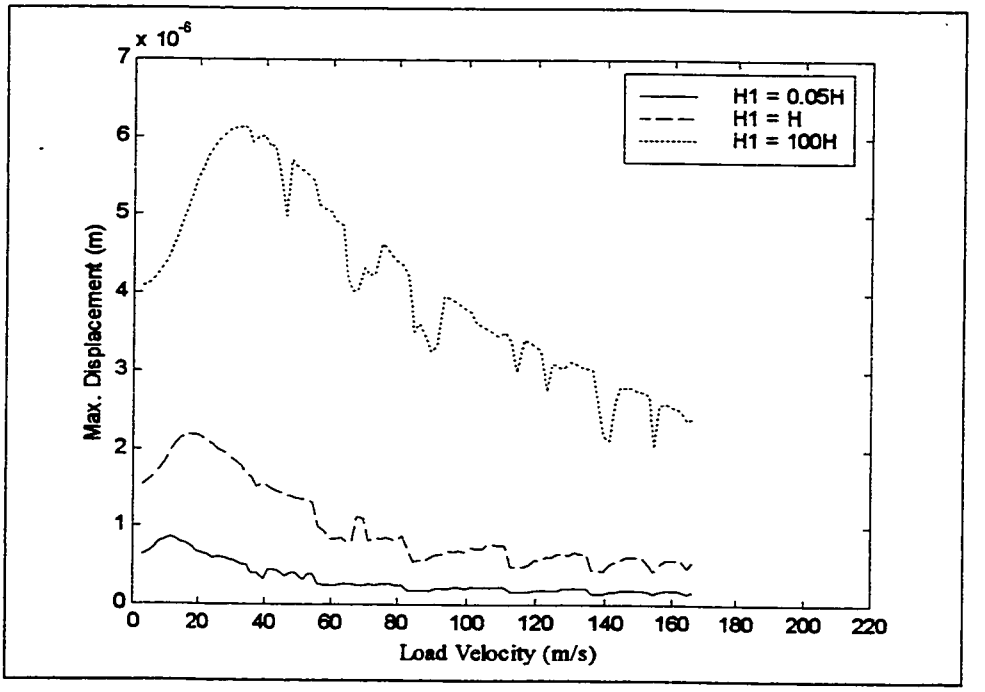

Figure 3.55: The upper liquid depth effect (H_1) on the maximum displacement versus load velocity curve for the 6-ply laminated plate

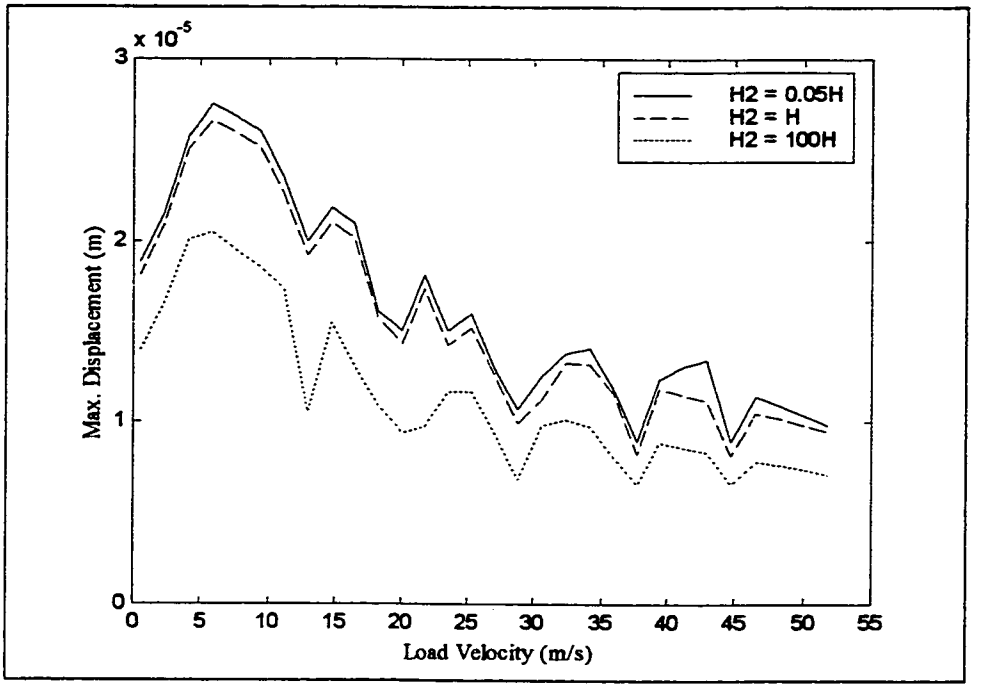

Figure 3.56: The lower liquid depth (H_2) effect on the maximum displacement versus load velocity curve for the isotropic plate

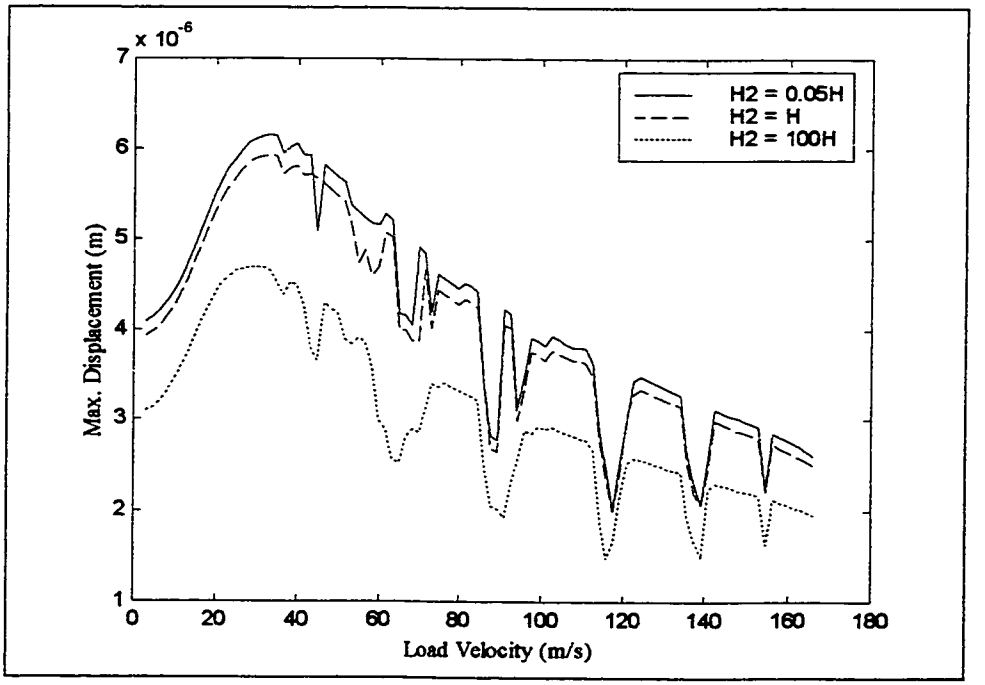

Figure 3.57: The lower liquid depth effect (H_2) on the maximum displacement versus load velocity curve for the 6-ply laminated plate

3.3 PLATES UNDER TWO MOVING LOADS

The last task of this work was to investigate the dynamic response of both the isotropic plate and the 6-ply laminated plate, with elastic foundation, when subjected to two simultaneous moving loads. Both loads were traveling with a velocity V in a direction parallel to η direction (refer to Figure 2.5 in Chapter 2), with a frequency of 10 *Hz*. The distance between the two loads are chosen to be as follows:

$L_\eta = 0.5\ m$, and $L_\varsigma = 0.0\ m$.

The effect of the phase difference between the two loads on the maximum displacement of both the isotropic and laminated plates was studied. Furthermore, the effect of the load velocities was also investigated.

3.3.1 THE ISOTROPIC PLATE

Figure 3.58 shows the relation between the maximum dynamic displacement divided by the maximum static displacement (displacement when the velocity is zero at a frequency near to zero) of the isotropic plate, and the phase difference between the two loads for various load speeds. The maximum displacement decreases, as the phase becomes close to 180° then it increases again. The curve is symmetric with respect of a phase of 180° for stationary harmonic loads (V = 0), but not for moving

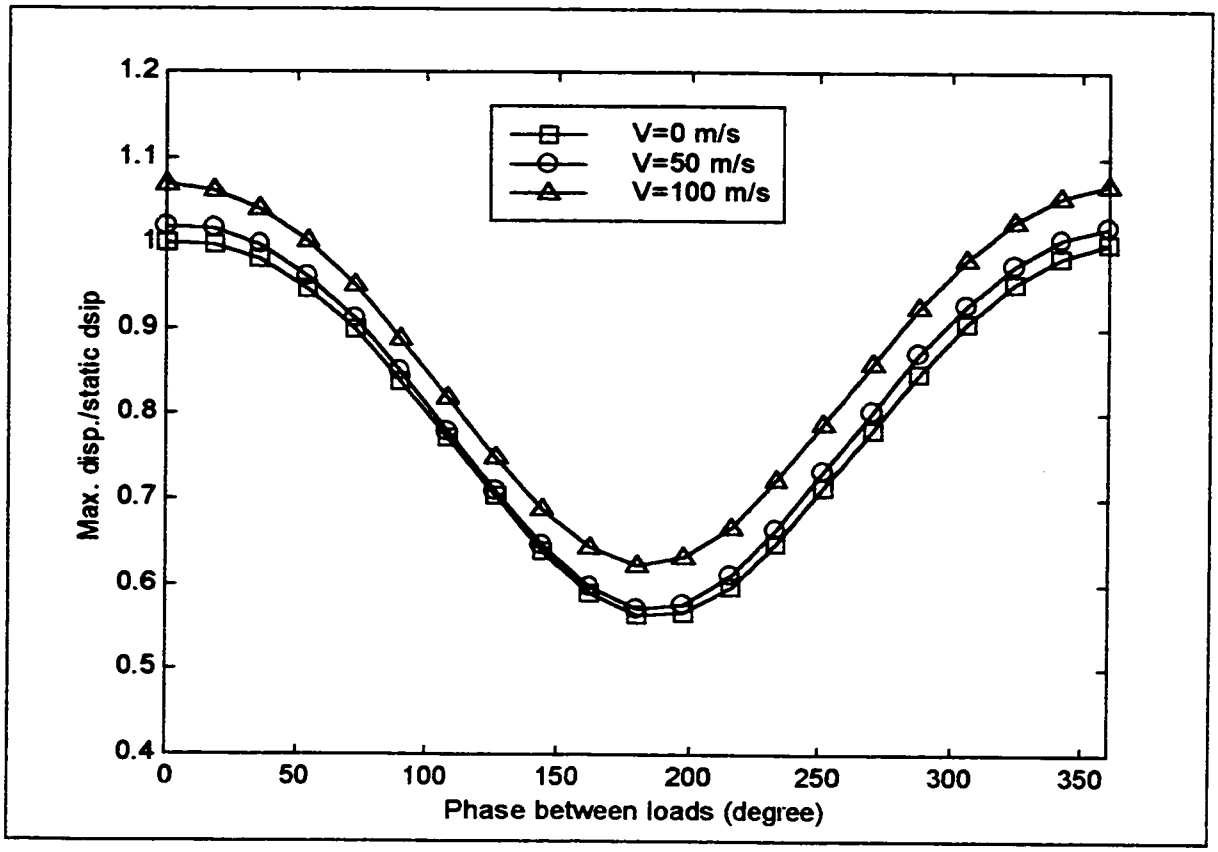

Figure 3.58: Effect of phase difference between the two moving loads on maximum displacement for the isotropic plate

loads ($V \neq 0$). One can observe the large difference between the maximum displacements for phase angles 0 and 180° (45% change). Therefore, a phase difference between loads can reduce the maximum displacement significantly. Moreover, it is obvious that the maximum displacement increases with the load speed for all the phase values, which is also shown below.

Next, the variation of the maximum displacement of the isotropic plate with increasing speed of various phase angles was investigated as shown in Figure 3.59. For all value of phase angles, the maximum displacement increases as the speed increases. Change in the maximum displacement with 0° and 90° phase angle is almost 6.50% whereas it is almost 9.60% with 180° phase angle. The figures also show that at low speed (less than 30.0 m/s) the change in maximum displacement is negligible.

3.3.2 THE 6-PLY LAMINATED PLATE

Figure 3.60 shows the relation between the maximum dynamic displacement divided by the maximum static displacement for 6-ply laminated plate, and the phase difference between the two loads for various load speeds. A large difference (about 55 %) between the maximum displacement for the phase angles of 0 and 180° is observed in this case. Notice that this percentage difference is greater than that of the isotropic plate (Figure 3.58). Thus, changing the phase angle can considerably reduce or increase the maximum displacement.

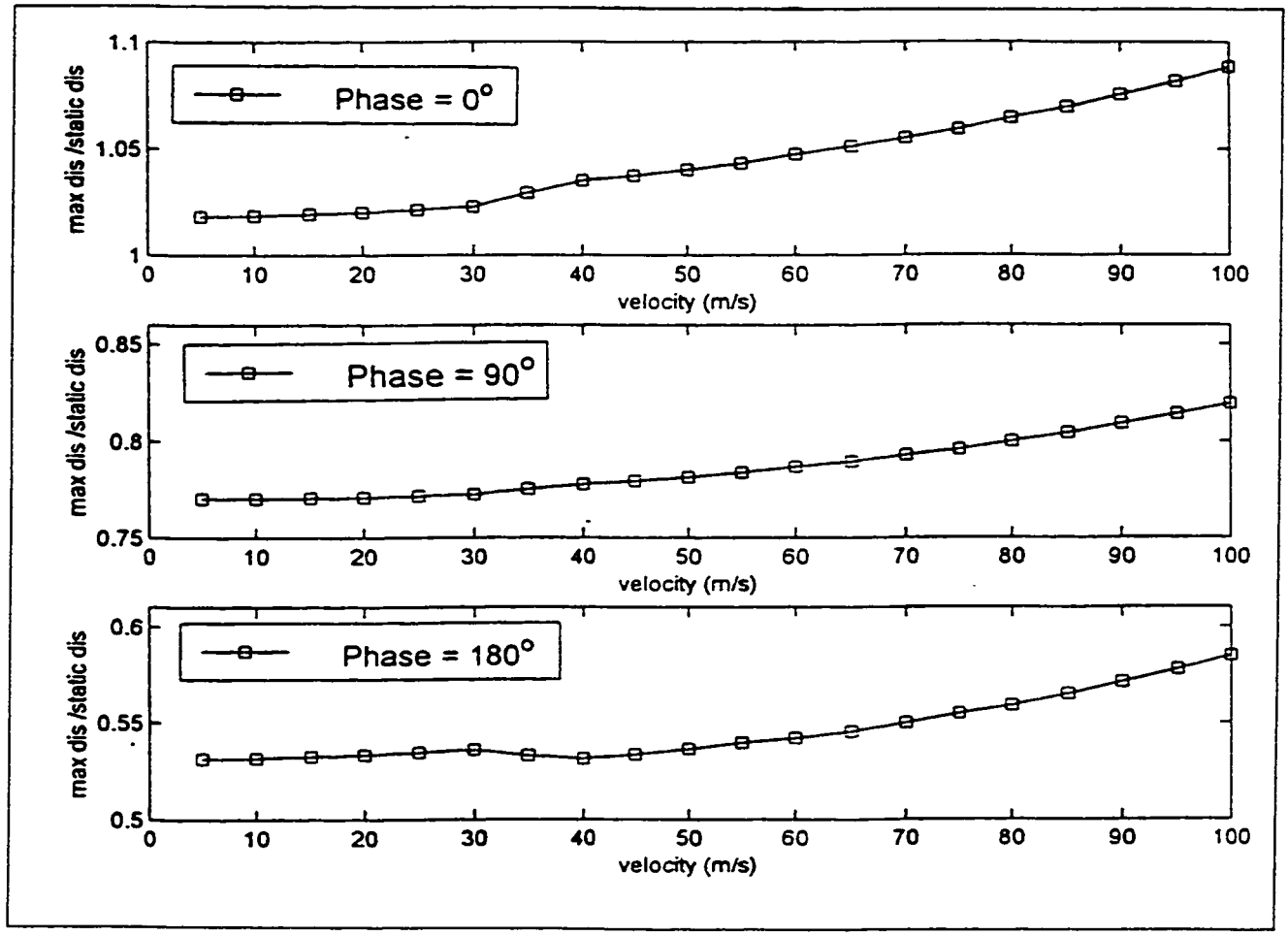

Figure 3.59: Effect of the two moving loads velocity for 0°, 90° and 180° phase respectively for the isotropic plate

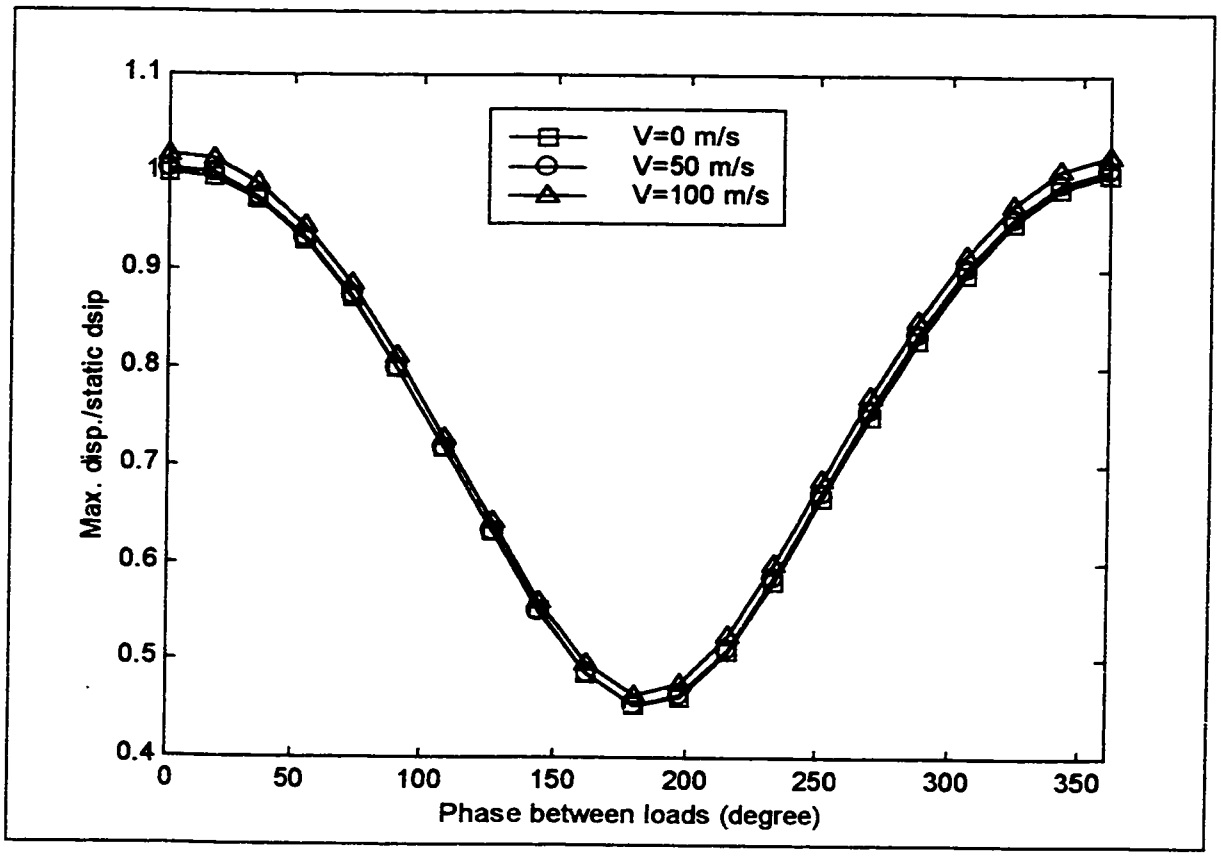

Figure 3.60: Effect of phase between the two loads on maximum displacement for the 6-ply laminated plate

Finally, the variation of the maximum displacement of the composite plate with increasing speed at various phase angles was studied for the laminated plate and shown in Figure 3.61. From the figure, it is noted that the maximum displacement increases as the speed increases. For 0° phase angle, a negligible change in maximum displacement can be noticed until the speed reaches 30 *m/s*, where the maximum displacement increases noticeably. For the same phase angle, the maximum displacement change is approximately 1.40 % when speed changes from 0 to 100 m/s. For 90° phase angle, this change is approximately 0.76 % whereas it is about 0.50 % for 180°. These percentages are much less than those of the isotropic plate. Furthermore, complexity of the composite plate appears in Figure 3.61 in terms of fluctuations especially for 180° phase angle.

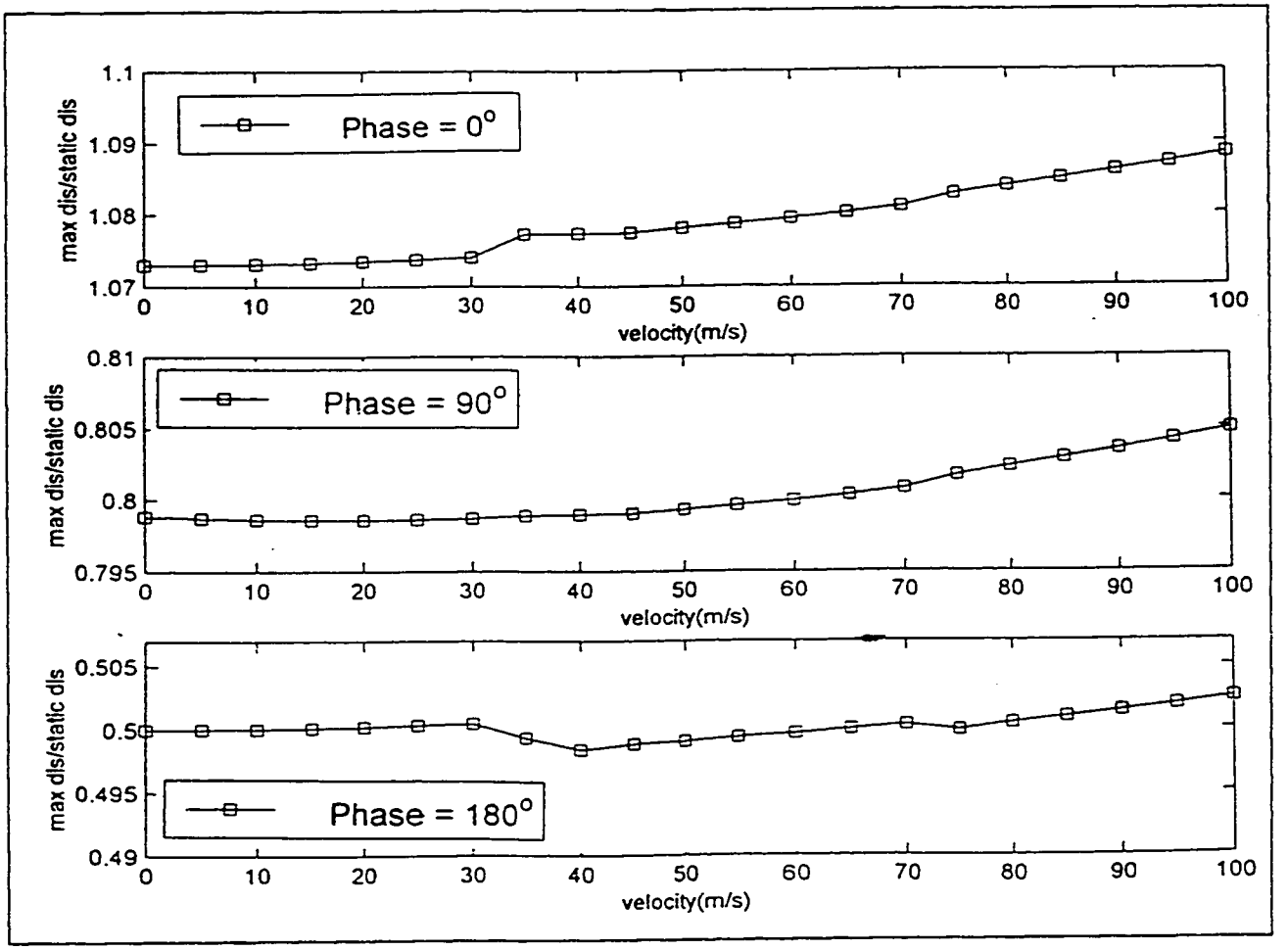

Figure 3.61: Effect of the velocity for 0°, 90° and 180° phase respectively for the 6-ply laminated plate

CHAPTER 4

CONCLUSIONS

The propagation of waves in laminated composite plates is more complex than that in isotropic plate. This is due to their higher degree of anisotropy (more elastic properties needed to describe the material), the fact that the composite plate may be constructed of several layers of different properties, and the interaction of the propagating waves with fibers and the layers interfaces. Most of the previous work done in the field of wave propagation in plates was performed for laminated plates without liquid loading and under a stationary load. However, in the present study, laminated plates behaviors were investigated under different loading conditions, specifically, liquid loads, stationary or moving loads, and two moving loads. Dispersion curves were constructed under different loading conditions. Normal transient responses were calculated for four plates; namely, isotropic, 3-ply, 6-ply, and 12-ply laminated plates along three main directions at three

different locations. Furthermore, plates subjected to a single or double harmonically moving load were investigated.

Dispersion curves of the 3-ply laminated plate under the liquid loadings were calculated at the three main directions. The wave propagation in plate was first modeled when the two liquids are different. The simulation was repeated for the plate under two identical liquid loadings and was validated for an isotropic plate by Bao [8]. It has been seen that the effect of the denser liquid on dispersion curves is more pronounced. We also saw that the dispersion curves were affected more by changing the depth of the lower liquid. The phase velocity increases as the depth of the lower liquid increases whereas it decreases as the depth of the upper liquid increases. Effects of density of both liquids on dispersion curves were studied as well and this was validated for an isotropic plate by Dabirikhah [2]. In contrast to the liquid depth effect, the effect of changing the liquid density is independent of the liquid location. In other words, the phase velocity decreases as the density of either liquid increases no matter which liquid density is chosen to be varied.

The normal transient responses were computed for an isotropic plate, and for the three laminated plates under liquid loadings. To perform this computation in laminated plates, multiple transform technique was applied to the higher order approximate solution for laminated plates. Even though, it was an approximate solution, the computational time was high. This was due to the irregular behavior of the integrated function. Also, this

solution required the double integration procedures to be done at discrete frequencies. To carry out the evaluation of such function, a one dimensional integration algorithm based on Romberg's method was modified to a two dimensional algorithm. This technique predicts transient responses of the flexural (a_o) mode only. Therefore, it is used at low (f*H) values where only the flexural mode is likely to exist. From the results, the phenomenon of anisotropy in laminated plates is found to be more pronounced when compared to isotropic plates. The effects of liquid loading on the normal transient responses of plates were discussed. We saw that as the lower liquid depth increases, the magnitude of the response decreases, and so does the group velocity.

The final part of the present work was to investigate the plates under moving loads. First, a harmonically single moving point load was used. For low frequency load, one critical velocity of the load is found, however, two critical velocities were found for higher frequencies. The critical velocity was found to be higher for the laminated plates. Moreover, the addition of liquid loading and/or the foundation stiffness to the system could considerably affect its critical velocities. Second, the plates were investigated under two harmonically moving point loads. Changing the velocity of the loads resulted in a bigger change in the maximum displacement of the plate. It has been also seen that the phase difference between the two loads can considerably affect the responses of the plate. A phase value of π produces the lowest response of a plate subjected to such loading. In this type of loading, the irregular behavior of the laminated composite plates can be

noticed here as well. The investigation of isotropic plates under a single or double moving loads was validated by Kim [14].

The major conclusions drawn from the present work can be summarized as

- As the upper liquid depth increases, the phase velocity decreases, whereas as the lower liquid depth increases the phase velocity increases.
- As the density of either liquid increases the phase velocity decreases.
- The group velocity is greater in the direction where more fibers exist.
- The attenuation of the normal transient response becomes larger as the number of the lamina increases.
- The amplitude of the normal response and the group velocity are greater when the liquid loading is absent.
- As the depth of the lower liquid increases the amplitude of the response decreases and the group velocity decreases.
- For moving loads, the critical velocity of the load decreases as the thickness of the plate decreases.
- For low frequency moving load (5 Hz), one critical velocity exists, however, for relatively high frequency moving load (5o Hz), two critical velocities exist.
- The existence of the water loading in moving load case shifts the critical velocity of the load toward zero whereas the existence of the elastic foundation smoothens the maximum displacement vs. load velocity curve.

- For two moving loads, the maximum displacement is the smallest when the phase difference between the loads is equal to π.

As an extension of this work, some suggestions can be introduced for future work in this area. An experimental work can be done for the laminated plates under the previously mentioned conditions and subsequently compared with the theoretical one. The type of the liquid can be changed to viscous compressible in order to be more analogous to the real life applications. Moreover, other systems can be investigated such as plate/fluid/plate system. Finally, other solving techniques such as Finite Element Method can be utilized and compared to those used here.

Appendix I

STATIONARY LOADS

The matrix $[M]$ for the approximate plate theory is defined as

$$\begin{bmatrix} -(\kappa A_{55}\xi_1^2 + \kappa A_{44}\xi_2^2 - \rho^* H\omega^2) + \rho_1\omega^2\Lambda_1\Gamma_1 - \rho_2\omega^2\Lambda_2\Gamma_2 & \kappa A_{55}\xi_1 i & \kappa A_{44}\xi_2 i \\ \kappa A_{55}\xi_1 i & D_{11}\xi_1^2 + D_{66}\xi_2^2 + \kappa A_{55} - I\omega^2 & (D_{12} + D_{66})\xi_1\xi_2 \\ \kappa A_{44}\xi_2 i & (D_{12} + D_{66})\xi_1\xi_2 & D_{22}\xi_2^2 + D_{66}\xi_1^2 + \kappa A_{44} - I\omega^2 \end{bmatrix}$$

Where

$$\Lambda_1 = \frac{1}{\beta\sinh(\beta\frac{H}{2}) - \beta\coth\left[\beta(H_1 + \frac{H}{2})\right]\cosh(\beta\frac{H}{2})}$$

$$\Gamma_1 = \cosh(\beta\tfrac{H}{2}) - \coth\left[\beta(H_1 + \tfrac{H}{2})\right]\sinh(\beta\tfrac{H}{2})$$

$$\Lambda_2 = \frac{1}{\beta\tanh\left[\beta(H_2 + \frac{H}{2})\right]\cosh(\beta\frac{H}{2}) - \beta\sinh(\beta\frac{H}{2})}$$

and,

$$\Gamma_2 = \cosh(\beta\tfrac{H}{2}) - \tanh\left[\beta(H_2 + \tfrac{H}{2})\right]\sinh(\beta\tfrac{H}{2})$$

with ,

$$\beta = \sqrt{\xi_1^2 + \xi_2^2}$$

The constitutive relations of Equation (2.10)

$$\begin{bmatrix} N_x \\ N_y \\ N_{xy} \\ M_x \\ M_y \\ M_{xy} \end{bmatrix} = \begin{bmatrix} A_{11} & A_{12} & A_{16} & B_{11} & B_{12} & B_{16} \\ A_{12} & A_{22} & A_{26} & B_{12} & B_{22} & B_{26} \\ A_{16} & A_{26} & A_{66} & B_{16} & B_{26} & B_{66} \\ B_{11} & B_{12} & B_{16} & D_{11} & D_{12} & D_{16} \\ B_{12} & B_{22} & B_{26} & D_{12} & D_{22} & D_{26} \\ B_{16} & B_{26} & B_{66} & D_{16} & D_{26} & D_{66} \end{bmatrix} \begin{bmatrix} \varepsilon_x^o \\ \varepsilon_y^o \\ \varepsilon_{xy}^o \\ \chi_x \\ \chi_y \\ \chi_{xy} \end{bmatrix}$$

where

$$(A_{ij}, B_{ij}, D_{ij}) = \int_{-H/2}^{H/2} Q_{ij}^{(K)} (1, z, z^2) dz \qquad i, j = 1,2,6$$

Appendix II

MOVING LOADS

The matrix $[\overline{M}]$ for the approximate plate theory is defined as

$$\begin{bmatrix} -(\kappa A_{55}\bar{\xi}_1^2 + \kappa A_{44}\bar{\xi}_2^2 - \rho^* H \underline{\underline{\omega}}^2) + \rho_1 \underline{\underline{\omega}}^2 \bar{\Lambda}_1 \bar{\Gamma}_1 - \rho_2 \underline{\underline{\omega}}^2 \bar{\Lambda}_2 \bar{\Gamma}_2 & \kappa A_{55}\bar{\xi}_1 i & \kappa A_{44}\bar{\xi}_2 i \\ \kappa A_{55}\bar{\xi}_1 i & D_{11}\bar{\xi}_1^2 + D_{66}\bar{\xi}_2^2 + \kappa A_{55} - I\underline{\underline{\omega}}^2 & (D_{12} + D_{66})\bar{\xi}_1\bar{\xi}_2 \\ \kappa A_{44}\bar{\xi}_2 i & (D_{12} + D_{66})\bar{\xi}_1\bar{\xi}_2 & D_{22}\bar{\xi}_2^2 + D_{66}\bar{\xi}_1^2 + \kappa A_{44} - I\underline{\underline{\omega}}^2 \end{bmatrix}$$

Where

$$\underline{\underline{\omega}} = \overline{\omega} - V_x\bar{\xi}_1 - V_y\bar{\xi}_2$$

$$\bar{\Lambda}_1 = \frac{1}{\bar{\beta}\sinh\left(\bar{\beta}\frac{H}{2}\right) - \bar{\beta}\coth\left[\bar{\beta}\left(H_1 + \frac{H}{2}\right)\right]\cosh\left(\bar{\beta}\frac{H}{2}\right)}$$

$$\bar{\Gamma}_1 = \cosh\left(\bar{\beta}\frac{H}{2}\right) - \coth\left[\bar{\beta}\left(H_1 + \frac{H}{2}\right)\right]\sinh\left(\bar{\beta}\frac{H}{2}\right)$$

$$\bar{\Lambda}_2 = \frac{1}{\bar{\beta}\tanh\left[\bar{\beta}\left(H_2 + \frac{H}{2}\right)\right]\cosh\left(\bar{\beta}\frac{H}{2}\right) - \bar{\beta}\sinh\left(\bar{\beta}\frac{H}{2}\right)}$$

and,

$$\bar{\Gamma}_2 = \cosh\left(\bar{\beta}\frac{H}{2}\right) - \tanh\left[\bar{\beta}\left(H_2 + \frac{H}{2}\right)\right]\sinh\left(\bar{\beta}\frac{H}{2}\right)$$

with ,

$$\bar{\beta} = \sqrt{\bar{\xi}_1^2 + \bar{\xi}_2^2}$$

Nomenclature

English Symbols

A_{ij},B_{ij},D_{ij}	Plate stiffness terms
c	Phase velocity
c_g	Group velocity
Cij	Elastic constants
F	Force vector
$f(t)$	Applied force
H	Plate thickness
H_1	Upper liquid depth
H_2	Lower liquid depth
L_η, L_ζ	Distance components between the two loads
[M]	Determinant matrix
N,M,Q	Force and moment resultant
Q_{ij}	Reduced stiffness terms
(u,v,w)	Displacement components

(u_o, v_o, w_o)	Displacement components of the middle surface
(x,y,z)	Stationary coordinate system
V_x, V_y	Load velocity components
$\overline{W}_o$	Transformed displacement

Greek Symbols

ϕ_i	Velocity potential
ρ	Plate density
ρ_1	Upper liquid density
ρ_2	Lower liquid density
ψ	Rotation
σ, τ	Stresses
ε, γ	Strains
Ψ	Transformed rotation
ω	Frequency
ξ	Wavenumber
η, ζ	Referred to moving coordinate

φ	Angle between wave direction and x-axis
κ	Shear factor
ν	Poisson ratio
$\Im$	Fourier Transform
λ, μ	Lame constants

REFERENCES

1. Schreier, V., and Fahy, 1. 1. "Point-Force Excited Vibrations of Thin, Infinite Panel Separating a Fluid Layer From a Fluid Half Space," Journal of Sound and Vibration," **74**(4), 465-476, (1991).

2. Dabirikhah H., and Turner, C. "The Coupling of the A_o and Interface Scholte Modes in Fluid-Loaded Plates," J. Acoust. Soc. Am., **100**(5), Nov. (1996).

3. Selezov, I., and Tkachenko V. "Analysis of Propagation of Transient Waves in an Elastic Plate on the Surface of a Liquid," Fluid Mechanics, **20**(3), 31-36, (1991).

4. Soedel, S., and Soedel, W. "On the Free and Forced Vibration of a Plate Supporting a Freely Sloshing Surface Liquid," Journal of Sound and Vibration, **71**(2), 159-171, (1994).

5. Wu, J. and Zhemin, Z. "The Propagation of Lamb Waves in a Plate Bordered with Layers of a Liquid, " J. Acoust. Soc. Am., **91**(2), 861-867, (1992).

6. Wu, S. and Zhu, J. "Effect of Mean Flow on Responses of a Fluid-Loaded Plate," J. Acoust. Soc. Am., **98**(3), 1786-1795, (1995).

7. Nagaya, K. and Nagai, K. "Transient Response of Plates with Arbitrary Shape in Contact with a Fluid Subjected to General Dynamic Pressure on a Fluid Surface," J. Acoust. Soc. Am., **81**(2), (1987).

8. Bao, X., P. Raju, and H. Uberall. "The Splitting of Dispersion Curves for Plates Fluid-Loaded on Both Sides, " J. Acoust. Soc. Am., **102**(2), 1246-1248, (1997).

9. Desmet, C., V. Gusev, C. Glorieux, W. Lauriks, and J. Theon. "All-Optical Investigations of the Lowest-Order Antisymmetrical Acoustic Modes in Liquid-Loaded Membranes, " J. Acoust. Soc. Am., **103**(1), 618-621, (1998).

10. Dickey, J., G.Maidanilk, and H. Uberall. "The splitting of Dispersion Curves for the Fluid-Loaded Plate," J. Acoust. Soc. Am., **98**(4), 2365-2362, (1995).

11. Langley, A. "The Sound Fields of an Infinite, Fluid-Loaded Plate Excited by a Point Force," J. Acoust. Soc. Am., 83(4), 1360-1365, (1988).

12. Hassan, W. and Nagy, P. "On the Low-Frequency Oscillation of a Fluid Layer Between Two Elastic Plates," J. Acoust. Soc. Am., **102**(6), 3343-3348, (1997).

13. Nugroho, W., K. Wang, R. Hosking, and F. Milinazzo. "Time-Displacement Response of a Floating Flexible Plate to an Impulsively Started Steadily Moving Load," Journal of Metal Mechanics, 381, 337-355, (1999).

14. Kim, S., and J. Roesset. "Moving Load on a Plate on Elastic Foundation," Journal of Engineering Mechanics, 1010- 1017, Sep, (1998)

15. Dieterman, H. and Metrikine, A. "Critical Velocities of a Harmonic Load Moving Uniformly Along an Elastic Layer," Journal of Applied Mechanics, **64**, 596-600, Sep. (1997).

16. Barber, J. " Surface Displacement Due to a Steadily Moving Point Force," Journal of Applied Mechanics, **63**,245-251, (1996).

17. Zaman, M., M. Taheri, and A. Alvappillai. "Dynamic Response of a Thick Plate on Viscoelastic Foundation to Moving Loads," International Journal for Numerical and Analytical Methods in Geomechanics, **15**,627-647, (1991).

18. Boldin, V., S. Malanov, and G Utkin. "Formulation of Boundary-Value Problems for the Dynamics of Two-Dimensional Systems with Moving Loads and Fastening," Prikl. Mat. Melch.,**56**(1),34-39,(1992).

19. Pesterev, A. and Bergman, L. "Response of a Non-conservative Continuous System to a Moving Concentrated Load," Journal of Applied Mechanics,**65**,436-444,June (1998).

20. Mindlin, R. "Influence of Rotary Inertia and Shear on Flexural Motions of Isotropic Elastic Plates," ASME J. App. Mech., **18**,31-38,(1951).

21. Yang, P. "Elastic Wave Propagation in Heterogeneous plates," Int. J. of Solids and Struct. ,**2**,665,(1966).

22. Whitney, J. *Structural Analysis of Laminated Anisotropic Plates.* Technomic Publishing Co. Lancaster,(1978).

23. Calcote, L. *The Analysis of Laminated Composite Structures.* Van Nostrand Reinhold Co. New York, (1969).

24. Szilard, R. Theory and Analysis of Plates. Prentice-Hall Inc. New Jersey, (1978)